COMBUSTION RESEARCH

Thesis by

Roy Earl Reichenbach

In Partial Fulfillment of the Requirements
For the Degree of
Doctor of Philosophy

California Institute of Technology
Pasadena, California
1960

To My Parents

ACKNOWLEDGMENTS

The author is indebted to Dr. S. S. Penner for suggesting these studies and for his helpful suggestions throughout the course of the work.

Financial support for this program has been provided by The Ramo-Wooldridge Corporation in the form of a fellowship granted for the academic years 1956-1958, by the California Institute of Technology through tuition scholarships for the years 1958-1960, and by the Office of Ordnance Research, United States Army, under Contract No. DA 04-495-Ord-1634. This support is gratefully acknowledged.

ABSTRACT

In Part 1 an iterative procedure is described for the solution of nozzle flow problems with one-step, reversible chemical reactions. The efficiency of the method of calculation is illustrated by comparing the results with data obtained through the use of machine computations for the recombination of hydrogen atoms in a deLaval nozzle.

Two topics concerned with droplet burning are considered in Part 2. Droplets of several important propellants, viz., RP-1, UDMH and N_2H_4, were burnt in air and in oxygen. The (effective) evaporation constants were determined experimentally for these fuels. The second topic involves the determination of the propagation rates and mechanism of propagation of a flame in a one-dimensional array of n-octane droplets. The flame propagation rates were found to be a function of the initial droplet size, of the droplet spacing, and directly of the depth of immersion of the droplet in the hot-gas zone.

Part 3 consists of a study of the effect of an inert diluent on spectral intensity ratios in propane-oxygen-nitrogen flames. Experiments were conducted with inert diluent contents of 50, 60, 70, and 80 percent nitrogen (by mass) and with equivalence ratios of 0.6, 0.8, 1.0, 1.2, 1.4 and 1.6. The spectral intensity ratio was found to be a function not only of the equivalence ratio but also of the percentage of inert diluent. Hence it is not possible, in general, to use spectral intensity ratios as measures of mixture composition, a procedure that has been used erroneously by a number of investigators.

TABLE OF CONTENTS

PART 1. THEORETICAL STUDIES ON CHEMICAL REACTIONS DURING FLOW THROUGH A DELAVAL NOZZLE

I. INTRODUCTION

The extent of the chemical changes occurring during nozzle flow in rocket engines has an important bearing on theoretical and actual performance evaluation, particularly for high-energy propellant systems.

It is common practice in rocket engineering to assume that the chemical processes go essentially to completion in properly designed combustion chambers. This assumption will be discussed in greater detail in the following section. If one accepts the assumption that complete combustion occurs in the chamber, it is a relatively simple matter to bracket the expected engine performance between frozen and equilibrium flow estimates. In the present context, frozen flow implies no composition change (the reaction rate is zero) and equilibrium flow implies that the reaction rate is infinite. Depending on the nature of the flow processes, i.e., on the extent of the chemical changes and on solid particle formation, the theoretical performance estimates for equilibrium flow may be as much as 10 to 15 percent higher than the corresponding values for frozen flow in the hottest propellant systems. The frozen and equilibrium flow estimates for conventional propellant combinations (specific impulse approximately 200 to 250 sec) generally do not differ by more than a few percent. It is important to note that differences in specific impulse of a few percent will have a large effect

on the range of large missile and satellite launching vehicles. Hence, theoretical and experimental efforts designed to define expected performance limits within close tolerances are of considerable practical importance. In the case of high-Mach number ramjet engines, chemical changes in high-velocity flow systems have a dominant influence on the performance.

Early theoretical studies on chemical reaction during nozzle flow[1, 2] involved approximate numerical calculations for one-step chemical processes. Because of the uncertainties inherent in estimates of high-temperature reaction rates, subsequent analytical studies were confined to the development of near-equilibrium and near-frozen flow criteria[3, 4, 5] designed to permit appropriate classification of reaction rates as "sufficiently fast to maintain nearly equilibrium throughout expansion" or "so slow that no significant composition changes will occur during expansion".* Thus, the application of the near-equilibrium and near-frozen flow criteria for known reaction rates is a useful first step in categorizing chemical processes and in obtaining approximate a priori estimates for the relation between nozzle dimensions, propellant composition and theoretical performance evaluation.

A useful analytical tool, that is intermediate in scope between the near-equilibrium and near-frozen flow criteria and exact numerical work[6, 7] (i.e., calculations by Krieger for the recombination of hydrogen atoms) utilizes the fact that many chemical reactions are maintained almost in

* For a summary of this work, see reference (5).

equilibrium up to a point in a nozzle and then remain practically "frozen" farther downstream. This type of physical behavior is to be expected in an adiabatically expanding gas mixture since initially the flow velocity is relatively low and also reaction rates generally decrease very rapidly when both the density and the temperature decrease.

Bray[8] has derived a simple and useful procedure using an approximate model suggested by Lighthill[9] for estimating the point in nozzle flow where significant deviations from equilibrium flow occur rapidly. Bray's procedure rests on the physical fact that for a reassociation process the following symbolic representation may be used:

rate of change with distance of mass fraction of molecules (dY/dx)

= rate of change with distance of mass fraction of molecules produced by association reactions (dY_A/dx)

- rate of change with distance of mass fraction of molecules produced by dissociation reactions (dY_D/dx).

Evidently dY/dx will be very small either when dY_A/dx is approximately equal to dY_D/dx (i.e., when the system is nearly in equilibrium) or when both dY_A/dx and dY_D/dx are approximately equal to zero (i.e., when all of the reaction rates are negligibly small). Furthermore, dY_D/dx decreases extremely rapidly with temperature. One expects equilibrium flow to persist for all values of dY_D/dx for which

$$(dY/dx)_{eq} \ll dY_D/dx$$

because then the equilibrium change in the mass fraction of molecules, which constitutes a theoretical upper limit for the mass fraction change,

is determined by the difference of two large, nearly equivalent quantities. When

$$(dY/dx)_{eq} >> dY_D/dx$$

then practically frozen flow must occur because the actual rate of change of mass fraction with distance is now determined largely by the recombination reactions which decrease with distance much less rapidly than dY_D/dx. If the two preceding inequalities are satisfied at points in the nozzle which are in close proximity, then the position at which departure from equilibrium flow and rapid freezing occurs is well defined. Plots of $(dY/dx)_{eq}$ and of dY_D/dx as functions of x are expected to exhibit the qualitative behavior sketched in Fig. 1. The point at which the two curves cross defines the approximate location where the expansion process changes from nearly frozen flow to nearly equilibrium flow.

Wegener[10] has recently demonstrated the utility of Bray's approach by performing careful calculations on his experimentally determined composition profiles for the system

$$X' + 2NO_2 \underset{k_b}{\overset{k_f}{\rightleftharpoons}} N_2O_4 + X'.$$

In the following sections, we consider the complete problem of recombination during nozzle flow with well justified physical approximations. It is our purpose to define a simple iteration procedure that allows solution of the nozzle flow problem by the use of desk machine computations. We

demonstrate the validity of our approach by a quantitative comparison with the results obtained on an IBM 709 Electronic Data Processing System. The calculations have been made using the same nozzle profile and reaction rates for hydrogen recombination as Krieger[6] used in his early numerical work, although his estimates of reaction rates may not constitute best values today. In fact, recent studies suggest that rather extensive revisions are needed.[11, 12, 13]

In the formulation of the complete nozzle flow problem with chemical reactions, we will make the following assumptions:[5]

1. The chemical processes go to completion in the combustion chamber, i.e., the equilibrium gas composition is assumed to exist at the nozzle entrance position prior to expansion. In justification of this assumption we note that, for many liquid-fuel and solid-fuel rocket engines, the observed values of the specific impulse are often intermediate between the calculated theoretical estimates for frozen and equilibrium flow. Caution should be exercised with this assumption since no empirical verification has been made with advanced engine types; furthermore, recent experiments with solid propellants containing metallic additives indicate that the combustion of the metal particles may be so slow that theoretical performance is unattainable in practice.

2. The expansion process is considered to involve one-dimensional flow of inviscid gases. These assumptions introduce negligibly small errors for conventional rocket engines with relatively slowly varying nozzle areas, and, therefore, the additional complications involved in

allowing for velocity components normal to the nozzle axis and for viscous flow do not appear to be justified, especially in view of the necessity of introducing the first assumption.

3. The gaseous mixture of reactants and products may be considered to follow the perfect gas law. The approach to ideal gas behavior may be calculated by using a suitable equation of state for the gas mixture. Penner[5] states that detailed calculations show that this assumption introduces small errors, of the order of 1% or less, into the calculated values of specific impulse for conventional rocket engines.

4. Concentration changes produced by diffusion currents may be neglected since the diffusion velocities are very small compared with the large translational velocities of the gases.

5. The expansion is assumed to be adiabatic, although heat transfer to the nozzle will introduce very small errors (of the order of 1% or less) into the calculated values of the specific impulse for engines of reasonable size.

II. BASIC EQUATIONS

In this section we derive the exact equations (exact in the sense that only the above listed approximations are used) and then obtain a set of approximate governing equations which we are able to solve through the use of an iterative procedure. The approximate equations may be used to obtain some physical insight into the variations of the dependent variables and their derivatives with nozzle location.

A. Conservation Equations

The appropriate set of conservation equations for one-dimensional, inviscid, flow problems with chemical reactions is easily derived from the well-known general expressions.*

We consider the three-body association reaction

$$2R + X' \underset{k_b}{\overset{k_f}{\rightleftharpoons}} P + X' , \tag{1}$$

where X' may be either R or P, and R and P are symbolic representations for reactant and product species. The one-dimensional continuity equation for species j is

$$\rho A v \frac{dY_j}{dx} = A w_j + \frac{d}{dx}\left[\rho A D_j \frac{dY_j}{dx}\right] \tag{2}$$

where ρ is the local density of the fluid mixture (g/cm^3); v is the mass weighted average velocity (cm/sec); Y_j is the mass fraction of species j; A(x) is the nozzle cross sectional area (cm^2); w_j is the net rate of production of species j per unit volume by chemical reactions (g/cm^3-sec);

* See, for example, reference (5), Chapter XVIII.

and D_j is the binary diffusion coefficient. Using the assumption made above that we may neglect diffusion, Eq. (2) reduces to

$$\rho v \frac{dY_j}{dx} = w_j \, . \tag{3}$$

For the general set of opposing chemical reactions

$$\sum_{j=1}^{n} \nu_j' \, M_j \underset{k_b}{\overset{k_f}{\rightleftharpoons}} \sum_{j=1}^{n} \nu_j'' \, M_j, \qquad j=1, 2, 3, \ldots, n \, , \tag{4}$$

it is well known that the law of mass action leads to the following equation for the production rate of species j:

$$w_j = W_j(\nu_j'' - \nu_j') \, k_f \left(1 - \frac{K'}{K}\right) \rho^{\delta} \prod_{j=1}^{n} \left(\frac{Y_j}{W_j}\right)^{\nu_j'} . \tag{5}$$

Here $\delta = \sum_{j=1}^{n} \nu_j'$ is the order of the chemical reaction; W_j is the molecular weight of species j (g/mole); k_f is the forward reaction rate constant, k_b is the backward reaction rate constant; the ν_j' are the stoichiometric coefficients for the reactants; the ν_j'' are the stoichiometric coefficients for the reaction products; n is the total number of chemical species involved; K represents the equilibrium constant; and K' is analogous to an equilibrium constant except that it is referred to the prevailing local concentrations rather than to equilibrium concentrations.

Throughout the remainder of the analysis we shall consider hydrogen recombination, i.e., in Eq. (1), R is H and P stands for H_2. Thus Eq. (5) reduces to

$$w_{H_2} = W_{H_2} k_f \left(1 - \frac{K'}{K}\right) \rho^3 \left(\frac{Y_H}{W_H}\right)^2 \left(\frac{Y_{X'}}{W_{X'}}\right)^1 . \tag{6}$$

Since X' may be either H or H_2, we have $Y_{X'} = 1$ and $W_{X'} = \overline{W}$, where $\overline{W}$ is the average molecular weight of the fluid mixture. The number of moles of species j is evidently equal to the ratio of the mass of species j ($\equiv m_j$) to the molecular weight of species j ($\equiv W_j$). Therefore, in the binary mixture containing only H and H_2,

$$\frac{m_T}{\overline{W}} = \frac{m_H}{W_H} + \frac{m_{H_2}}{W_{H_2}} \tag{7}$$

where m_T is the total mass. Since $Y_j = m_j/m_T$, the preceding expression becomes

$$\frac{1}{\overline{W}} = \frac{Y_H}{W_H} + \frac{Y_{H_2}}{W_{H_2}} = \frac{2 - Y_{H_2}}{W_{H_2}} . \tag{8}$$

Furthermore, since

$$Y_H + Y_{H_2} = 1, \tag{9}$$

Eq. (2) may be rewritten in the form

$$w_{H_2} = 4k_f \left(1 - \frac{K'}{K}\right) \frac{\rho^3}{W_{H_2}^2} \left(2Y_H^3 + Y_H^2 Y_{H_2}\right). \tag{10}$$

It is now convenient to introduce the fraction of the reaction completed, ξ, through the expression

$$\varepsilon = \frac{Y_{H_2} - Y_{H_2}^{o}}{1 - Y_{H_2}^{o}} , \qquad 0 \leq \varepsilon \leq 1 . \tag{11}$$

Here $Y_{H_2}^{o}$ denotes the initial mass fraction of H_2 which corresponds to the equilibrium value formed in the chamber. Now substituting into Eq. (3), we find

$$w_{H_2} = \rho v \frac{dY_{H_2}}{dx} = \rho v (1 - Y_{H_2}^{o}) \frac{d\varepsilon}{dx} , \tag{12}$$

where ρv (in g/cm^2-sec) corresponds to the mass flow rate per unit area, and the conservation of mass equation for H_2 reduces to the form

$$\frac{d\varepsilon}{dx} = \frac{4k_f \rho^2}{v W_{H_2}^2} \left(1 - \frac{K'}{K}\right) (1 - Y_{H_2}^{o}) (1-\varepsilon)^2 \left[1 + (1-\varepsilon)(1 - Y_{H_2}^{o})\right] . \tag{13}$$

Neglecting axial diffusion and heat conduction, the one-dimensional energy equation is

$$h + (1/2)v^2 = h_s = \text{constant}, \tag{14}$$

where

$$h = \sum_{i=1}^{n} Y_i (\Delta hf_i^* + \int_{T^*}^{T} c_{p_i} dT)$$

and is the local enthalpy, h_s is the specific stagnation enthalpy including chemical enthalpy; Δhf_i represents the standard specific enthalpy of formation for species i evaluated at a suitably chosen reference temperature T*, c_{p_i} is the specific heat at constant pressure for species i, and T is the local temperature of the fluid mixture.

For hydrogen recombination, using the definition of ε, the energy equation may thus be expressed as

$$\left[Y_{H_2}^{o} + \varepsilon(1-Y_{H_2}^{o})\right](\Delta hf^{*}_{H_2} + \int_{T^*}^{T} c_{p_{H_2}} dT)$$

$$+ \left[(1-\varepsilon)(1-Y_{H_2}^{o})\right](\Delta hf^{*}_{H} + \int_{T^*}^{T} c_{p_H} dT) + \frac{v^2}{2} = h_s. \qquad (15)$$

We choose $T^* = 298.16^{o}K$, and, therefore, $\Delta hf^{*}_{H_2} = 0$, $\Delta hf^{*}_{H} = 51,675.6$ cal/g of H. Solving Eq. (15) for v we find

$$v\left(\frac{cm}{sec}\right) = \sqrt{2}\,(4.184 \times 10^{7})^{1/2}\left[h_s - (\Delta hf^{*}_{H} + \int_{298.16}^{T} c_{p_H} dT)\right.$$

$$\left. -\left[(Y_{H_2}^{o}) + \varepsilon(1-Y_{H_2}^{o})\right](-\Delta hf^{*}_{H} + \int_{298.16}^{T} \left(c_{p_{H_2}} - c_{p_H}\right) dT\right]^{1/2} \qquad (16)$$

where the numerical factor arises because of our particular choice of units.

The overall continuity equation is

$$\rho A v = m \qquad (17)$$

where m is the constant total mass flow rate (in g/sec).* Solving for the

---

* The mass flow rate is actually an eigenvalue and must be determined from an iteration procedure. This problem will be discussed more fully in Section IV.

density ρ we find now that

$$\rho\left(\frac{g}{cm^3}\right) = \frac{m}{Av} = \frac{m}{\sqrt{2}\,(4.184 \times 10^7)^{1/2} A} \left[h_s - \left(\Delta hf_H^* + \int_{298.16}^{T} c_{p_H}\, dT\right)\right.$$

$$\left. - \left(Y_{H_2}^{o} + \varepsilon(1 - Y_{H_2}^{o})\right)\left(-\Delta hf_H^* + \int_{298.16}^{T} \left(c_{p_{H_2}} - c_{p_H}\right) dT\right)\right]^{-\frac{1}{2}} . \quad (18)$$

Using the perfect gas law,

$$p = \rho \frac{R}{\overline{W}}\, T \,, \quad (19)$$

where p is the local static pressure in atmospheres and R is the molar gas constant (cal/mole-^{o}K), we find after substitution for ρ, $\overline{W}$, and T that

$$p(atm) = \frac{41.298m\, RT\left[1 + (1-\varepsilon)(1 - Y_{H_2}^{o})\right]}{(4.184 \times 10^7)^{1/2}\sqrt{2}\; W_{H_2} A} \left[h_s - \left(\Delta hf_H^* + \int_{298.16}^{T} c_{p_H}\, dT\right)\right.$$

$$\left. - \left(Y_{H_2}^{o} + \varepsilon(1 - Y_{H_2}^{o})\right)\left(-\Delta hf_H^* + \int_{298.16}^{T} \left(c_{p_{H_2}} - c_{p_H}\right) dT\right)\right]^{-1/2} . \quad (20)$$

For one-dimensional, inviscid flow, the overall momentum equation is

$$v \frac{dv}{dx} = -\frac{1}{\rho}\, dp \,. \quad (21)$$

The use of Eqs. (16), (18), and (20) in Eq. (21) leads to the following basic equation in terms of ε and T:

$$\frac{dT}{dx} = \left[\frac{dA}{dx} \frac{RT}{W_{H_2} A} \left[1+(1-\varepsilon)(1-Y_{H_2}^{o}) \right] - (1-Y_{H_2}^{o}) \frac{d\varepsilon}{dx} \left[\beta(-\Delta hf_H^{*} + \int_{298.16}^{T} (c_{p_{H_2}} - c_{p_H}) dT) \right. \right.$$

$$\left. \left. - \frac{RT}{W_{H_2}} \right] \right]$$

$$\Bigg/ \left[\beta \left\{ \left[Y_{H_2}^{o} + \varepsilon(1-Y_{H_2}^{o}) \right] c_{p_{H_2}, T} + \left[(1-\varepsilon)(1-Y_{H_2}^{o}) \right] c_{p_{H, T}} \right\} \right.$$

$$\left. + \frac{R}{W_{H_2}} \left[1 + (1-\varepsilon)(1-Y_{H_2}^{o}) \right] \right] \qquad (22)$$

where we have set

$$\beta = \left\{ \frac{RT \left[1+(1-\varepsilon)(1-Y_{H_2}^{o}) \right]}{2W_{H_2}} \left[h_s - (\Delta hf_H^{*} + \int_{298.16}^{T} c_{p_H} dT) \right. \right.$$

$$\left. \left. - (Y_{H_2}^{o} + \varepsilon(1-Y_{H_2}^{o})) (-\Delta hf_H^{*} + \int_{298.16}^{T} (c_{p_{H_2}} - c_{p_H}) dT) \right]^{-1} \right\} - 1. \qquad (22a)^{*}$$

In order to complete the formulation of the exact flow problem, it is now necessary to rewrite Eq. (13) in terms of ε, T and x. Using Eqs. (13), (16), and (18) we obtain the result

---

* In terms of the Mach number $M^2 = v^2 \overline{W} / \gamma RT$, it is easily shown that

$$\beta = \frac{1}{\gamma M^2} - 1.$$

$$\frac{d\varepsilon}{dx} = \frac{4k_f m^2 (1-\frac{K'}{K})(1-Y_{H_2}^{o})(1-\varepsilon)^2 \left[1 + (1-\varepsilon)(1-Y_{H_2}^{o})\right]}{(2 \times 4.184 \times 10^7)^{3/2} A^2 W_{H_2}^{2}}$$

$$\times \left[h_s - (\Delta hf_H^* + \int_{298.16}^{T} c_{p_H} dT) \right.$$

$$\left. -(Y_{H_2}^{o} + \varepsilon(1-Y_{H_2}^{o}))(-\Delta hf_H^* + \int_{298.16}^{T} (c_{p_{H_2}} - c_{p_H}) dT) \right]^{-3/2} \qquad (23)$$

where ε and T are the dependent variables and the numerical factor occurring in the denominator arises again because of the previously specified choice of dimensions for k_f, m, A, and W_{H_2}. The dimensionless ratio

$$\frac{K'}{K} = \frac{K_c'}{K_c} = \frac{1}{K_c} \frac{(\rho Y_{H_2}/W_{H_2})}{(\rho Y_H/W_H)^2} = \frac{1}{K_p RT} \frac{W_{H_2} Y_{H_2}}{4\rho(1-Y_{H_2})^2} \qquad (24)$$

may also be expressed readily in terms of ε and T by using Eqs. (11) and (18). Thus

$$\frac{K'}{K} = \frac{(2 \times 4.184 \times 10^7)^{1/2} W_{H_2} A \left[Y_{H_2}^{o} + (1-Y_{H_2}^{o})\right]}{4 \times 41.298\ RT\, m\, K_p (1-\varepsilon)^2 (1-Y_{H_2}^{o})^2} \left[h_s - (\Delta hf_H^* + \int_{298.16}^{T} c_{p_H} dT) \right.$$

$$\left. -(Y_{H_2}^{o} + \varepsilon(1-Y_{H_2}^{o}))(-\Delta hf_H^* + \int_{298.16}^{T} (c_{p_{H_2}} - c_{p_H}) dT) \right]^{1/2} \qquad (25)$$

where K_P is the equilibrium constant $p_{H_2}^e/(p_H^e)^2$ if $p_{H_2}^e$ and p_H^e denote equilibrium partial pressures. The quantity K_P^* is a sensitive function

of temperature and hence K'/K is a complicated function of ε, T, and the constants of the flow.

We have now reduced the nozzle flow problem with recombination reactions to the solution of the coupled, non-linear differential equations given in Eqs. (22) and (23). It is obvious that, upon imposition of suitable initial conditions, these equations may be solved by the use of numerical techniques on an electronic computer.

The above equations [Eqs. (22) and (23)] do not provide significant physical insight into the forms of ε, $d\varepsilon/dx$, or T as functions of distance along the nozzle. Hence we will reformulate the flow problem in terms of ε and M, where M represents the Mach number, viz.,

$$M = \frac{v^2}{\gamma R_g T} = \frac{v^2}{\gamma \frac{R}{\overline{W}} T} \quad . \tag{26}$$

Here R_g is the specific gas constant for the gaseous mixture (in cal/g-$^{\circ}$K) and γ is the ratio of the specific heat at constant pressure for the gaseous mixture.

In the following formulation we shall make the additional assumption that we may use constant average values for the ratio of the specific heats (γ) and for the specific heat at constant pressure ($\overline{c}_p$), since both γ and $\overline{c}_p$ are relatively weak functions of the temperature and of the composition of the gaseous mixture.

---

* K_p is tabulated as a function of temperature in several references, for example see reference (5), page 127 or reference (14).

Using the above approximations in Eq. (14) and noting that

$$h = \overline{c}_p(T-T^*) + \sum_{i=1}^{n} Y_i \, \Delta hf_i^*,$$

we find that the one-dimensional energy equation becomes

$$\frac{v^2}{2} + \overline{c}_p T + Y_H \Delta hf_H^* + Y_{H_2} \Delta hf_{H_2}^* = \frac{v_o^2}{2} + \overline{c}_p T_o + Y_H^o \Delta hf_H^* + Y_{H_2}^o \Delta hf_{H_2}^* . \tag{27}$$

where the subscript and superscript o again identify initial conditions, and all other symbols have the previously stated meanings. Here we define the initial stagnation enthalpy h_o (excluding the chemical enthalpy) through the equation

$$h_o \left(\frac{cal}{g}\right) = \overline{c}_p \, T_o + \frac{v_o^2}{2} . \tag{28}$$

The heat release q (in cal/g) per unit mass of mixture for complete recombination of hydrogen atoms is

$$q = (1-Y_{H_2}^o)(\Delta hf_H^* - \Delta hf_{H_2}^*) = (1-Y_{H_2}^o) \, \Delta hf_H^* \tag{29}$$

if $T^* = 298.16^oK$. Equations (11) and (27) to (29) lead to the following relation:

$$\frac{v^2}{2} + \overline{c}_p T - \mathcal{E} q = h_o . \tag{30}$$

If we now use the definition of Mach number [cf. Eq. (26)] and the ideal gas equation with $R_g/c_p = (\gamma-1)/\gamma$, it is easily shown that

$$T = \frac{h_o + \varepsilon q}{\bar{c}_p \left[1+(\gamma-1)M^2/2\right]} \quad . \tag{31}$$

Equations (30) and (31) may be combined to yield the following explicit relation for the linear flow velocity v:

$$v = (4.184 \times 10^7)^{1/2} \frac{M\left[(\gamma-1)(h_o+\varepsilon q)\right]^{1/2}}{\left[1+(\gamma-1)M^2/2\right]^{1/2}} \quad . \tag{32}$$

Using now the overall continuity equation, $\rho Av = m$, leads to

$$\rho = \frac{m}{Av} = \frac{(4.184 \times 10^7)^{-1/2} m\left[1+(\gamma-1)M^2/2\right]^{1/2}}{AM\left[(\gamma-1)(h_o+\varepsilon q)\right]^{1/2}} \quad . \tag{33}$$

An explicit expression in terms of ε and M may be derived for the local pressure by using the defining relation for the Mach number together with the overall mass conservation equation and the ideal gas equation of state, viz.,

$$M^2 = \frac{v^2}{\gamma R_g T} = \frac{v^2}{\gamma p/\rho} = \frac{v^2(m/Av)}{\gamma p} = \frac{vm}{A\gamma p}$$

whence

$$p(\text{atm}) = \frac{(4.184 \times 10^7)^{1/2}}{1.01325 \times 10^6} \frac{m\left[(\gamma-1)(h_o+\varepsilon q)\right]^{1/2}}{\gamma AM\left[1+(\gamma-1)M^2/2\right]^{1/2}} \quad . \tag{34}$$

Introducing Eqs. (32), (33), and (34) into the one-dimensional momentum equation [Eq. (21)] leads to the working equation

$$\frac{dM^2}{dx} = \frac{M^2\left[1+(\gamma-1)M^2/2\right]}{1-M^2}\left[\frac{(1+\gamma M^2)q}{h_o+\varepsilon q}\frac{d\varepsilon}{dx} - \frac{2}{A}\frac{dA}{dx}\right]. \tag{35}$$

In order to find the other basic working equation needed to complete the formulation of the approximate flow problem, we must rewrite the $d\varepsilon/dx$ equation [Eq. (13)] in terms of ε, M, and x. Thus

$$\frac{d\varepsilon}{dx} = \frac{4k_f m^2}{M^3 A^2 W_{H_2}^2}\,\frac{(1-\frac{K'}{K})(1-\varepsilon)^2(1-Y_{H_2}^o)\left[1+(1-\varepsilon)(1-Y_{H_2}^o)\right]}{(4.184\times 10^7)^{3/2}}$$

$$\frac{\left[1+(\gamma-1)M^2/2\right]^{3/2}}{\left[(\gamma-1)(h_o+\varepsilon q)\right]^{3/2}}\,. \tag{36}$$

Using Eqs. (11), (24), (31) and (33) we may express the dimensionless ratio K'/K in terms of ε and M; thus

$$\frac{K'}{K} = \frac{156.8\gamma AM\left[Y_{H_2}^o+\varepsilon(1-Y_{H_2}^o)\right]\left[1+(1-\varepsilon)(1-Y_{H_2}^o)\right]}{4K_p\, m\,(1-\varepsilon)^2\,(1-Y_{H_2}^o)^2}\,\frac{\left[1+(\gamma-1)M^2/2\right]^{1/2}}{\left[(\gamma-1)(h_o+\varepsilon q)\right]^{1/2}} \tag{37}$$

where K_P has been defined previously.

Equations (35) and (36) [with K'/K specified by Eq. (37)] constitute the two coupled, non-linear differential equations that describe the adiabatic expansion with hydrogen recombination through a deLaval nozzle. After imposition of suitable initial conditions, i.e., $\varepsilon = 0$ at $x = 0$ and $M^2 \neq 0$ at $x = 0$ for any finite nozzle entrance area. We also note that $(d\varepsilon/dx)_{x=0} = 0$ since $M^2 \neq 0$ and $(K'/K)_{x=0}=1$ if we assume that expansion begins with the equilibrium composition; finally

$$\left(\frac{dM^2}{dx}\right)_{x=0} = \left\{\frac{M^2\left[1+(\gamma-1)M^2/2\right]}{1-M^2}\right\}_{x=0}\left[-\frac{2}{(A)_{x=0}}\left(\frac{dA}{dx}\right)_{x=0}\right].$$

After appropriate (numerical) solutions have been obtained of Eqs. (35) and (36), we may compute explicit values for the (dimensional) observables T, v, ρ, and p by straightforward applications of Eqs. (31), (32), (33), and (34).

It is interesting to note that Eqs. (23) and (36) show, in the limiting case of $k_f = 0$ (or frozen flow), that $d\varepsilon/dx = 0$. Thus ε remains constant at the entrance value of $\varepsilon = 0$, and the system of equations reduces to one equation in one unknown without chemical reactions. In the second limiting case of $k_f \rightarrow \infty$ we observe that the $\left[1-(K'/K)\right]$ term must equal zero for $d\varepsilon/dx$ to remain finite. Thus $K' = K$, i.e., we have chemical equilibrium everywhere. Hence, for the case of chemical equilibrium, Eqs. (22) and (25) with $K'/K = 1$ describe the flow process completely and may be solved simultaneously to obtain ε and T as functions of x. Similarly, we may solve the approximate equations [Eqs. (35) and (37)] simultaneously to obtain ε and M as functions of x.

III. AN ITERATIVE PROCEDURE FOR THE SOLUTION OF THE APPROXIMATE EQUATIONS

Careful analysis of Eq. (36) indicates that $d\varepsilon/dx$ has the following properties:

1. $d\varepsilon/dx$ equals zero at the nozzle entrance since we have assumed that the equilibrium composition exists at the chamber exit ($K'/K \neq 1$), and $M_{x=0} \neq 0$ for any mass flow rate for any nozzle with a finite entrance area.

2. $d\varepsilon/dx$ has a maximum in the vicinity of the nozzle throat ($x=x_i$) for a sufficiently converging-diverging nozzle since $d\varepsilon/dx \sim 1/A^2$, and $1/A^2$ is the only term in Eq. (36) that is not continuously increasing or decreasing with axial distance.

3. $d\varepsilon/dx$ decreases continuously for $x >> x_i$ since k_f is either constant or changes only slightly, $(1-\varepsilon^2)\left[1+(1-\varepsilon)(1-Y_{H_2}^{o})\right] / \left[(\gamma-1)(h_o+\varepsilon q)\right]^{3/2}$ decreases, $\left[1+(\gamma-1)M^2/2\right]^{3/2}/M^3$ approaches the constant value $\left[(\gamma-1)/2\right]^{3/2}$, $1/A^2$ decreases, and $\left[1-(K'/K)\right]$ is bounded and cannot exceed unity even for completely frozen flow. Thus $d\varepsilon/dx$ must approach zero asymptotically as x becomes very large.

We are thus led to searching for a trial function (zeroth approximation) for $d\varepsilon/dx$ that satisfies the above requirements. We choose the simple function

$$\frac{d\varepsilon_z}{dx} = c_1 \frac{x}{x_i^2} \exp\left[-(x-ax_i)^2/(ax_i)^2\right] \tag{38}$$

and impose the condition

$$\left(\frac{d^2\varepsilon_z}{dx^2}\right)_{x=x_i} = 0 \tag{39}$$

whence it follows that the parameter a must equal 0.732. We further note that

$$\left(\frac{d\varepsilon_z}{dx}\right)_{x=x_i} = \xi_i \tag{40}$$

may be calculated from Eq. (36) as a function of $(\varepsilon_z)_{x=x_i}$ if we assume that $M^2 = 1$ at $x = x_i$, i.e., we assume that the flow velocity at the nozzle throat is sonic for the reacting gas mixture in zeroth approximation. We believe that the approximation implied by this assumption must be at least as good as the assumed profile for ε_z specified through Eq. (38) since it is well known that the Mach number equals unity at the nozzle throat for a non-reacting gas. This may be shown from our equations as follows. In order for dM^2/dx to be finite everywhere the numerator of Eq. (35) must vanish at the point where M^2 equals unity. Thus

$$\left[\frac{(1+\gamma M^2)q}{h_o + \varepsilon q}\ \frac{d\varepsilon}{dx} - \frac{2}{A}\ \frac{dA}{dx}\right]_{M=1} = 0, \tag{41}$$

or

$$\frac{(1+\gamma)q}{h_o + [\varepsilon]_{M=1}\, q}\ \left(\frac{d\varepsilon}{dx}\right)_{M=1} = \left(\frac{2}{A}\ \frac{dA}{dx}\right)_{M=1}. \tag{42}$$

For a non-reacting gas $d\varepsilon/dx$ equals zero and hence the sonic location occurs at the nozzle throat. Every quantity on the left-hand side of Eq. (42) is positive in the region of interest for the case of a reacting gas, and hence $dA/dx > 0$ at the sonic location. Thus the Mach number equals unity aft of the nozzle throat. For a complete discussion of the subtleties in the statement of sonic velocity of a reacting gas mixture we refer to the literature.[15,16]

From Eqs. (38) and (40) it is apparent that

$$c_1 = x_i \, \xi_i \exp(0.134)$$

whence

$$\frac{d\varepsilon_z}{dx} = \xi_i \left[\exp(0.134)\right] \frac{x}{x_i} \exp\left[-(x-0.732\,x_i)^2/(0.732\,x_i)^2\right]. \tag{43}$$

A zeroth approximation to $(\varepsilon_z)_{x=x_i}$ may be obtained by integrating Eq. (43) from $\varepsilon = 0$ at $x = 0$, to $\varepsilon_z = (\varepsilon_z)_{x=x_i}$ at $x = x_i$. In this manner it is found that

$$\frac{(\varepsilon_z)_{x=x_i}}{\xi_i} = 0.516\,x_i \, . \tag{44}$$

A second relation between $(\varepsilon_z)_{x=x_i}$ and ξ_i has been specified in Eq. (40) which may be written in the following explicit form:

$$\xi_i = \frac{4k_f m^2}{A_i^2 W_{H_2}^2} \frac{\left[1-(\varepsilon_z)_{x=x_i}\right]^2 (1-Y_{H_2}^o)\left\{1+\left[1-(\varepsilon_z)_{x=x_i}\right](1-Y_{H_2}^o)\right\}}{2.715 \times 10^{11}}$$

$$\times \frac{\left[1+(\gamma-1)/2\right]^{3/2}}{\left\{(\gamma-1)\left[h_o + (\varepsilon_z)_{x=x_i}\, q\right]\right\}^{3/2}}$$

$$\left\{1 - \frac{1.568 \times 10^2 \; A_i \left\{1+\left[1-(\varepsilon_z)_{x=x_i}\right](1-Y_{H_2}^o)\right\}}{4m K_{p,i}\left[1-(\varepsilon_z)_{x=x_i}\right]^2 (1-Y_{H_2}^o)^2} \frac{\left[Y_{H_2}^o + (\varepsilon_z)_{x=x_i}(1-Y_{H_2}^o)\right]}{1}\right.$$

$$\left. \frac{\left[1+(\gamma-1)/2\right]^{1/2}}{\left\{(\gamma-1)\left[h_o + (\varepsilon_z)_{x=x_i}\, q\right]\right\}^{1/2}} \right\} . \tag{45}$$

Here $K_{p,i}$ is a known function of the temperature, i.e., in view of Eq. (31), of $(\varepsilon_z)_{x=x_i}$ for $M^2 = 1$. Simultaneous solution of the two preceding expressions leads to explicit values of ξ_i, $(\varepsilon_z)_{x=x_i}$, c_1, and $(d\varepsilon_z/dx)$. Now using Eq. (43) with value of ξ_i (found by the method stated above) gives us $d\varepsilon_z/dx$ at every value of x. Then the zeroth approximation for $\varepsilon = \varepsilon_z$ can be obtained by graphical integration.

To demonstrate the utility of the procedure we have solved the problem of hydrogen atom recombination using a nozzle of the same geometry as that employed by Krieger.[6] We have also used the same initial conditions, namely the gas enters the nozzle at a temperature of $3500^{\circ}K$ and a pressure of 20 atm. The mass flow rate for this nozzle is 1000 g/sec. The nozzle considered is shown in Fig. 2. The entrance area A_c of the nozzle is twice the throat area A_i. The convergent section is spherical with a radius r_c, and is tangent to the rounded throat section at a point where the slope makes an angle of $28^{\circ}31'$ with respect to the nozzle axis. The diverging section is a diverging cone with a half angle of θ ($\theta = 15^{\circ}$) tangent to the rounded throat section. The expression describing the area of the spherical section as a function of x (distance along the nozzle axis, with the origin at the nozzle entrance) is

$$A = \pi(r_c^2 - x^2), \qquad 0 \leq x \leq 0.47741\, r_c. \tag{46}$$

For the area of the rounded throat section we have

$$A = \pi\left[6.5\, r_c^2 - \frac{6r_c}{2}\sqrt{2r_c^2 - (x-x_i)^2} - (x-x_i)^2\right],$$

$$0.47741\, r_c \leq x \leq 1.5186\, r_c\ ; \tag{47}$$

the area of the divergent section may be expressed as

$$A = \pi \left[(0.75529\, r_c)^2 + \frac{1.51058\, r_c (x - 1.5186\, r_c)}{\cot \theta} + \frac{(x - 1.5186\, r_c)^2}{\cot^2 \theta} \right],$$

$$1.5186\, r_c \leq x \,. \tag{48}$$

Since $A_c = 2A_i$ we know that $r_c = \sqrt{2}\, r_i$, $r_i = 3.00000$ cm, and $r_c = 4.24264$ cm. Hence from Eqs. (46), (47), and (48) we may compute the nozzle area at any station. We may also find dA/dx as a function of x from the preceding equations.

For the above example the quantity $d\varepsilon_z/dx$ has been plotted in Fig. 4 as a function of x. The zeroth approximation for $\varepsilon = \varepsilon_z$ is plotted in Fig. 3. The corresponding zeroth approximation for dM^2/dx is readily derived from Eq. (35) by using ε_z for ε and $d\varepsilon_z/dx$ for $d\varepsilon/dx$ on the right-hand side of Eq. (35). Graphical integration of dM^2_z/dx yields M_z^2 as a function of x. The constant of integration $(M_z^2)_{x=0}$ may be evaluated explicitly by using the initial temperature, pressure, and equilibrium composition, and the mass flow rate and nozzle entrance area together with the perfect gas relation and the definition of Mach number. The resulting curves for M_z^2 and dM_z^2/dx as functions of x are shown in Figs. 5 and 6, respectively. Finally, we have plotted the pressure and temperature profiles in Figs. 7 and 8.

Better approximations to the true solutions may be obtained by straightforward, but laborious iteration calculations. The most efficient approach found by us involves the trial-and-error computation of a first approximation ε_1 by using $d\varepsilon_z/dx$ and M_z in Eq. (36). This involved

approach was found to be necessary because the term $\left[1-K'/K\right]$ is an exceedingly sensitive function of ε and M. There are two extreme ranges of values which ε may assume, viz., (a) ε_1 is intermediate between ε_z and the correct value ε_c or (b) ε_c is intermediate between ε_z and ε_1, i.e., ε_1 "overshoots". In either case the next iteration will produce values of $\varepsilon=\varepsilon_2$ closer to ε_c than ε_1 if we use $\varepsilon_2 = (1/2)(\varepsilon_z + \varepsilon_1)$ rather than ε_1. For this reason we compute $\varepsilon_2 = (1/2)(\varepsilon_z + \varepsilon_1)$ and then use Eq. (35) to find dM_1^2/dx with $M^2 = M_z^2$, $d\varepsilon/dx = d\varepsilon_2/dx$, and $\varepsilon=\varepsilon_2$ on the right-hand side of Eq. (35). We also find a third iteration, $\varepsilon=\varepsilon_3$, from Eq. (36) by using the previously determined values of M_1^2 and $d\varepsilon_2/dx$. Finally a fourth iteration has been worked out in the downstream section of the nozzle, where we have obtained ε_4 using M_2^2 and $d\varepsilon_3/dx$.

IV. SOLUTION OF THE EXACT EQUATIONS

The exact working equations [Eqs. (35) and (36)] were solved numerically, using the Runge-Kutta method,[17] on an IBM 709 Electronic Computer. The program was written in Fortran (Formula Translation) language,[18] and appropriate initial conditions, constants of the flow, and values of the thermochemical parameters (i.e., K_p, $c_{p_{H_2}}$, $\int_{298.16}^{T} c_{p_{H_2}}\, dT$) at various temperatures were fed in as input data. A six point Lagrange's interpolation formula[19] was used to determine K_p, $c_{p_{H_2}}$, and $\int_{298.16}^{T} c_{p_{H_2}}\, dT$ at any temperature from the input data.

The method of solution which was employed was found to be unstable unless very small intervals were used. However, the solutions which were obtained were essentially independent of the size of the intervals provided the intervals were sufficiently small. For example, calculations with intervals of 0.0025 cm and 0.00125 cm, respectively, yielded at 15.5 cm from the nozzle entrance location, differences in T of approximately 4 parts in 10^5 and in $\mathcal{E}$ of approximately 5 parts in 10^6.

The error estimate for a particular computation was evaluated as follows (cf. Fig. 9):

$$E = \frac{\left[T_{x_o} + (x_1 - x_o) \left(\frac{dT}{dx} \right)_{x_o} \right] - (T_{\text{Runge-Kutta}})_{x_1}}{(T_{\text{Runge-Kutta}})_{x_1}}$$

where E represents the error per calculation. The quantity E was maintained smaller than 10^{-7}. The length interval used in most of our calculations was 0.0025 cm. Since the nozzle length required to expand

the gases to one atmosphere was approximately 16 cm, approximately 6400 calculations were required for a complete solution. But 6400 x $10^{-7} \lesssim 10^{-3}$, i.e., the overall error in the calculated parameters at the nozzle exit location should be less than 0.1%.

It is well known that the mass flow rate is an eigenvalue for a supersonic converging-diverging nozzle. Thus there is only one mass flow rate for specified values of the initial pressure, initial temperature, reacting gas composition, and fixed nozzle geometry for which the gas mixture will accelerate continuously from subsonic through sonic to supersonic flow velocities. If the mass flow rate is less than the correct eigenvalue (called the critical mass flow rate, m_c) the gas will accelerate until it reaches the vicinity of the nozzle throat and then it will decelerate in the diverging section of the nozzle, remaining subsonic everywhere. If a mass flow rate greater than m_c is chosen, the solutions will diverge in the vicinity of the throat (physically, the flow is choked).

Reference to Eq. (22) indicates that the denominator has a zero at a Mach number equal to unity since

$$\left[\left(\frac{1}{\gamma M^2} - 1\right) c_{p_{Mix}} + R_g\right]_{M=1} =$$

$$c_{p_{Mix}}\left[\frac{1-\gamma M^2}{\gamma M^2} + \frac{R_g}{c_{p_{Mix}}}\right]_{M=1} =$$

$$c_{p_{Mix}}\left[\frac{(1-\gamma M^2)}{\gamma M^2} - \left(\frac{1-\gamma}{\gamma}\right)\right]_{M=1} = 0 . \qquad (49)$$

But $(dT/dx)_{M=1}$ must remain finite and non-zero. We may therefore conclude that the numerator of Eq. (22) has the value zero for $M < 1$ for a mass flow rate less than m_c, i.e., $dT/dx = 0$ at some location x upstream of the throat. Similarly, it may be seen that the numerator equals zero for $M > 1$ for a mass flow rate which is larger than m_c, i.e., $dT/dx \rightarrow -\infty$. Hence, we may locate the correct mass flow rate by calculating from the nozzle entrance position downstream to the throat region with a chosen value for m; then, by comparing the results with the criteria stated above, it is possible to make new and better estimates for the mass flow rate; etc. This trial and error procedure was repeated until sufficiently accurate values had been obtained for m slightly larger and slightly smaller than m_c. Next we plotted T, ε, dT/dx, and $d\varepsilon/dx$ (see Figs. 10 to 13) as functions of x near the throat. It seems physically plausible to require that T, ε, dT/dx, and $d\varepsilon/dx$ shall be smooth, continuous functions of x; this hypothesis led us to the conclusion that smooth curves should be drawn for T and ε through the throat region. In practice, we introduced "jump conditions" in order to avoid difficulties, since we would need to know m_c to very many significant figures before the computor would yield meaningful data in the vicinity of the nozzle throat. Reference to Figs. 10 to 13 shows that it is possible to determine ε and T quite accurately through the requirements that T, ε, dT/dx, and $d\varepsilon/dx$ shall be continuous functions of x. We expect that the introduction of "jump conditions" has led to very small errors in the final computed results. From the figures we observe that M=1 occurs downstream of the nozzle throat in accord with

our earlier expectations based on an analysis of Eq. (35).

Complete solutions were obtained also for frozen flow and for equilibrium flow. The results of the computations are also plotted on Figs. 3 to 8.

V. RESULTS

The results calculated using the approximate equations and the exact equations are plotted in Figs. 3 to 8. It is apparent from Fig. 3 that ε_4 is in close agreement with the results of the "exact" machine computations. Comparison of our results with those calculated by Krieger shows that differences of order of a few percent exist presumably because Krieger assumed erroneously that the expansion was isentropic.

In so far as comparisons between the "exact" calculations and our iteration procedure are concerned, we note the following conclusions. Reference to Fig. 5 shows that the plots of M_2^2 vs. x and M^2_{exact} vs. x are very nearly identical at the larger value of x. The small pressure discrepancies (primarily at small values of x) shown in Fig. 7 are attributed to small errors in Mach number and the use of a constant γ. The temperature profile shown in Fig. 8 is also fairly close to the exact profile, but does not appear to converge to it. We are inclined to attribute this fact and any remaining discrepancies to the approximations implicit in our use of constant values for γ and $\bar{c}_p$. We probably could have obtained better agreement if we had computed γ and $\bar{c}_p$ as functions of x after determining ε and T from the zeroth approximation, and then used these values in the higher order iterations, etc.

VI. CONCLUSIONS

Our iteration procedure for describing recombination reactions during nozzle flow should be useful for high-energy propellant systems because the easily derived zeroth approximation constitutes a fair representation to the actual profiles of $\mathcal{E}$, M, p, and T (see Figs. 3, 5, 7, and 8) in deLaval nozzles. The higher order iterations converge relatively slowly and are obtainable only at the expense of considerable computational effort. For this reason, we are inclined to regard the present procedure as a useful supplement to the other flow criteria although precise solutions of the nozzle flow problem with chemical reactions require machine computations.

The use of an isentropic flow assumption by Krieger[6] introduced errors of approximately five percent in the results obtained from his machine computations.

PART 2. EXPERIMENTAL STUDIES ON DROPLET BURNING

I. INTRODUCTION

The combustion of sprays is of great practical importance in the design and use of liquid-propellant rocket engines, gas turbines, diesel engines, etc. Theoretical and experimental studies[20-24] on the burning of single fuel droplets and of multiple arrays of fuel droplets have been performed with the hope of obtaining basic information that might be utilized in describing spray combustion. Most of the experimental studies[20, 21, 22, 24] have been carried out with droplets suspended from fine quartz fibers and burning in an oxidizing atmosphere. These studies have shown that the square of the droplet diameter (D^2) decreases linearly with time (t), viz.,

$$D^2 = D_o^2 - K't, \tag{50}$$

where D_o is the initial droplet diameter and K' is called the (effective) evaporation constant. The quantity K' is a convenient parameter for comparing burning rates of different fuels for arbitrary droplet sizes. An approximate theoretical prediction of mass burning rate for single droplets may be obtained on the assumption that mass transport by diffusion to the flame surface and heat conduction to the burning droplet control the burning rate.[5, 23]

Williams[24] has developed a comprehensive theory of spray combustion and has shown that the numerical value of the evaporation constant determined from studies of single droplets has a direct bearing on the

overall combustion rate of sprays. This last conclusion is underscored by some recent successes in correlating the performance of liquid fuel rocket engines with diffusion-flame theories.

In view of the importance of the evaporation constant for spray burning, it is of obvious interest to obtain basic data on fuels such as RP-1, UDMH and N_2H_4 burning in air and in oxygen. As a first step in this program, we have measured the effective evaporation constants for these propellants in air and in oxygen at room temperature. The procedure used and the results obtained are described in Section II.

Since little is known of the manner in which a flame propagates through a fuel spray, a study was carried out on a one-dimensional array in order to determine the factors that influence the rate of flame transfer between adjacent droplets in one-dimensional arrays. Only natural convection occurred in these studies and care has been taken to eliminate all extraneous effects as far as possible. Hence the results obtained are not truly representative of the high turbulence conditions existing within a combustion chamber. The two main objectives were the measurement of flame propagation velocities for a range of droplet diameters and spacings, and the examination of the mechanism of flame transfer from one droplet to the next. The procedure and results are described in Section III.

II. EVAPORATION CONSTANTS FOR RP-1, UDMH AND N_2H_4 BURNING IN AIR AND IN OXYGEN*

A. Apparatus and Experimental Procedure

The apparatus which was assembled to obtain the effective evaporation constants for RP-1, UDMH and N_2H_4 is shown schematically in Fig. 14. The droplets were suspended on a quartz fiber (stem diameter = 0.025, head diameter = 0.04) which was secured to a metal rod. A ball bearing of known diameter, silver-soldered to a wire and attached to the metal rod, provided a suitable reference dimension on the film for determining the actual size of the droplets.

Droplets of fuel were suspended from the quartz fiber by depositing the fuel onto the fiber with a CaLab micro syringe which permitted fuel dispersal accurate to 0.00003 ml. The droplets were ignited with a match for the experiments conducted in air, whereas for the experiments conducted in oxygen a Tesla coil was discharged across the droplet to the ball bearing.

The droplets were contained in a lucite flow chamber for the experiments in oxygen. Oxygen was fed into the flow chamber under a positive pressure of 6 psig. The chamber was provided with an orifice plate having holes with diameters of 5/64 in and a series of screens was used to insure nearly uniform oxygen flow velocities across the chamber.

The operating procedure for the oxygen experiments using RP-1 as fuel involved suspension of the droplet followed by flushing of the flow

* Supported under contract through Rocketdyne Division, North American Aviation Corporation, Canoga Park, Calif.

chamber for 3.5 min, a quiescent period of 0.5 min, and ignition through the use of the Tesla coil. The procedure for burning UDMH and N_2H_4 involved flushing of the flow chamber for two minutes, suspension of the droplets (since these droplets evaporated more rapidly), and then burning. Gas samples from the lucite chamber were absorbed in an alkaline solution of pyrogallic acid and analyzed; these tests proved that the ambient gases in the chamber were practically pure oxygen under our operating conditions.

An Arriflex 35 mm movie camera was used for photographing the burning droplets while they were illuminated from the back with a bright light. An adapter tube and telephoto lens were used in order to obtain large images on each frame of the film. A stroboscope giving 3.75 flashes per second served as a time standard. The light from the stroboscope produced dark images on both the liquid drop and the reference sphere. The camera speeds were adjusted to 22.5 and 28.8 frames per second, respectively, for the air and oxygen experiments, with a precision of approximately three percent. The film was read with a microfilm reader and a millimeter scale. The maximum measured horizontal dimension of the burning droplets was used to calculate D^2 as a function of time.

B. Results

The experimentally determined D^2 (cm^2) vs. t (sec) curves for the experiments performed in air are shown in Figs. 16 to 18 together with the straight lines from which the constants K' were computed.

The RP-1 droplets changed their shape during burning and became pear-shaped. The magnitude of this effect may be estimated by reference to Table I where the ratio of droplet diameter to droplet length is listed according to definitions implicit in the sketch shown in Fig. 15. As burning progressed, the RP-1 droplets became more nearly spherical. For this reason, it appeared preferable to use the terminal stages of burning for the determination of K' in air (see Fig. 16). Our "best value" for K'_{RP-1} is about 0.0078 cm^2/sec and this value is clearly larger than the value which would have been obtained if data points during the initial burning process had been used.

In Fig. 17 we show our results for UDMH burning in air. As burning progresses, the D^2 vs. t curves become less steep because the droplets are largely consumed and significant heat losses occur to the supports. We find $(K'_{UDMH})_{air} \simeq 0.011(4)$ cm^2/sec.

In Fig. 18 we have plotted D^2 vs. t for N_2H_4 burning in air. During the terminal stages of burning, the droplets tended to become abruptly ellipsoidal with an increase in burning rate. This phenomenon is not understood. We estimate $(K'_{N_2H_4})_{air} \simeq 0.016(6)$ cm^2/sec.

The experimentally determined D^2 (cm^2) vs. t (sec) curves for the experiments performed in oxygen are shown in Figs. 19 to 21 together with the straight lines from which the evaporation constants K' were computed. In general, all the curves have relatively small slopes initially. This behavior is probably associated with heat transfer to the quartz fiber during the ignition (i.e., pre-steady state) period. The observed variations during the ignition period reflect, in part, the fact

Table I. Representative experimental results obtained for RP-1 burning in air.

Frame No.	D (cm)	D^2 (cm^2)	$D_o^2-D^2$, cm^2	D/L
0	.193	.0373	.0000	0.60
6	.192	.0368	.0005	0.63
12	.189	.0358	.0015	0.63
18	.184	.0340	.0033	0.64
24	.182	.0332	.0041	0.65
30	.178	.0317	.0056	0.66
36	.174	.0304	.0069	0.68
42	.169	.0285	.0088	0.70
48	.161	.0259	.0114	0.71
54	.154	.0238	.0135	0.76
60	.148	.0219	.0154	0.80
66	.138	.0191	.0182	0.86

that the origin at t = 0 is not necessarily chosen in the same manner in successive tests. The film was not read during the terminal stages of burning because the droplets tended to become distorted.

The RP-1 droplets burning in oxygen showed marked oscillation between various ellipsoidal shapes after ignition (cf. Table II). This phenomenon may be partly responsible for the discrepancies between the observed results ($K' = 0.0107$ to 0.0150 cm^2/sec). In the tests with RP-1, the flame was very bright, presumably because of carbon formation. The tests using RP-1 were difficult to perform because the droplets tended to fall off the quartz fibers during the ignition period.

We find that K' equals approximately 0.030 and 0.036 cm^2/sec, respectively, for UDMH and N_2H_4 droplets burning in oxygen.

C. Discussion and Conclusions

The values obtained for the (effective) evaporation constants for burning in air and in oxygen are summarized in Table III.

Reference to Table III shows that the observed values of K' are nearly doubled or tripled when the oxygen concentration is increased from about 20 percent to 100 percent. The largest relative change in K' was observed for UDMH (from 0.011 to 0.030 cm^2/sec) and the smallest relative change for RP-1 (from 0.0078 to 0.011-0.015 cm^2/sec). If the combustion processes in rocket engines using LOX as oxidizer are controlled by mass-transfer rates, then the present results suggest appreciably smaller burning times for N_2H_4 and UDMH than for RP-1. Oscillatory combustion of RP-1 may possibly be associated with

Table II. Representative length measurements on burning RP-1 droplets which illustrate droplet oscillations between various ellipsoidal shapes.

Frame No.	Maximum diameter (in arbitrary units)	Maximum length (in arbitrary units)	Frame No.	Maximum diameter (in arbitrary units)	Maximum length (in arbitrary units)
0	94	174	21	88	137
1	93	182	22	89	135
2	94	170	23	88	135
3	98	146	24	86	134
4	94	161	25	85.5	131
5	94	157	26	87	130
6	96.5	149	27	86	128
7	94	158	28	86	125
8	97	144	29	84.5	125
9	93.5	152	30	84	123
10	96	142	31	84	121
11	92.5	150	32	83	118
12	95.5	142	33	82	118
13	92	147	34	81	116
14	92.5	140	35	80	115
15	91.5	142	36	80	114
16	91.5	143	37	78.8	112
17	91.5	140	38	78	110
18	90	140	39	76	108
19	89.5	139	40	75	105
20	89	138	41	73	103
			42	72	100

Table III. Summary of measured evaporation constants for RP-1, UDMH and N_2H_4 burning in air and oxygen.

	RP-1	UDMH	N_2H_4
K' (cm^2/sec) for burning in air	0.0078	0.011(4)	0.016(6)
K' (cm^2/sec) for burning in oxygen	0.011-0.015	0.030	0.035

selective fractionation of the fuel constituents which, in turn, may conceivably bear some relation to instabilities in engine performance.

III. FLAME PROPAGATION IN LIQUID-FUEL DROPLET ARRAYS

A. Apparatus and Experimental Procedure

The apparatus which was assembled to measure the rate of flame propagation between adjacent droplets and to study the mechanism of ignition is shown schematically in Fig. 22. The experimental arrangement involved essentially a horizontal, one-dimensional array of fibers with suspended droplets, a schlieren system,[26] and a high speed camera.

The droplet array was formed by suspending fuel droplets on quartz fibers that were attached to a lucite locating fixture. The quartz fibers had head diameters that were maintained at 0.0395 ± 0.0005 in to help insure uniform droplet size. Furthermore, the stem diameters were controlled at 0.016 ± 0.003 in in order to minimize variations in the heat capacities of the fibers. The lucite fixture was constructed by milling parallel grooves with spatial separations of 0.175, 0.200, 0.225 and 0.250 in on a piece of lucite. The separation between grooves was accurate to within ± 0.001 in. A jig was devised and used when installing the quartz fibers on the locating fixture to assure accurate horizontal alignment of the fiber heads. The fibers were then secured in position. The holding fixture was arranged properly within the optical system with the fibers inclined at angles of approximately 45° with respect to the vertical. This procedure minimized heat absorption by the stem and distortion of the droplet shape. A lucite box was placed around the array of fibers to prevent extraneous convection currents that might be caused by air currents in the room.

The schlieren system involved the usual elements mounted on a rigid angle-iron framework. A Bausch and Lomb mechanical feed carbon arc lamp served as a primary source. The light emitted by the crater on the positive electrode was focused by means of a condensing lens on a vertical slit that was constructed from razor blades. The vertical slit served as an effective line source. The effective source was located at the focal plane of a 6 in parabolic mirror (42 in focal length) and hence the light reflected by mirror was very nearly parallel. The beam of parallel light passed through the test section (i.e., the location of the one-dimensional array) and was then reflected and focused by a second 6 in parabolic mirror. An adjustable knife edge, constructed from a common wood plane, was located at the focal plane of the second mirror since an image of the effective source existed at that plane. The knife edge was adjusted to obtain maximum definition of the density gradients consistent with the illumination and the film speed that were available. The test section was mounted so that the focus of the working system (i.e., the secondary light system) was at a convenient location with respect to the other components. The image of the array was then focused by means of an objective field lens on the film in the camera. A film plate holder from a Speed-Graphic camera was installed in the system at the focus of the working section to provide provisions for taking still photographs of the droplet array. A shutter assembly from a camera was mounted near the knife edge to attain proper exposure times.

An Eastman Kodak 16 mm high speed camera was positioned in the system to photograph the flame propagation across the arrays of fuel

droplets. A rheostat, which was incorporated in the camera, was used for the purpose of adjusting the framing speeds. Normally, from 200 to 400 frames per second were used. A neon timing light in the camera put 120 timing marks per second on the edge of the film and served as a time standard. Dupont Superior 4 film was used in all of the experiments.

All of the measurements were performed on Phillips research grade normal octane. This fuel was selected because it is readily available, its volatility is low, and the surface tension is sufficiently high to maintain the droplet shape during burning.

The droplets of fuel were suspended from the fibers by depositing fuel onto each fiber with a CaLab micro syringe, which permitted fluid dispersal accurate to about ± 0.00003 ml. The droplets were suspended in succession from the end at which ignition occurred. The total time involved in preparing the experiment was about one to two minutes, of which considerably less than a minute was required to load the portion of the array that was photographed (6 to 8 fibers, depending on the spatial separation). Droplet evaporation during the preparation time was negligibly small (see below). Droplets of 0.003, 0.004, 0.005 and 0.006 ml volume were used in the course of the experiments; with the accuracy of dispersal stated above, the volumes of the droplets agreed within ± 1 percent.

Ignition of the droplet array was initiated by loading the first fiber (a wire with a loop at the end, which acted as one pole of a spark gap) with ether and igniting the ether droplet with a spark generated by means

of an automotive ignition system.

The flame propagation time from one droplet to the next was obtained by reading the film on a microfilm reader. In particular, the time required for ignition was estimated by counting the number of timing marks on the edge of the film between the ignition times for adjacent droplets. The process of "ignition" occurred in a very short period of time and was characterized by the very rapid symmetric development of the heated-gas region as seen on a schlieren photograph.

The immersion depth, which is defined as the minimum depth to which the unburned droplet is immersed in the hot-gas region of the adjacent burning droplet (see Fig. 23), was measured with a millimeter scale from an enlarged image produced on a screen with a Bell and Howell 16 mm time and motion projector. Also the maximum horizontal dimensions and the approximate lengths of the droplets were measured. These measurements were probably accurate only to ± 5 percent because of insufficient resolution on the film. The total distance across the photographed portion of the array provided a suitable standard dimension.

Observations of the projected image indicated that the droplets as suspended from the fibers were not accurately spherical; this was especially true of the larger droplets. The calculated diameters (including the volume of the fiber heads), assuming that the droplets were spherical in shape, were 0.0745, 0.0810, 0.0865 and 0.0914 in for the droplets containing 0.003, 0.004, 0.005 and 0.006 ml, respectively. In Table IV we have indicated that the maximum horizontal dimensions, averaged over the photographed portion of the array, were somewhat

smaller than the calculated values; the discrepancies probably result from the non-spherical shapes of the droplets.

The effective evaporation constants in room temperature (approximately $75^{\circ}F$) of the non-burning droplets were determined by taking still photographs of a droplet at 1/2 minute intervals. The diameter of a droplet was measured using a long focal length lens assembly. The effective evaporation constant was found to be 9.7×10^{-6} in^2/sec (see Fig. 24). Thus for a droplet with an initial diameter equal to 0.08 in., the diameter decreased by somewhat less than 5 percent in one minute.

Tests were performed for each of the four different droplet spacings with droplets having four different volumes initially. The normal procedure involved fixing the fibers at a given spatial separation, then performing several runs with a given initial volume, then with another initial volume, etc.

B. Experimental Results and Discussion

Representative results for the flame propagation time from one droplet to the next ($\equiv \tau_D$) are shown in Figs. 25 through 27. These results indicate that the scatter becomes larger as the spacing between droplets is increased. Most of the scatter is probably associated with small differences in the actual spacings at the droplets; direct observation of the projected images of the arrays indicated that the spatial separation varied by as much as ± 5 percent. Since the grooves of the holding fixture were defined within ± 0.001 in, the differences in spacing were probably caused by slight bending of the fibers. However, reasonable results should be obtained by averaging over a section of the

droplet array. The measured immersion depths were similarly averaged. The results are summarized in Table IV.

In Fig. 28 we have plotted the propagation time per droplet τ_D as a function of droplet spacing for each of the initial droplet volumes used in our experiments. The results of all of the tests have been averaged arithmetically. It is interesting to observe that the propagation time was essentially independent of the droplet size for the smallest droplet spacing and that, as the spacing increased the propagation time increased relatively faster for the smaller droplets. These results indicate that the time delay is dependent on the droplet size for a given spacing. Further examination of the results show that the propagation time is not proportional either to a power of droplet spacing or droplet size.

From a close examination of the photographs, it is possible to construct a picture for the mechanism of flame transfer. The results are illustrated schematically in Fig. 29 for a droplet spacing of 0.20 in. After a given droplet has ignited and is burning stably, it is surrounded by a luminous flame and hot gases. At some distance from the flame a very marked density and temperature gradient occurs that defines the extent of the hot-gas zone (see Fig. 29). Representative schlieren photographs defining the sharp density gradient are shown in Fig. 30. The uniform exposure of the film within the hot-gas zone indicates that a nearly constant density gradient exists until near the flame surface. This observation suggests that the temperature varies inversely with distance from the flame surface to the edge of the hot-gas zone.

Table IV. Experimental results for flame propagation in a droplet array.

Run No.	Nominal droplet spacing in inches	Nominal droplet volume, in ml	Average droplet diameter in inches	Average droplet height, in inches	Average propagation time τ_D, sec	Average immersion depth in inches
7	.200	.005	.0725	.0886	.1165	.1101
8	.200	.005	.0742	.0876	.0958	.1119
9	.200	.005	.0749	.0866	.0869	.1127
10	.200	.005	.0737	.0880	.1081	.1077
11	.200	.005	.0751	.0876	.0936	.1127
12	.200	.004	.0713	.0798	.1057	.1126
13	.200	.004	.0679	.0802	.0999	.1110
14	.200	.004	.0653	.0756	.1037	.1088
15	.200	.004	.0675	.0796	.0918	.1127
16	.200	.006	.0747	.0952	.0812	.1269
17	.200	.006	.0739	.0952	.0817	.1237
18	.200	.006	.0761	.0984	.0973	.1193
19	.200	.006	.0755	.0952	.0928	.1116
20	.200	.003	.0637	.0719	.0948	.1077
21	.200	.003	.0631	.0719	.1138	.1164
22	.200	.003	.0639	.0733	.1094	.1107
23	.200	.003	.0635	.0743	.1104	.1017
24	.200	.003	.0647	.0750	.1156	.1155
26	.200	.005	.0738	.0866	.0859	.1193
27	.200	.005	.0751	.0889	.0896	.1210
28	.200	.005	.0736	.0883	.0943	.1237
29	.175	.005	.0737	.0880	.0666	.1513
30	.175	.005	.0740	.0888	.0775	.1484
31	.175	.005	.0740	.0873	.0666	.1506
32	.175	.005	.0738	.0862	.0633	.1516
33	.175	.005	.0744	.0873	.0658	.1484
34	.175	.005	.0734	.0873	.0720	.1488
35	.175	.004	.0709	.0786	.0612	.1480
36	.175	.004	.0711	.0793	.0887	.1257
37	.175	.004	.0699	.0771	.0683	.1442
38	.175	.004	.0706	.0786	.0614	.1516
39	.175	.004	.0691	.0771	.0699	.1520
40	.175	.004	.0707	.0771	.0699	.1563
41	.175	.003	.0648	.0698	.0683	.1504
42	.175	.003	.0638	.0727	.0683	.1448
43	.175	.003	.0631	.0698	.0716	.1412
44	.175	.003	.0644	.0742	.0650	.1490
45	.175	.003	.0639	.0727	.0691	.1591
46	.175	.003	.0634	.0727	.0641	.1451
48	.175	.006	.0769	.1006	.0670	.1765
49	.175	.006	.0773	.0967	.0683	.1744
50	.175	.006	.0773	.0970	.0733	.1690

Table IV (cont.)

Run No.	Nominal droplet spacing in inches	Nominal droplet volume, ml	Average droplet diameter in inches	Average droplet height, in inches	Average propagation time τ_D, sec	Average immersion depth in inches
51	.175	.006	.0763	.0999	.0683	.1764
52	.175	.006	.0774	.0977	.0741	.1685
53	.175	.006	.0776	.0977	.0650	.1773
54	.225	.005	.0714	.0840	.1570	.0870
55	.225	.005	.0700	.0840	.1667	.0879
56	.225	.005	.0715	.0840	.1493	.0922
57	.225	.005	.0697	.0860	.1598	.0916
58	.225	.005	.0710	.0880	.1640	.0957
59	.225	.005	.0707	.0880	.1542	.0925
60	.225	.004	.0673	.0798	.1850	.0896
61	.225	.004	.0663	.0798	.1825	.0866
62	.225	.004	.0663	.0798	.1940	.0884
63	.225	.004	.0669	.0798	.1970	.0838
65	.225	.003	.0608	.0724	.2063	.0759
66	.225	.003	.0610	.0693	.1951	.0745
67	.225	.003	.0608	.0714	.1825	.0751
68	.225	.003	.0604	.0714	.2369	.0695
69	.225	.006	.0748	.0945	.1441	.0966
70	.225	.006	.0772	.0966	.1471	.0992
71	.225	.006	.0753	.0955	.1613	.0985
72	.225	.006	.0760	.0997	.1377	.0989
73	.225	.006	.0786	.1008	.1375	.0970
74	.225	.005	.0749	.0987	.1621	.1031
75	.225	.005	.0753	.0955	.1468	.1026
76	.225	.005	.0744	.0934	.1266	.0991
77	.225	.005	.0734	.0924	.1641	.0996
78	.250	.005	.0736	.0916	.317	.0509
79	.250	.005	.0717	.0933	.5194	.0399
80	.250	.006	.0777	.0999	.261	.0613
81	.250	.006	.0777	.0989	.3054	.0470
82	.250	.004	.0675	.0812	.4820	.0277
84	.250	.003	.0628	.0760	.1101	.0213

Similar results were obtained previously for single droplets by Kumagai and Isoda.[27] A schematic diagram of the resulting temperature profile is shown in Fig. 31.

Since the hot-gas zone as defined by the schlieren photographs has approximately constant dimensions for a given droplet size, it appears that prior to ignition the unburnt droplet will be immersed in the hot-gas zone to a varying depth depending on the droplet spacing. Since the temperature increases as the depth of immersion increases, it follows that the rate of evaporation of the unburnt droplet will also vary. Convection currents within the hot-gas zone transport the fuel vapor upward and the fuel vapor will eventually mix with the hot combustion products and with the surrounding ambient atmosphere. When the fuel vapor concentration is sufficiently high and the mixture is sufficiently hot, ignition will occur in the region above the unburnt droplet and the flame then propagates downward and sideways around the droplet. The flame finally stabilizes at the steady-state configuration and the ignition cycle is repeated.

The specified mechanism suggests that the propagation time τ_D is dependent on both the droplet size and spacing and that a quantitative measure for τ_D should be obtainable in terms of immersion depth. In Fig. 32 we have plotted the logarithm of the average immersion depth as a function of the logarithm of the propagation time τ_D. A least squares fit[19] to the data indicates that

$$\tau_D(\text{immersion depth})^{1.5} = \text{constant}. \qquad (51)$$

It is probable that most of the scatter in the data is the result of erroneous measurements of the immersion depth rather than of errors in the

estimate of the propagation time. However, the scatter of the points surrounding the best curve is actually not very large and it may therefore be concluded that the immersion depth provides a reasonable criterion for estimating flame propagation rates between droplets. This idea may be useful for application in spray combustion theories.

PART 3. RADIATION AND BURNING VELOCITY STUDIES ON PROPANE-OXYGEN-NITROGEN MIXTURES

I. INTRODUCTION

The authors of several published papers have used the ratios of apparent peak intensities of two rotational lines belonging to different emitters (e.g., CH and C_2) as a measure of the mixture ratio in hydrocarbon flames. The procedure involves first the determination of the spectral intensity as a function of equivalence ratio (actual moles of fuel per mole of oxygen divided by the moles of fuel per mole of oxygen for the stoichiometric mixture ratio) using a known fuel-air input to a laminar flame. Then, using a calibration curve obtained in this manner for a given fuel-oxidizer system, the spectral intensity ratios are employed, in turn, to determine local equivalence ratios in turbulent flames, reverse-jet flames, etc.

Clark[28] found the intensity ratios of C_2 to CH bands to be a good index of the equivalence ratios of flames for a given fuel. He measured intensity ratios in different regions of laminar and turbulent ethylene-air flames and found that the intensity ratios were constant in the laminar flames. Clark and Bittker[29] found that the radiation per unit area of a laminar flame depends only on the equivalence ratio. They proposed to use this result for the measurement of burning velocities. John and Summerfield[30] have shown that the relative changes of C_2 and CH intensity for a turbulent flame (propane-air) enclosed in a duct are nearly equal, and hence turbulence did not alter appreciably the correlation of the spectral intensity ratio with equivalence ratio. In several studies

dealing with flame stabilization, the spectral intensity ratio method has been used.[31, 32, 33] Fuhs[33] has used the result that the apparent intensity (assuming that the population temperature and the effective temperature in the formula for the line radiancy are equal) from optically thin gases, observed with a spectroscope having a slit width large compared to the line width, is proportional to the ratio of the population of emitters in the excited states.

The radiation from C_2 and CH in flames is probably not of thermal origin but rather is the result of chemical reactions which produce molecules in excited states (chemiluminescence). In laminar flames, the C_2 and CH radiation occurs predominantly in the inner cone; it is unlikely that self-absorption affects the measurements of intensity for C_2 and CH emitters.[34, 35]

In the work using the spectral intensity method discussed earlier, the investigators have stated or assumed, without convincing proof, that the spectral intensity ratio is a function only of the local equivalence ratio for a given fuel-oxidizer system. The prime objective of the present studies was to see if this assumption is indeed correct. It was decided to determine the effect of various amounts of inert diluent on the spectral intensity ratio as a function of equivalence ratio. A propane-oxygen-nitrogen system was used. Chemically pure propane was selected because it had been used in some of the studies mentioned earlier in this discussion. By varying the amount of inert diluent, the adiabatic flame temperature is changed appreciably; hence our results should provide

some information concerning the effect of temperature on the spectral intensity method.

The laminar burning velocities for propane-oxygen-nitrogen mixtures were also measured in order to serve as an additional check for comparing our results with those of other investigators. The burning velocity is defined as the normal rate of propagation of the flame front into the initial combustible mixture.[36] The angle method and the area method are commonly used to determine the burning velocity of stationary laminar flames on cylindrical burners. The burning velocity, as determined by the area method, is equal to the volume flow rate of the mixture divided by the area of the inner cone surface of the flame. The area method gives a burning velocity that is averaged over the total flame surface. Since a considerable fraction of the total surface of the cone lies close to the burner rim, cooling undoubtedly lowers the burning velocity; on the other hand, the gas near the tip is heated from all sides of the cone, thus increasing the burning velocity in this region.[37]

The angle method consists of drawing tangents to the straight portion of the inner cone (the region where the tip and base effects are negligible). The laminar burning velocity is found by using the relation $V_b = V_m \sin \alpha$,[37] where V_b equals the burning velocity, V_m is the average velocity in the burner tube, and α is the half angle of the inner cone (obtained from the tangent data). The accuracy of this method depends on how closely the following assumptions apply to the flame studied:[36] (1) the divergence of the gas stream from the axial direction between the burner port and burning surface is negligible; (2) the nature of the flame reactions in the

straight portion of the cone is nearly constant and is representative of the reaction under study; (3) the flow is laminar; (4) the straight portion of the cone includes the stream tube where the velocity is the average velocity passing through the burner (0.707 times the burner radius); (5) the surface of maximum temperature gradient is parallel to the region defined by the onset of luminosity.

Many variations of the above methods have been used. It is actually debatable as to which method is superior. Comprehensive surveys and extensive references to the published literature on this subject may be found in the books by Lewis and von Elbe,[38] Gaydon and Wolfhard,[39] and Jost[40] as well as in surveys by Poorman,[36] Linnett,[37] and Fiock.[41]

In the studies discussed in this paper, the angle method was used because the apparatus needed was simple and inexpensive and, furthermore, the results obtainable are satisfactory for showing the relative changes of burning velocities with changes of composition.

II. APPARATUS AND EXPERIMENTAL PROCEDURE

The apparatus which was assembled to obtain laminar flames of gas mixtures of known equivalence ratio and percentage of inert diluent content is shown schematically in Fig. 33. Also shown is the optical system used to obtain information needed for a determination of laminar burning velocities. The gases were supplied to the system from standard commercial high-pressure tanks. Chemically pure propane, oil-pumped nitrogen, and extra-dry-grade oxygen were the gases used in all experiments. The gas pressure was reduced by a high-pressure regulator and an accurate low-pressure regulator connected in series in each line. Pressure gauges, sensitive to about 1/16 psig, were attached downstream of each low-pressure regulator.

Fischer and Porter precision bore metering tubes with ball-type floats were used to meter the gases. These rotameters deliver within ± 2 percent of the calibrated flow, except near the limits of their respective operating ranges. The flow rate of each gas was controlled by a needle valve placed downstream of the rotameter in each line.

Each gas line was tapped into the upstream end of a mixing chamber, which consisted of a steel pipe about 2.5 inches in diameter and 24 inches long, capped at each end. The chamber was filled with small tubular glass beads to promote mixing and also to make the chamber an effective flashback arrester. It was concluded that good mixing was achieved since the observed flames were steady and reproducible. Copper tubing was used to connect the outlet from the downstream end of the mixing chamber to the burner.

The burners used for the studies were hard copper tubing with inside diameters of 1.012, 0.704, and 0.386 cm. The burners of various inside diameters were needed to achieve laminar flow and reasonable flow rates, and to keep the quenching effect of the burner to a minimum for the large number of mixtures of gases used during the studies.

An objective lens system from a motion picture camera was used to magnify and project the image of the inner cone of the flame onto a ground-glass screen. A plane mirror was used in the system to place the image on a horizontal surface for ease in tracing the outline of the inner cone image. A magnification of about 4:1 was used. The system was aligned and focused by placing an illuminated square grid network in the plane of the flame cone. Then the system was adjusted to obtain a clear magnified image of identical vertical and horizontal proportions of the grid network on the ground glass screen. Originally a double-convex lens was used in the system but pincushion distortion was found to be severe. With the final system it is estimated that errors in optical alignment could not contribute an error of more than 1 percent to the measured value of the burning velocity.

Figure 34 shows schematically the experimental equipment that was used to obtain the data needed to compute the spectral intensity ratios. A Jarrell Ash spectroscope with an f-number of 6.5 and a linear dispersion of 18 Å/mm was used. An RCA 1P28 photomultiplier tube (glass) located at the exit slit of the spectroscope served as a detector. The spectra were recorded on a Leeds and Northrup Speedomax Recorder. The voltage input to the photomultiplier tube was maintained constant

and relatively low throughout all of the experiments. By using this method, a lower noise level was achieved and, furthermore, the output current of the photomultiplier was kept low, thus helping to avoid the difficulties associated with fatigue of the photomultiplier tube.[42] The output of the photomultiplier tube was amplified and then fed to the recorder unit. A given spectral intensity ratio varied by less than 2 percent with different amplifications; this discrepancy was smaller than the lack of reproducibility (5 percent) observed when identical tests were conducted on different days.

An image of the inner cone was formed on the slit of the spectroscope by suitable adjustment of the condensing lens. The slit was masked to prevent radiation from the tip and base of the inner cone from entering the spectroscope. Also the slit was located so that radiation from the edge (or leg) of the cone did not enter the spectroscope because it was found the spectral intensity ratio from the edge increased, remained the same, or decreased, depending on the specific fuel-oxygen-nitrogen mixture. This effect may be understood in terms of the relative positions of the radicals in the reaction zone.[43, 44, 45] Spectral intensity ratios determined from any part of the straight portion of the inner cone (excluding the cone edge) were the same for identical fuel-oxygen-nitrogen input to the flame. In all tests, the axis of the inner cone image was placed on the slit and a slit width of several hundred microns was used. The spectral intensity ratio was found to be independent of the monochromator scanning speed, for all practical purposes. A scanning rate of 50 Å/min was used to get sufficient line detail and still not make the time required to get the desired spectral regions prohibitively long.

The following rotational lines were selected for the computation of spectral intensity ratios:

Wavelength, Å	Transitions	Emitter
5165	$^3\Pi \rightarrow {}^3\Pi$ (0, 0)	C_2
4737	$^3\Pi \rightarrow {}^3\Pi$ (1, 0)	C_2
4324	$^2\Delta - {}^2\Pi$ (0, 0)	CH
4312	$^2\Delta - {}^2\Pi$ (0, 0)	CH

These lines were selected because they are well isolated; furthermore, the spectral intensity ratios of several combinations of lines could be compared. For a given equivalence ratio, the spectral intensity ratios based on the stronger lines (5165 Å, 4312 Å) were reproducible to within about 5 percent when using the same rotameters.

All tests were conducted in a darkened room and a flat black screen was used behind the flame. These precautions were taken to reduce scattered light and radiation reflection, stop air movement from disturbing the flame, and make the image of the flame on the ground glass screen distinct. The temperature of the room was at all times between 71 and 75°F while the experiments were in progress.

The procedure followed in the tests involved first the calculation of the necessary flow rates for each gas to obtain a gas mixture of a desired equivalence ratio and a desired percentage of nitrogen (by mass). It turned out to be difficult to obtain a total flow rate of a desired gas mixture such that the flame neither blew off nor flashed back and, at the same time, had a suitable "inner cone". We considered the inner cone

suitable when the straight portion of the cone was large compared to the base and tip sections (this was usually a height/radius ratio of greater than 5 or 6). Flames from gas mixtures of low equivalence ratios and large percentages of nitrogen were very sensitive to blowoff and flashback (a very narrow range of flows could be used), while flames from rich gas mixtures containing large amounts of nitrogen are not very steady (air currents caused slight movements). When a suitable flame was obtained, the radiation entering the slit was scanned with the spectroscope. A wavelength interval on each side of a desired line was taken so that one could determine the magnitude of background continuum (see Fig. 35). The background radiation was always subtracted in measurements of line intensities, thus insuring that only radiation from the desired emitters was used in the calculation of the intensity ratio. This scanning operation was repeated so that one could determine the average height of the lines and determine the amount of variation. Usually the variation was less than 2 percent of the total line height.

Tangents to the image of the inner cone of the flame (see Fig. 36 for a typical image) were drawn on tracing paper. These tangents were drawn parallel to the upstream side of the bright image. Consecutive measurements of the angle between the tangents for the same flame showed a reproducibility of about five percent. This variation would affect the burning velocity reproducibility by the same amount. Attempts to reproduce the burning velocity data on different days resulted in variations as large as 10 percent in some cases.

III. EXPERIMENTAL RESULTS AND DISCUSSION

The results of the experimental studies are presented in Figs. 37 through 44. In Figs. 37 through 44 the spectral intensity ratio (the intensity of a C_2 line divided by the intensity of a CH line) is plotted against the equivalence ratio of the mixture (the actual fuel-oxygen ratio divided by the stoichiometric fuel-oxygen ratio). Curves have been drawn through the points obtained from mixtures containing the same percentages of nitrogen (by mass). Figures 37 through 40 are believed to be more accurate than Figs. 41, 42 and 43 since in the former the lines (5165 Å, 4312 Å) used to determine the spectral intensity ratio are stronger and, therefore, the signal to noise levels were much larger. It was found experimentally that the intensity ratios of the 5165 Å to the 4312 Å lines were reproducible to within about 5 percent on different days, even with different total flow rates, as long as the same diameter burner and the same combination of flowmeters were used. If different combinations of flowmeters were used, the reproducibility was not as good in general. This fact emphasizes the need to use flowmeters with the proper flow range. In this work, the same combination of flowmeters usually proved satisfactory for obtaining all of the needed information for mixtures of a fixed percentage nitrogen content and for a certain burner tube. The reproducibility of the ratios obtained from the weaker lines was found to be poorer.

Figures 37, 38, 41 and 42 show that the maximum intensity ratio occurs at a larger equivalence ratio as the percentage of nitrogen con-

tent is reduced in the gas mixture. Also the maximum intensity ratio of the stronger lines tends to be larger with decreasing inert diluent content while, to a lesser extent, the opposite is observed to be the case for the maximum intensity ratio based on the weaker lines. The curves seem to become flatter with increasing diluent content. Thus it is obvious that, in general, the intensity ratio is a more sensitive function of the equivalence ratio for mixtures containing smaller amounts of nitrogen.

Smaller diameter burner tubes were needed to prevent the flow from becoming turbulent as mixtures containing lower percentages of nitrogen (faster burning) were used. Figures 39 and 43 show the changes in spectral intensity ratio with different burner tubes. The curves for the 0.386 cm burner (60 percent nitrogen) are somewhat higher than the curves for the 0.704 cm burner (60 percent nitrogen). In fact, the curves of 60 percent nitrogen for the 0.386 cm burner are quite similar to the curves of 70 percent nitrogen for the 0.704 cm burner. These changes of intensity ratios with change of burners were probably due to increased quenching with the smaller tube.

The curves on Fig. 40 show that quenching had very little effect when the 0.704 cm tube and 1.012 cm tube were used. The relatively large scatter of the points for the curve obtained with a 1.012 cm tube was due to changes of the initial mixture temperatures of about 11 to 14°F. The larger spectral intensity ratios were found on days when the room temperature was approximately 82 to 85°F, instead of the normal 71 to 75°F room temperature.

Wohl and Welty[46] have studied radiation intensity as a function of position in reaction zones for butane-air flames. They found that the decay of C_2-radiation in a lean flame was very rapid as compared to CH-radiation decay. As they used progressively richer mixtures, the decay rate of C_2-radiation began to approach that of CH radiation. On the basis of these results, they concluded that the reaction between C_2 and O_2 was especially fast. Possibly the shift of the maximums of the curves in Figs. 37, 38, 41 and 42 to richer mixtures with decreasing percentages of nitrogen in our results was partially due to the more intimate contact of the C_2 with O_2, thus promoting fast removal of C_2 from the reaction zone for mixtures of lower equivalence ratios.

Thomas[47] measured the effect of preheating on the C_2 and CH emission from ethylene-air flames of fixed equivalence ratio. His results showed that the ratios of C_2 to CH intensities were functions of the initial mixture temperature. Since preheating and inert diluent content both change the final flame temperature, it is believed that the changes of our curves with amount of inert diluent are largely determined by changes in temperature.

Clark[28, 29] found curves of spectral intensity ratio as a function of equivalence ratio for propane-air flames that are very similar to the curves we found for mixtures containing 70 percent nitrogen (by mass). Clark stated that leveling off at equivalence ratios of approximately 1.3 might be due to the surrounding air mixing with the richer flames, thus causing the actual equivalence ratios to remain near 1.3. The curves on

Figs. 37 and 41 tend to prove the above observation to be false, as the curves for 75 percent and 80 percent nitrogen leveled off at equivalence ratios where there was a surplus of oxygen.

Clark[28] also found that the intensity ratios were constant in different regions of laminar flames. We found changes at the tip, the base, and at the edges of the cone during preliminary tests. We believe that Clark did not find changes because he used a much larger slit width than we did. We minimized this change with position in our results by always looking at a portion of the central axis not containing parts of the flame tip or flame base of the inner cone.

In Fig. 44 the laminar burning velocity (in cm/sec) is plotted as a function of the percentage of inert diluent (nitrogen) by mass. The large scatter of the points obtained from richer mixtures was primarily due to the slight unsteadiness of very rich flames, which made the procedure of drawing tangents to the inner cone inaccurate. Burning velocity data were not taken for lean-mixture flames, since in some cases the flame tended to lift off the burner slightly and the inner cone became flatter. When this happened, the diameter of the base of the cone was larger than the burner diameter, and the angle method was no longer useful. It was impossible to get stable flames from any mixtures containing 90 percent nitrogen. The burning velocities of mixtures containing 80 percent nitrogen were the same for all practical purposes. Hence, it may be assumed that the mixtures containing 80 percent nitrogen are very near the flammability limit.

The use of the angle method for determining burning velocities of relatively slow-burning hydrocarbon flames probably fails to satisfy the requirement that the divergence of the gases from the axial direction between the port and the burning surface be negligible. This and the above mentioned difficulties seem to indicate that it is very difficult to obtain accurate burning velocities of slow-burning hydrocarbon flames over a wide range of equivalence ratios by either the angle method or the total area method. We may conclude that the method used was inaccurate for absolute determination of burning velocities, but was satisfactory for showing the relative change of burning velocities with composition.

IV. CONCLUSIONS

The spectral intensity ratios of C_2 and CH lines from laminar flames were found to be dependent on the percentage of inert diluent and the equivalence ratio of the gas mixtures. The chemical reaction rates producing CH and C_2 are known to be functions of the amount of inert diluent. Our results show that the spectral intensity ratios of CH to C_2 are not unique functions of the mixture ratio but rather of the chemiluminescent processes producing the emitting species. Hence the use of the spectral intensity ratio method for measuring local equivalence ratios in turbulent flames, reverse-jet flames, etc., is questionable.

The burning velocities of nearly stoichiometric mixtures were found to be a more sensitive function of the amount of inert diluent than of rich mixtures.

REFERENCES

1. S. S. Penner and D. Altman, J. Franklin Institute 245, 42 (1948).

2. D. Altman and S. S. Penner, J. Chem. Phys. 17, 56 (1949).

3. S. S. Penner, J. Franklin Institute 249, 441 (1950).

4. S. S. Penner, J. Chem. Phys. 19, 877 (1951).

5. S. S. Penner, Chemistry Problems in Jet Propulsion, Pergamon Press, London 1957.

6. F. J. Krieger, J. American Rocket Society 21, 179 (1952).

7. S. P. Heims, NACA TN No. 4144, Washington, D.C., January 1958.

8. K.M.C. Bray, Aeronautical Research Council Paper 19, 983, March 1958.

9. M. J. Lighthill, J. Fluid Mechanics 2, (1957).

10. P. P. Wegener, Progress Report No. 20-388, Jet Propulsion Laboratory, California Institute of Technology, Pasadena, Calif., June 1959.

11. D. L. Bunker and N. Davidson, J. Amer. Chem. Soc. 80, 5085 (1958).

12. G. Porter and J. A. Smith, "The Recombination of Atoms", ASTIA Document No. 211443, December 1958.

13. M. Carmac, J. Keck and C. Petty, "Relaxation Phenomena in Air Between 3000 and 8000°K", AVCO Research Report 22, Everett (Mass.) 1958.

14. NBS Circular 500, "Selected Values of Chemical Thermodynamic Properties", February 1952.

15. B. T. Chu, Wright Air Development Center TN-57-213, Dayton (Ohio), May 1957.

16. J. G. Kirkwood and W. W. Wood, J. Chem. Phys. 22, 1915 (1954); 25, 1276 (1956).

17. F.B. Hildebrand, Introduction to Numerical Analysis, McGraw-Hill Book Company, New York 1956.

18. IBM 709 Fortran Reference Manual, 1959, International Business Machine Corporation, 590 Madison Avenue, New York 52, New York.

19. W. E. Milne, Numerical Calculus, Princeton University Press, Princeton, New Jersey 1949.

20. J. F. Rex, A. E. Fuhs and S. S. Penner, Jet Propulsion 26, 179 (1956).

21. G. A. E. Godsave, Fourth (International) Symposium on Combustion, Williams and Wilkins Company, Baltimore 1952, p. 819.

22. A. R. Hall and J. Diedericksen, Fourth (International) Symposium on Combustion, Williams and Wilkins Company, Baltimore 1952, p. 837.

23. M. Goldsmith and S. S. Penner, Jet Propulsion 24, 245 (1954).

24. M. Goldsmith and C. K. Perkins, "Experiments on the Burning of Single Drops of Fuel in Oxygen-Inert Gas Mixtures", Technical Report No. 4, Contract No. DA 04-495-Ord-446, California Institute of Technology, Pasadena, May 1954.

25. F. A. Williams, Ph.D. Thesis, California Institute of Technology, Pasadena, June 1958.

26. D. W. Holder and R. J. North, Aeronautical Research Council Technical Report No. 2780, 1953.

27. S. Kumagai and H. Isoda, Sixth (International) Symposium on Combustion, Reinhold Publishing Company, New York 1957, p. 726.

28. T. P. Clark, NACA Technical Note 4266, June 1958.

29. T. P. Clark and D. A. Bittker, NACA Research Memorandum E54F29, August 24, 1954.

30. R. R. John and M. Summerfield, Jet Propulsion 27, 169-175, (178-179 (1957).

31. R. R. John, E. S. Wilson and M. Summerfield, Jet Propulsion 25, 535 (1955).

32. E. S. Wilson, R. R. John and M. Summerfield, Jet Propulsion 27, 892-894 (1957).

33. A. E. Fuhs, Ph.D. Thesis, California Institute of Technology, Pasadena (1958), p. 91-107.

34. S. S. Penner, Quantitative Molecular Spectroscopy and Gas Emissivities, Addison-Wesley Co., Reading, Mass., 1959.

35. N. Thomas, Physical Measurements in Gas Dynamics and Combustion (Volume IX, High Speed Aerodynamics and Jet Propulsion Series, Princeton, New Jersey; Princeton University Press, 1954) Section N, p. 563.

36. H. R. Poorman, A.E. Thesis, California Institute of Technology, Pasadena (1953).

37. J. W. Linnett, Fourth (International) Symposium on Combustion, Williams and Wilkins Company, Baltimore 1952, p. 20.

38. B. Lewis and G. von Elbe, Combustion, Flames and Explosions of Gases, Academic Press, Inc., New York 1951.

39. A. G. Gaydon and H. G. Wolfhard, Flames, Chapman & Hall Ltd., London 1953.

40. W. Jost, Explosion and Combustion Processes in Gases, Croft Translation, McGraw-Hill Book Co., New York 1946.

41. E. F. Fiock, Physical Measurements in Gas Dynamics and Combustion: Volume IX, High Speed Aerodynamics and Jet Propulsion Series, Princeton University Press, Princeton, New Jersey 1954; Section K, p. 409.

42. G. H. Dieke, Trans. Instr. Measurements Conference, Stockholm 1947.

43. A. G. Gaydon and H. G. Wolfhard, Fourth (International) Symposium on Combustion, Williams and Wilkins Company, Baltimore, Mass., 1952, p. 212.

44. K. Wohl, F. Welty, L. Bernath et al., Inst. Mech. Engrs. London J. & Proc., Sept. 1951.

45. R. E. Ferguson and H. P. Broida, Fifth (International) Symposium on Combustion, Reinhold Publishing Company, New York 1955, p. 761.

46. K. Wohl and F. Welty, Fifth (International) Symposium on Combustion, Reinhold Publishing Company, New York 1955, p. 746.

47. N. Thomas, Transactions of Faraday Society 47, 958 (1951).

Figures

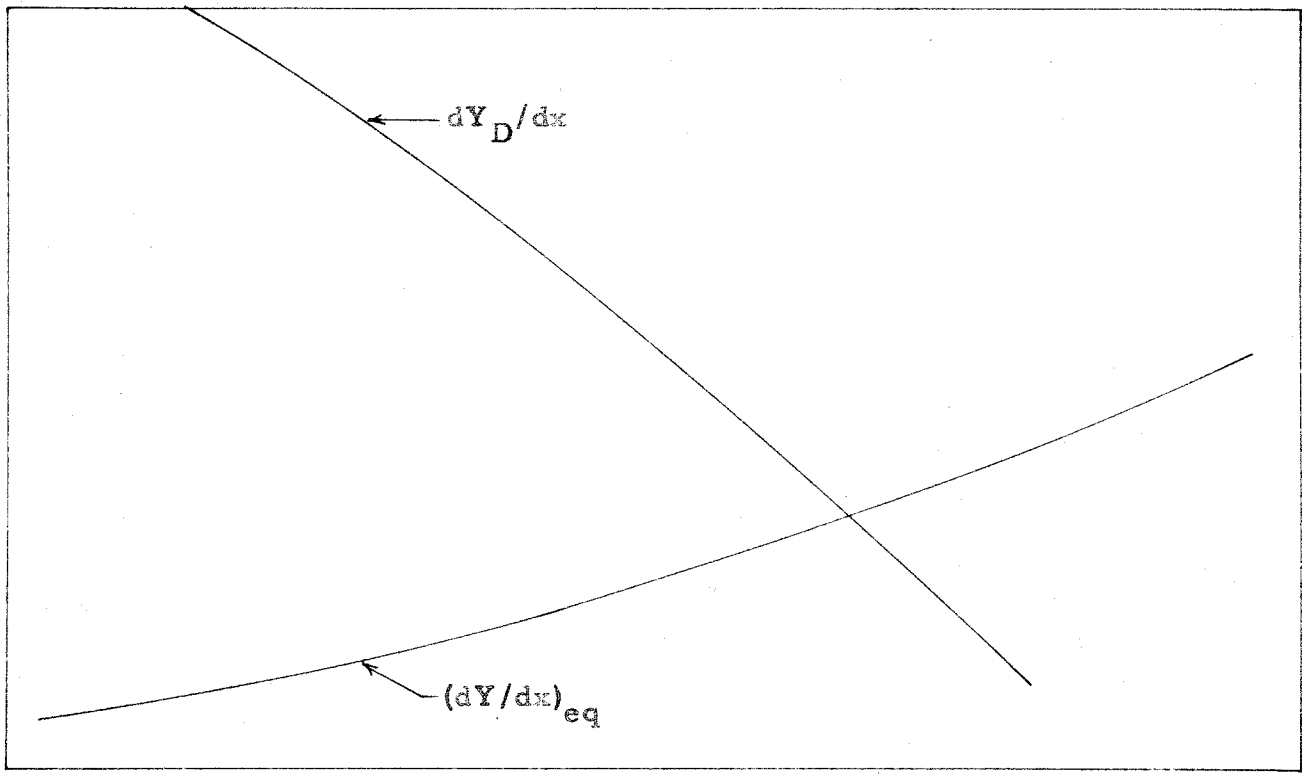

Figure 1. A schematic diagram showing $(dY/dx)_{eq}$ and dY_D/dx as functions of distance along the nozzle axis.

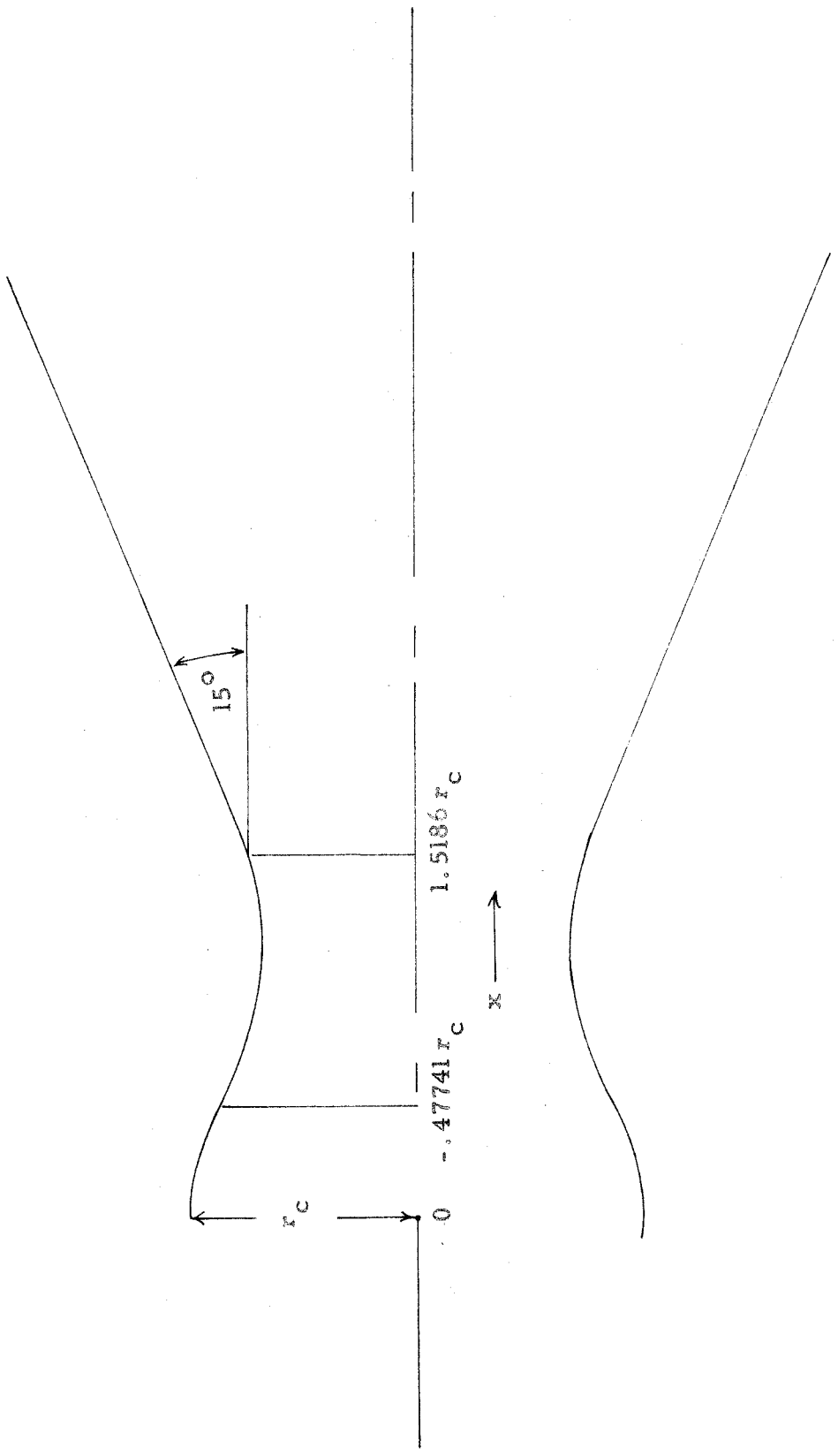

Figure 2. A cross section through the rocket nozzle.

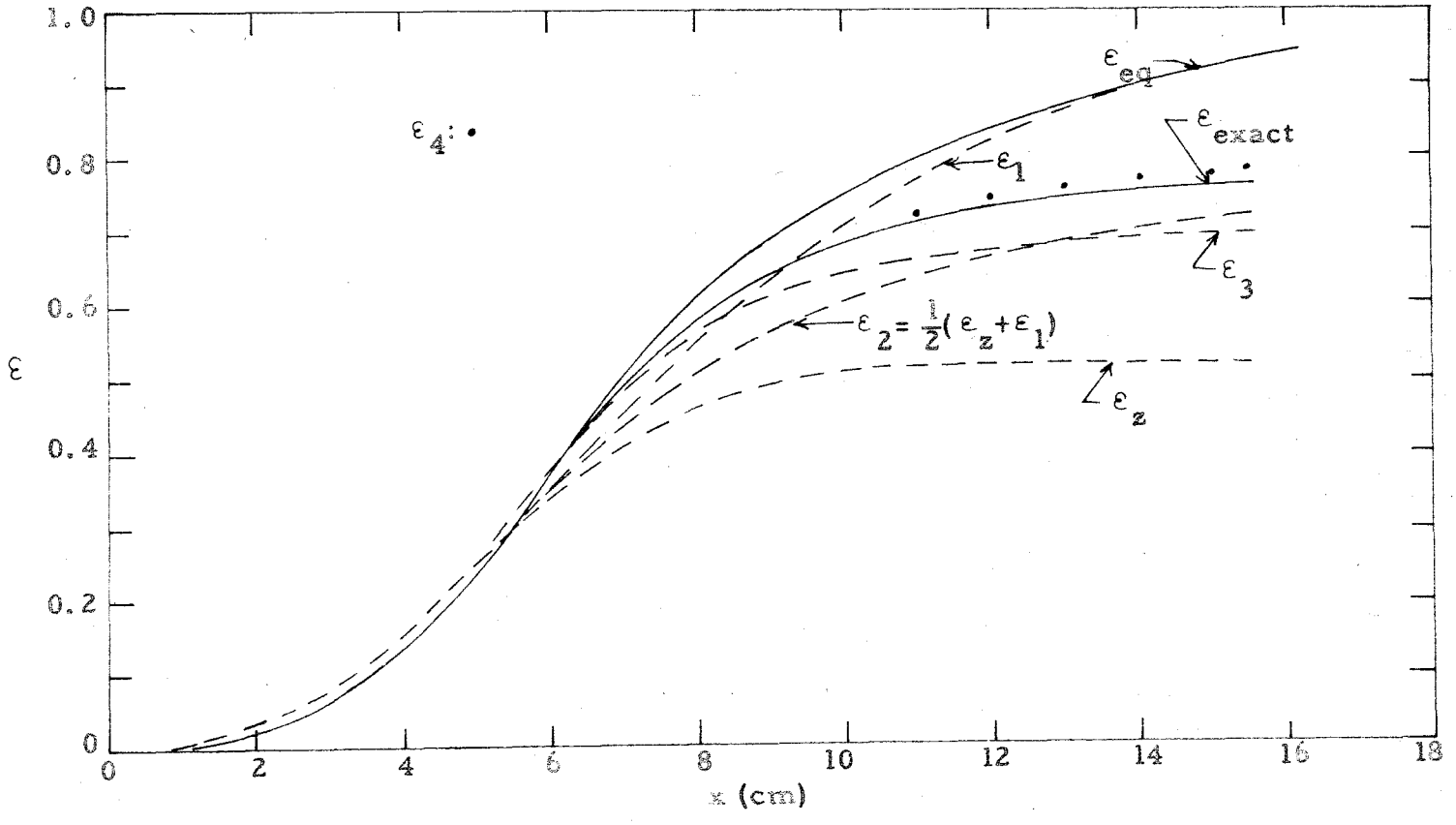

Figure 3. The fraction of the reaction completed (ε) as a function of distance along the nozzle axis (x); ε_{eq} identifies the chemical equilibrium value; ε_{exact} identifies the results from the 709 for case with finite reaction rate; ε_z, ε_1, ε_2, and ε_3 represent successive iterations.

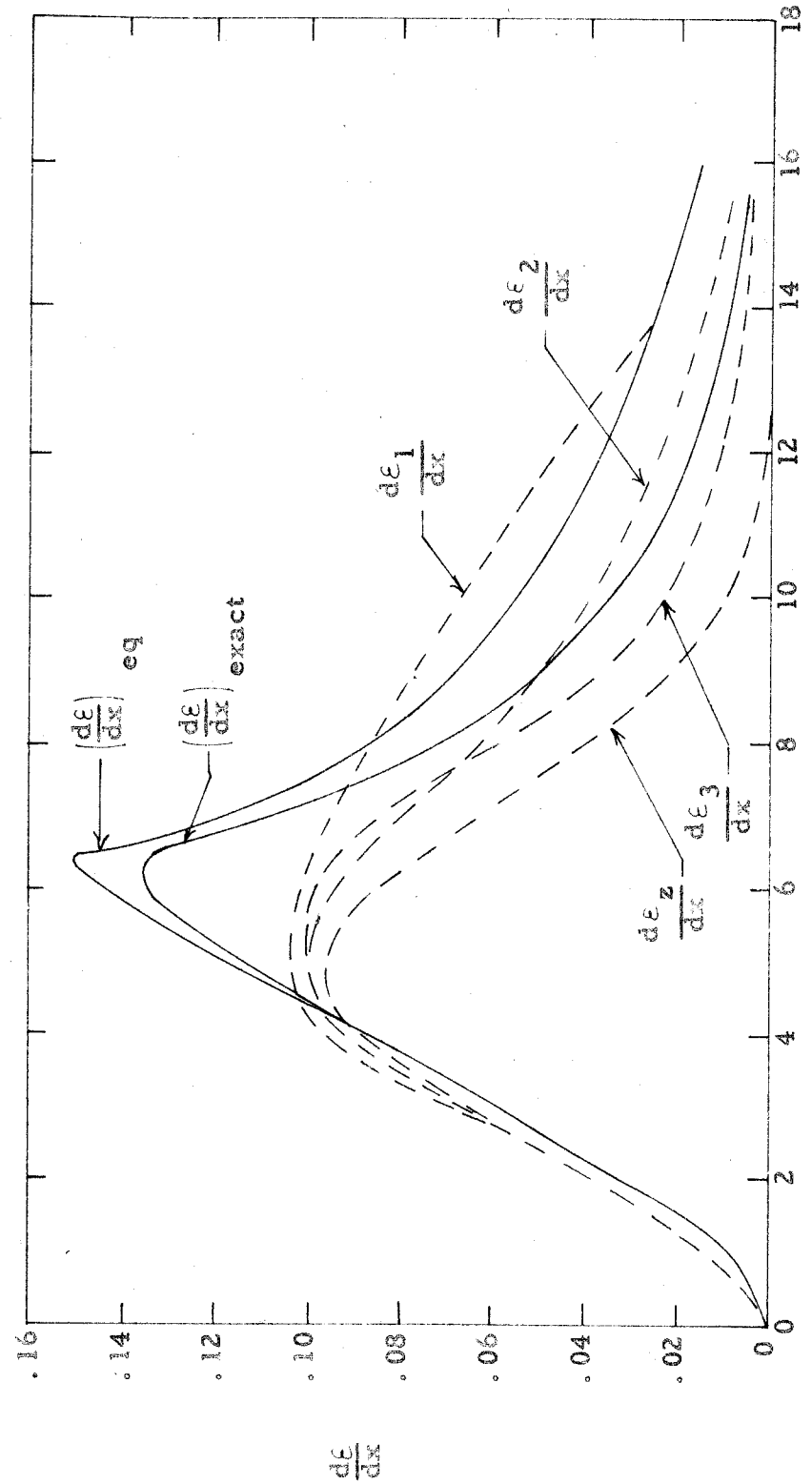

Figure 4. The parameter $d\epsilon/dx$ as a function of distance along the nozzle axis (x); see Fig. 1 for identification of subscripts.

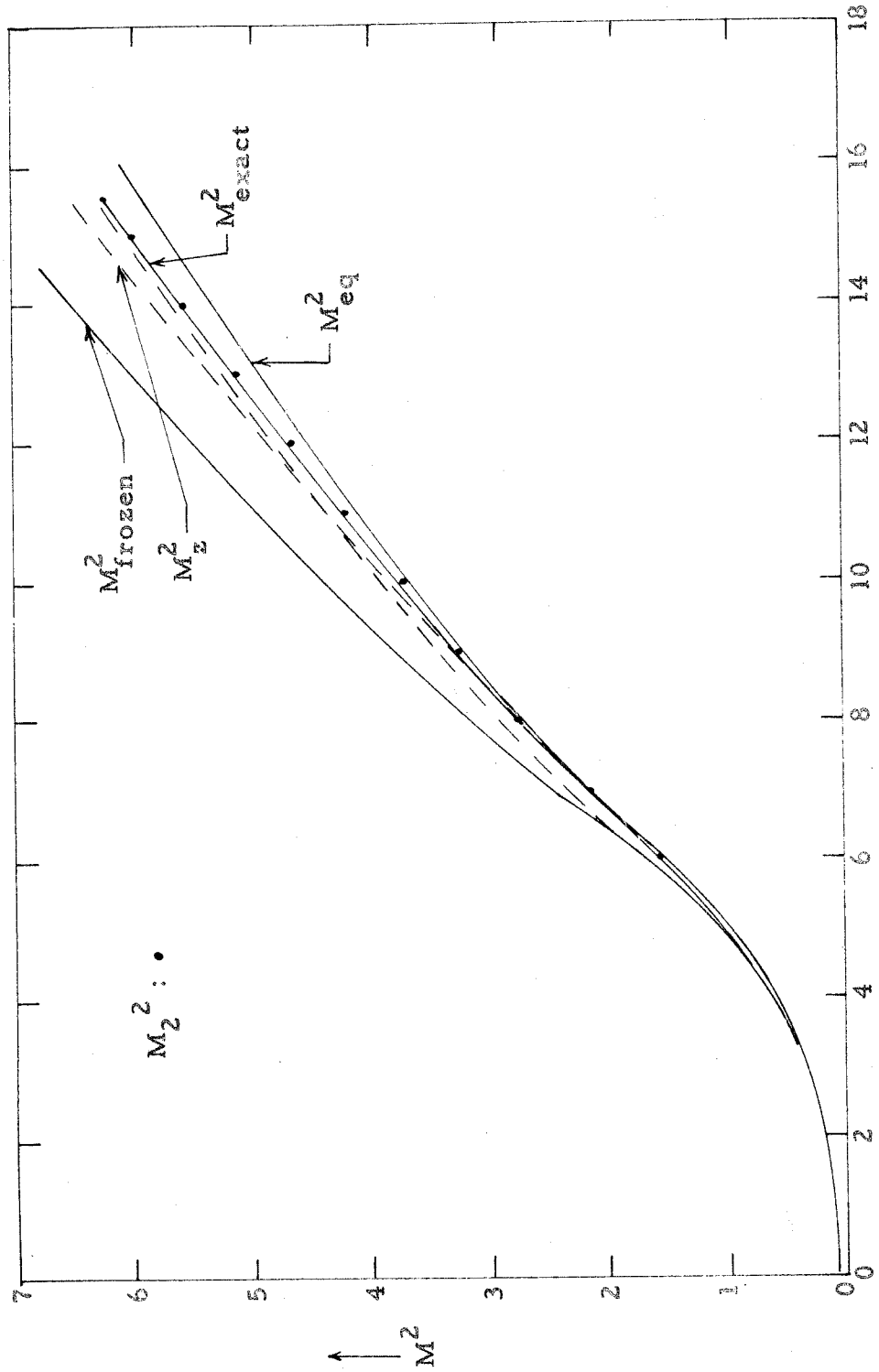

Figure 5. The square of the Mach number as a function of distance along the nozzle axis (x).

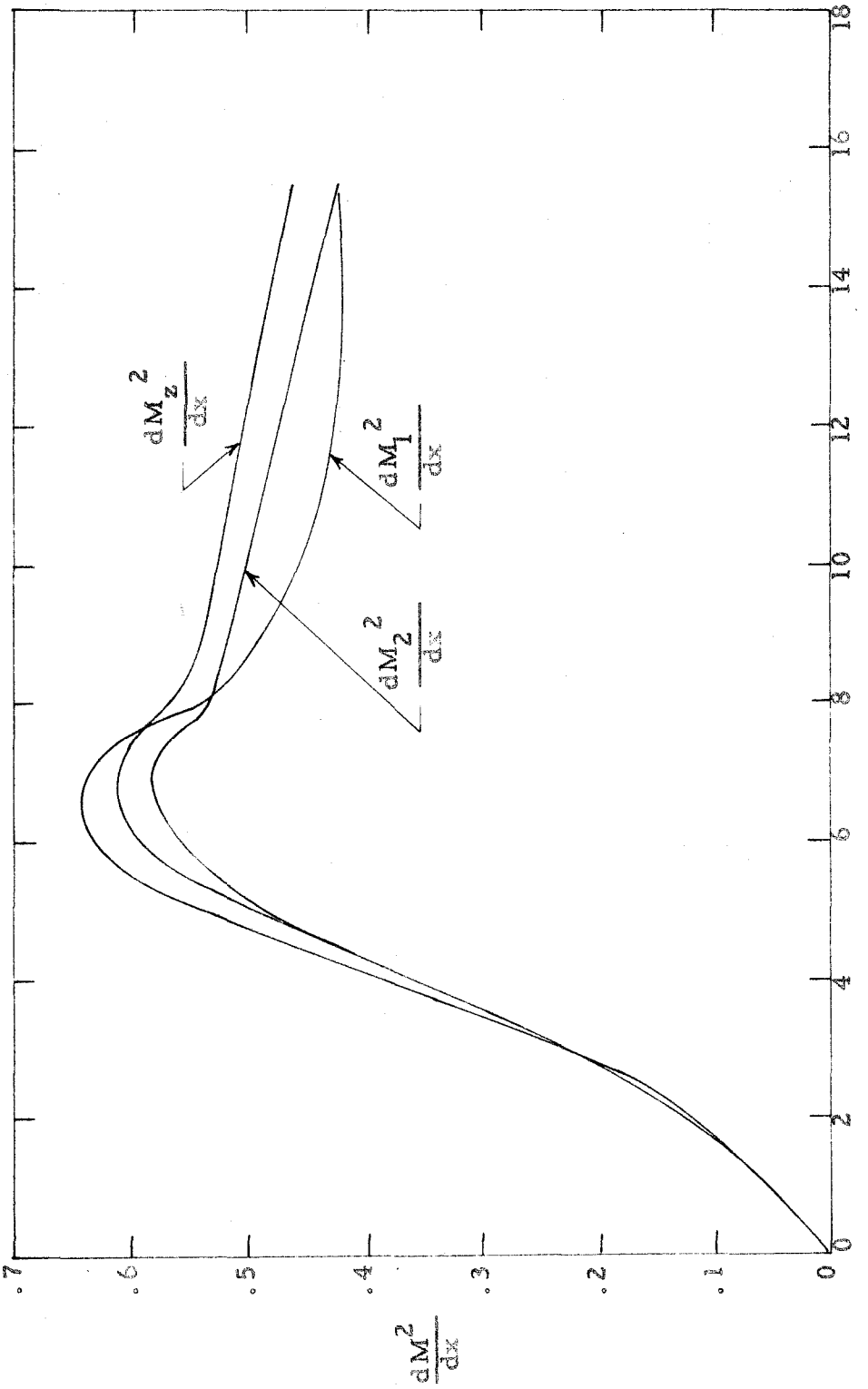

Figure 6. The parameter dM^2/dx as a function of distance along the nozzle axis (x).

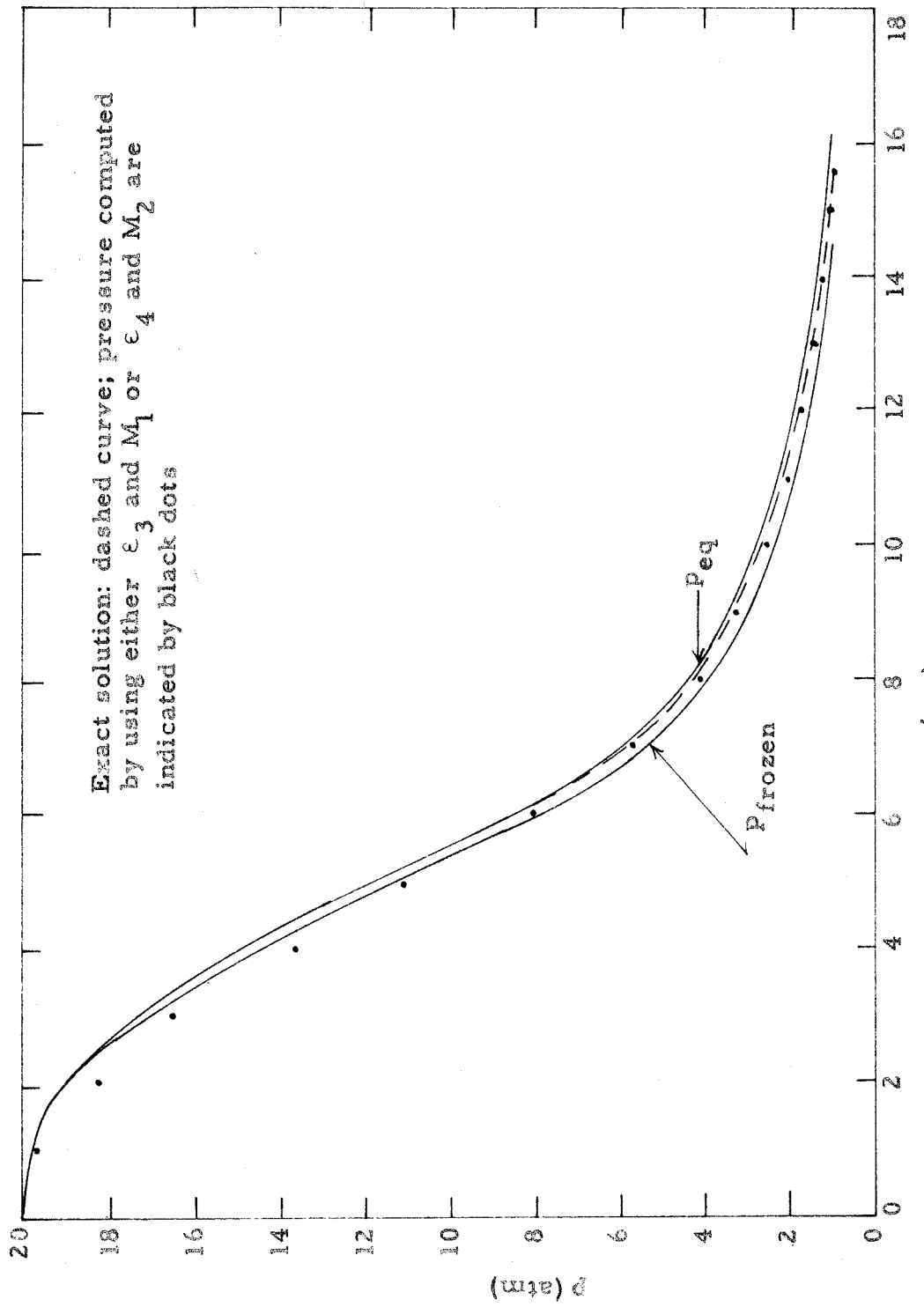

Figure 7. The pressure as a function of distance along the nozzle axis (x).

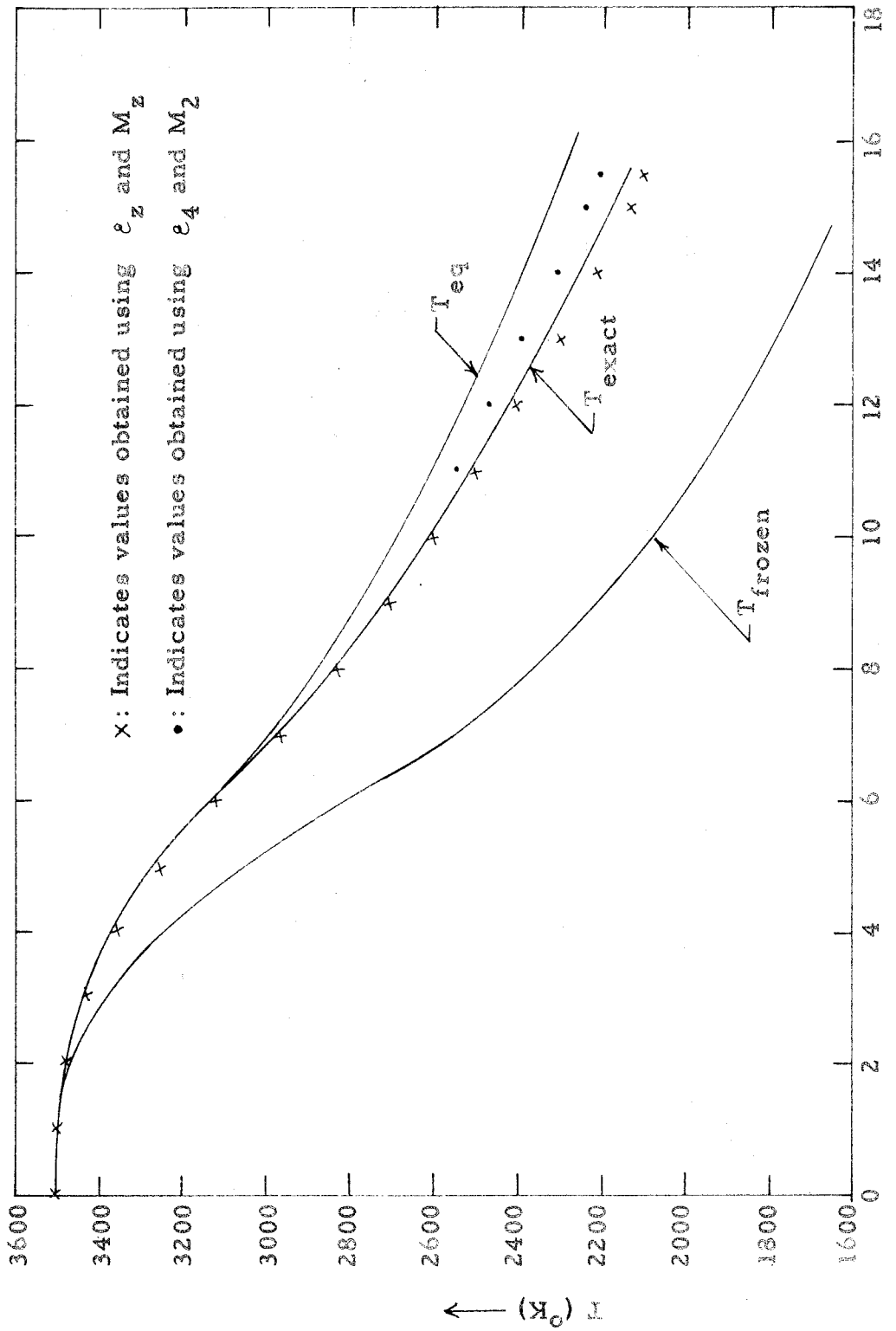

Figure 8. The temperature as a function of distance along the nozzle axis (x).

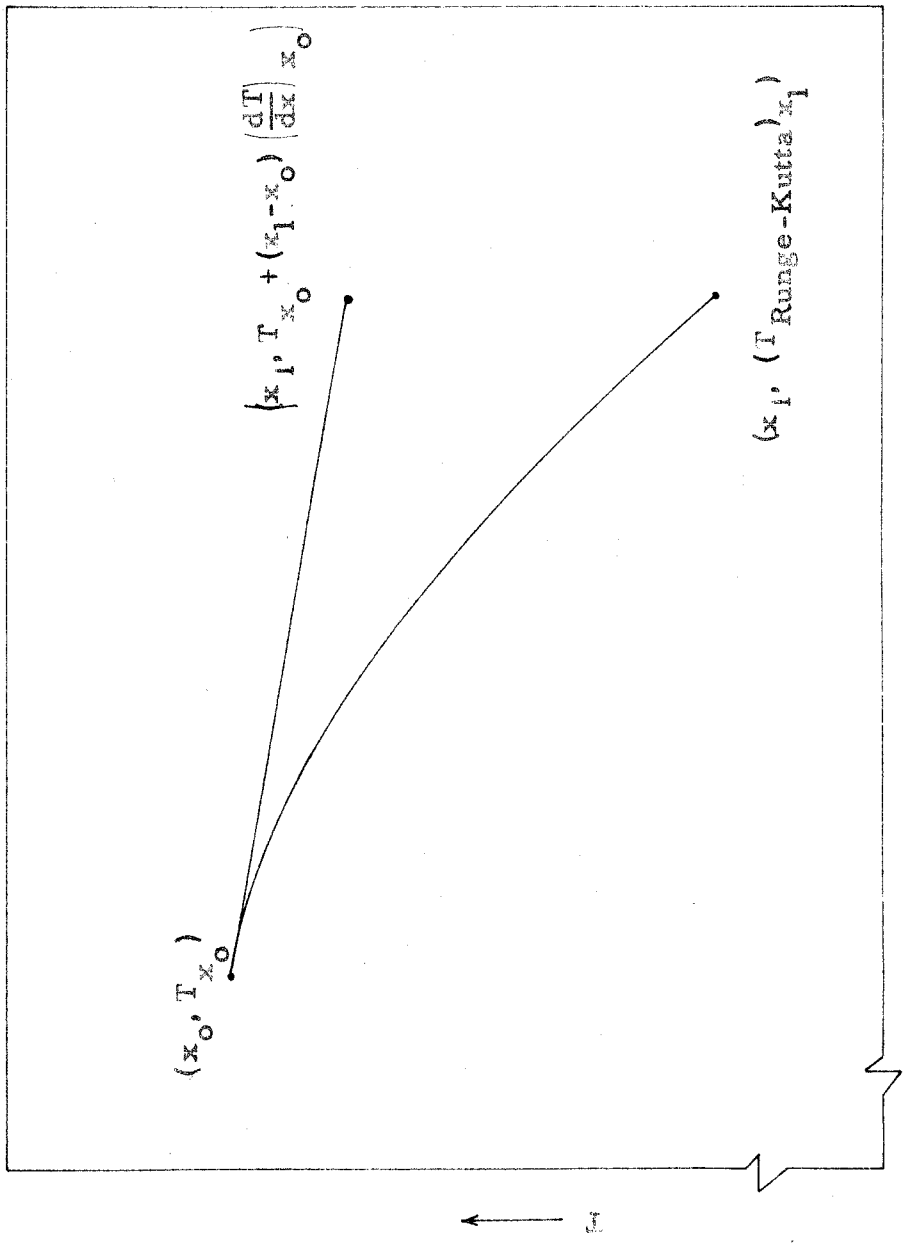

Figure 9. A sketch of the elements used to determine the error estimate.

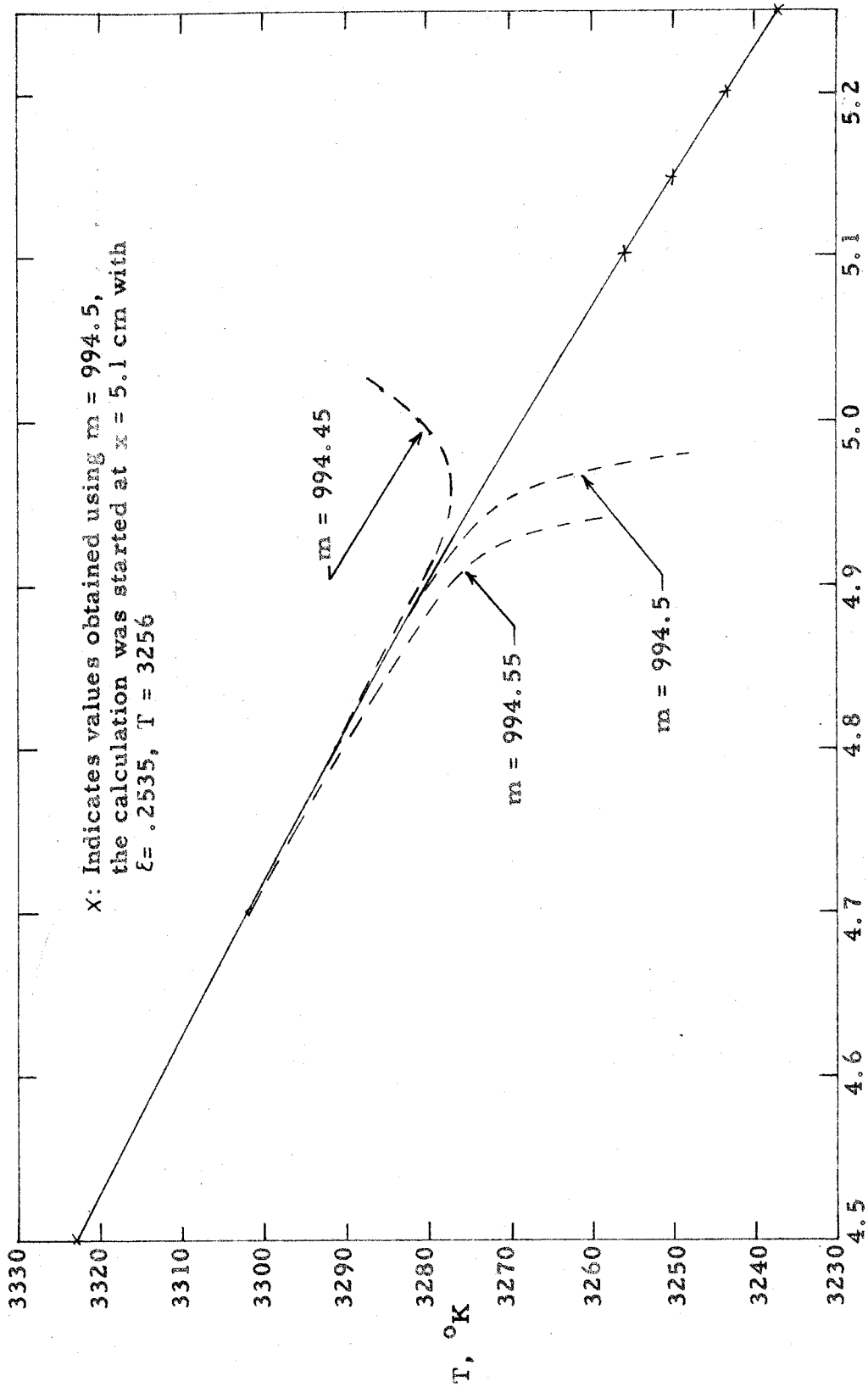

Figure 10. A plot of T as a function of x in the throat region with the mass flow rate as a parameter.

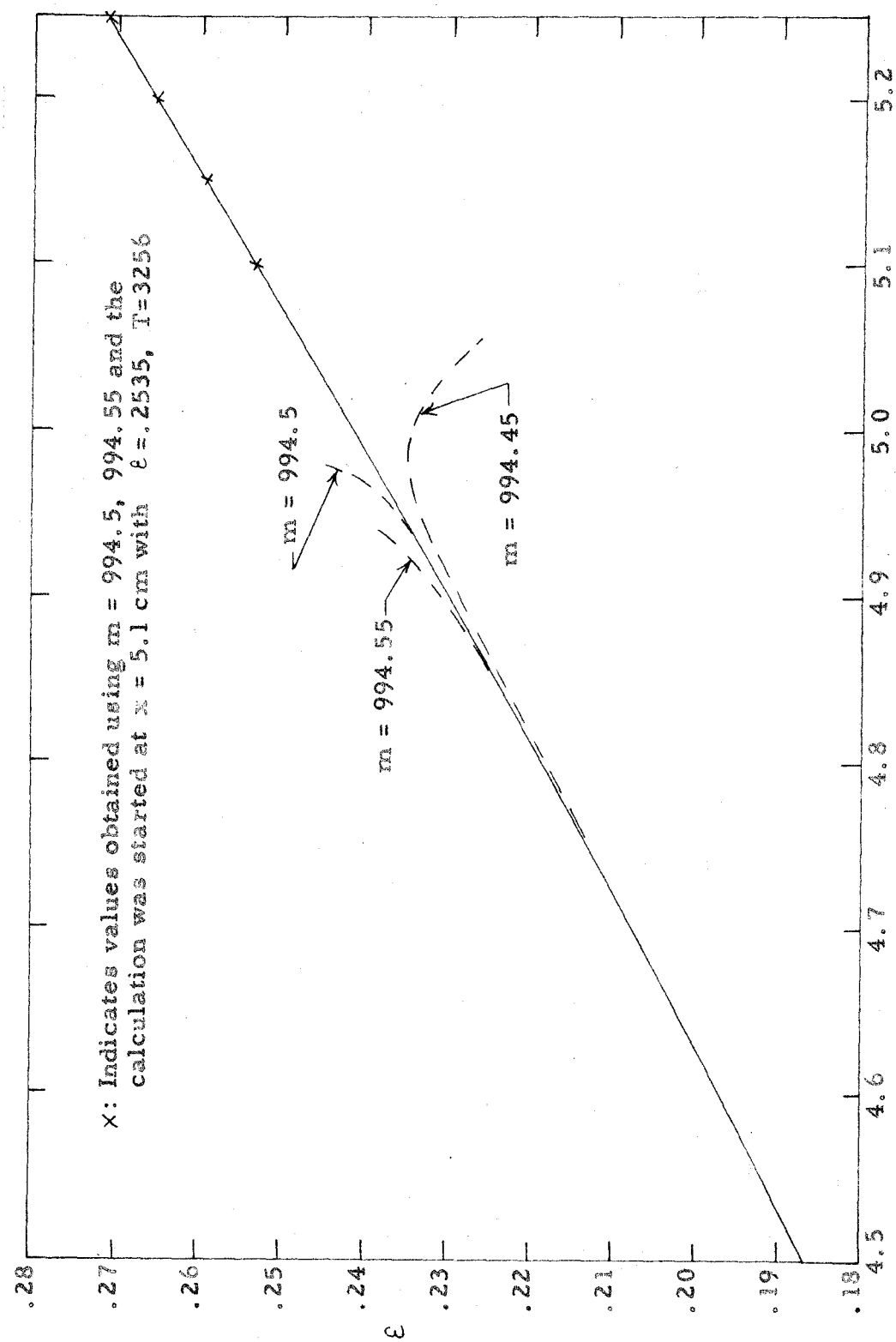

Figure 11. A plot of ε as a function of x in the throat region with the mass flow rate as a parameter.

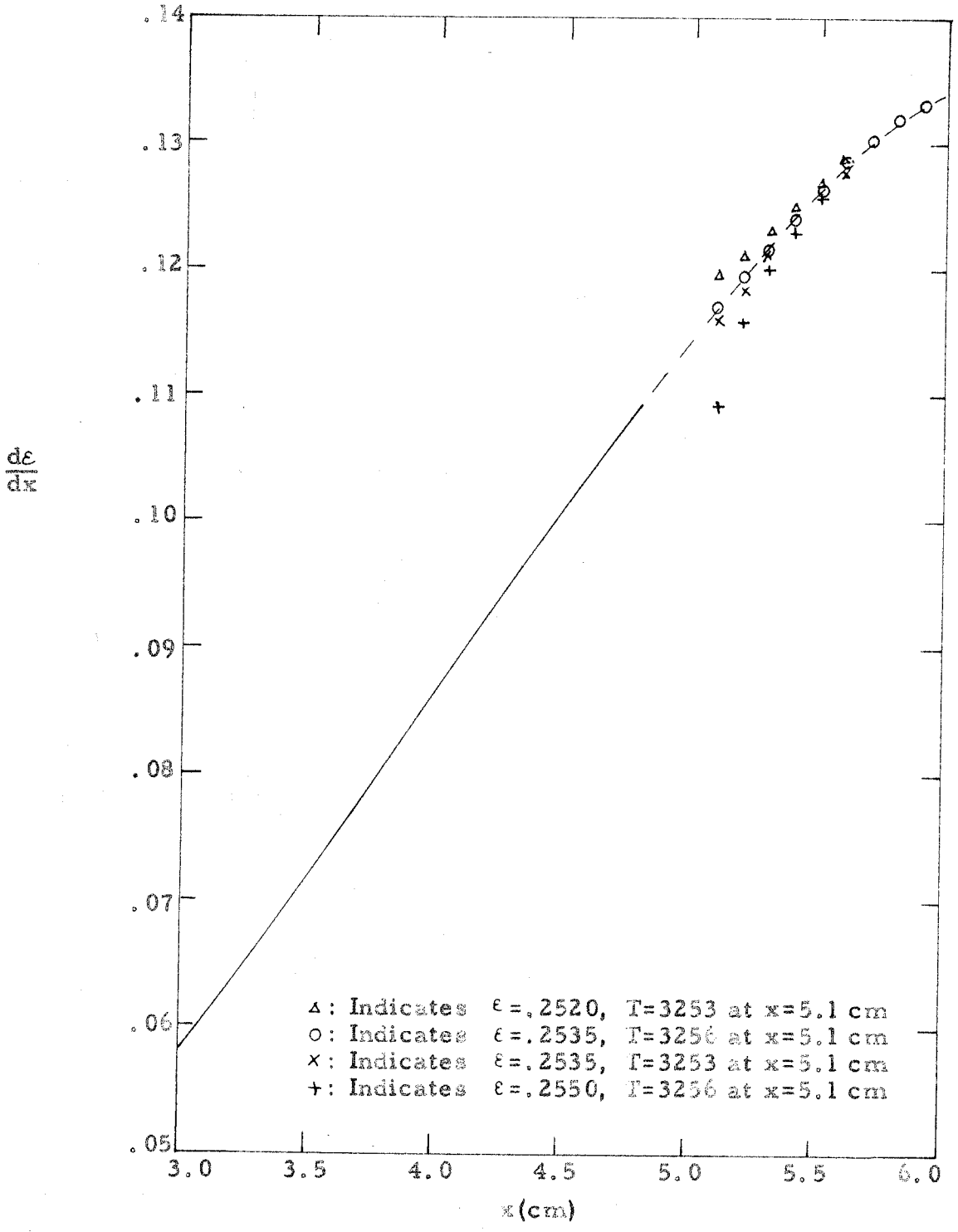

Figure 12. An illustration of the use of the $d\varepsilon/dx$ curve to find ε and T at the restart location (m = 994.5 g/sec).

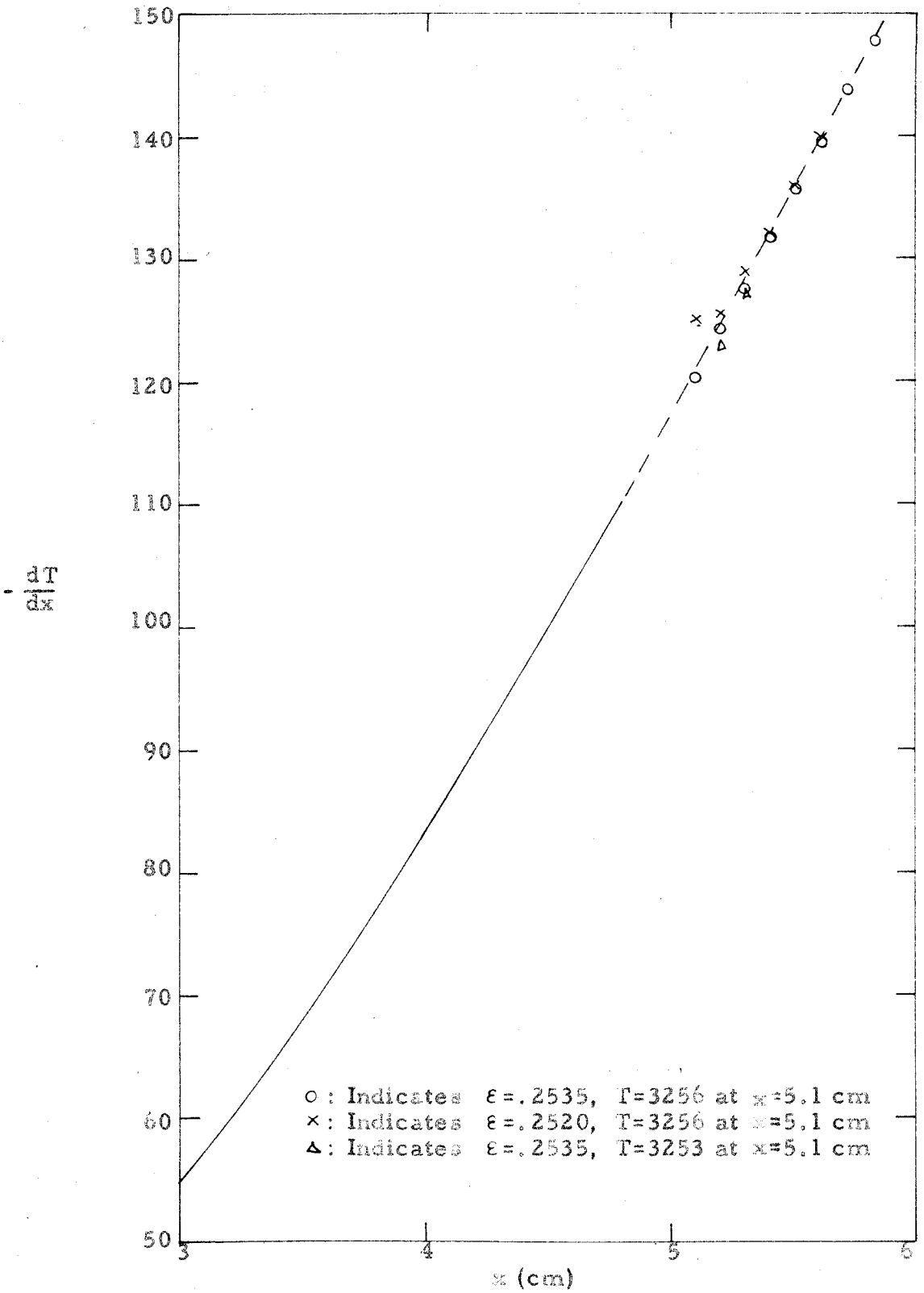

Figure 13. An illustration of the use of the dΓ/dx curve to find ε and T at the restart location (m = 994.5 g/sec).

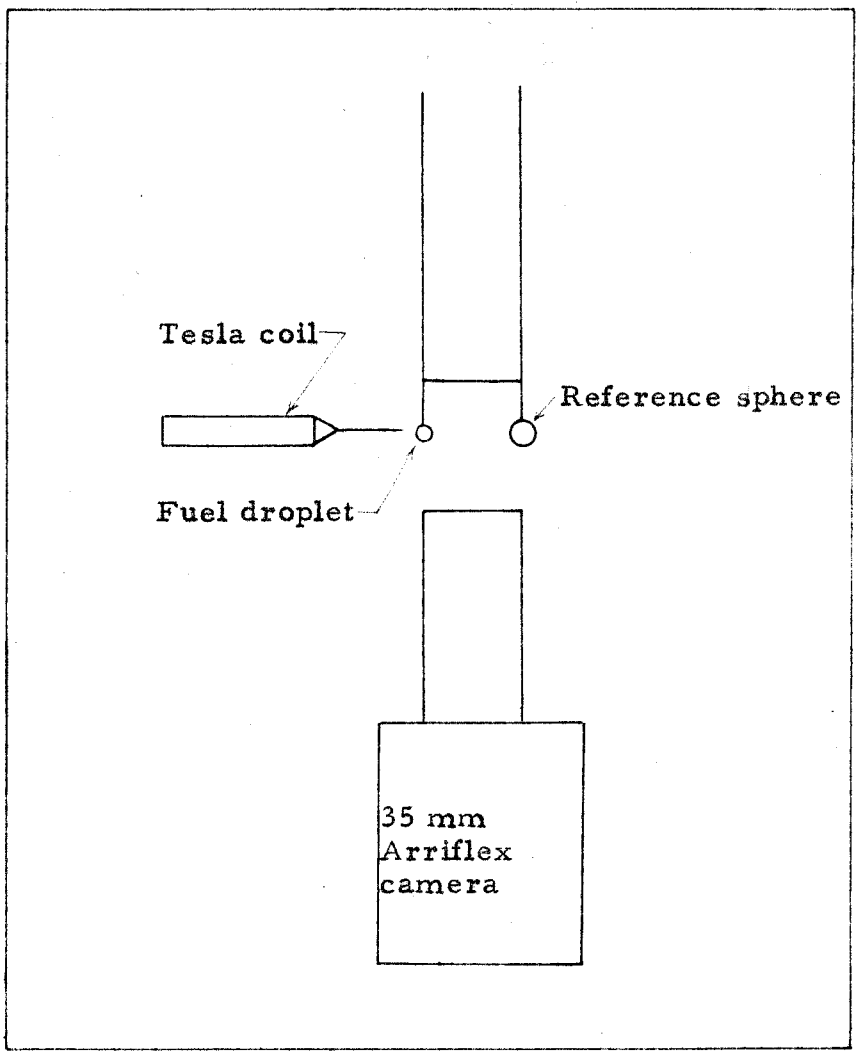

Figure 14. A schematic diagram of the apparatus used to obtain evaporation constants.

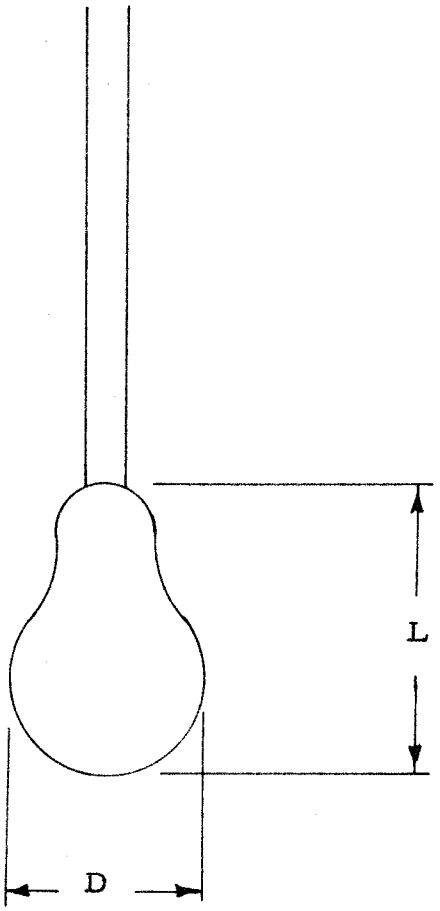

Figure 15. A sketch showing the shape of a RP-1 droplet burning in air and the dimensions listed in Table I.

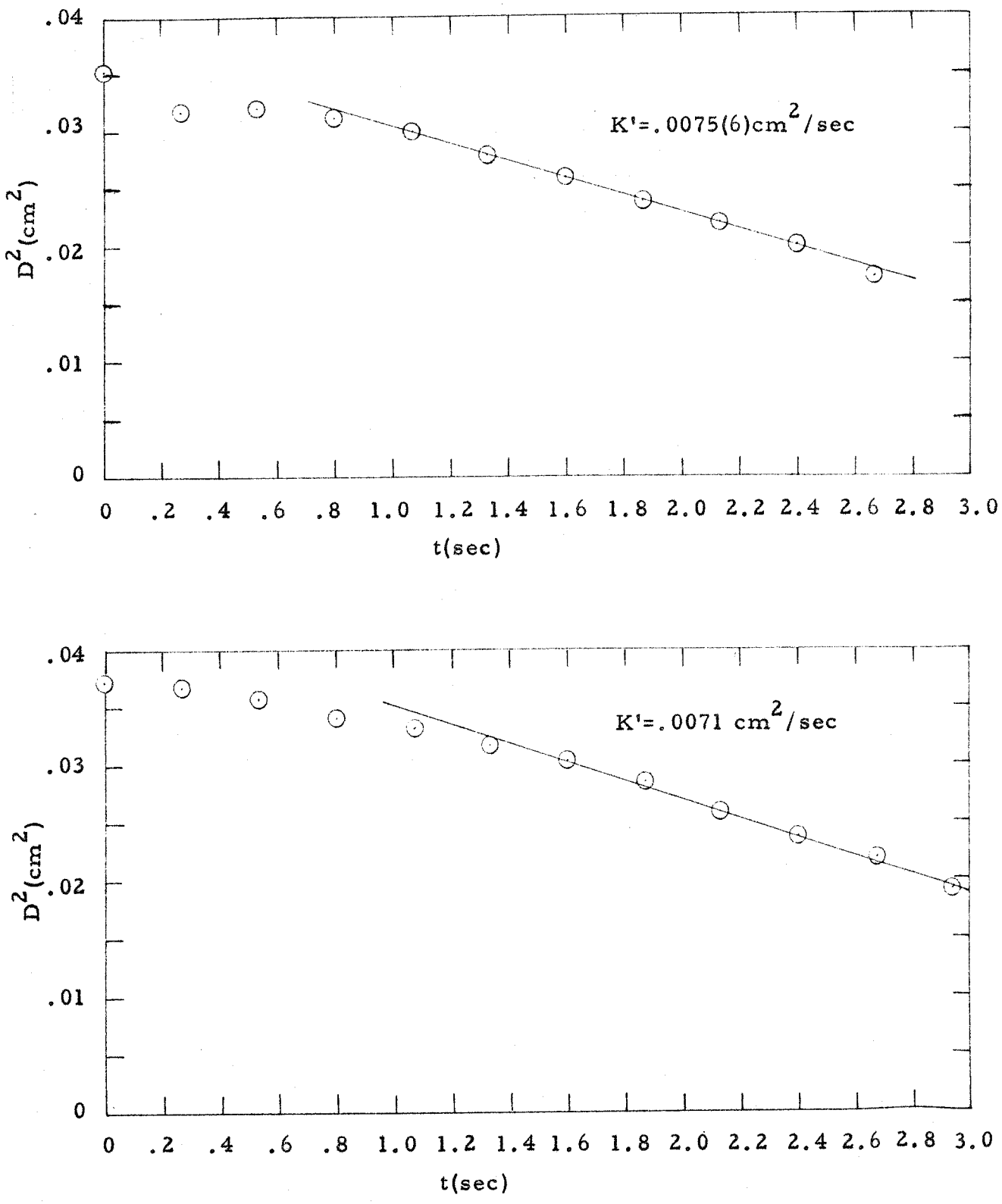

Figure 16. Experimental studies on the burning of RP-1 droplets in air.

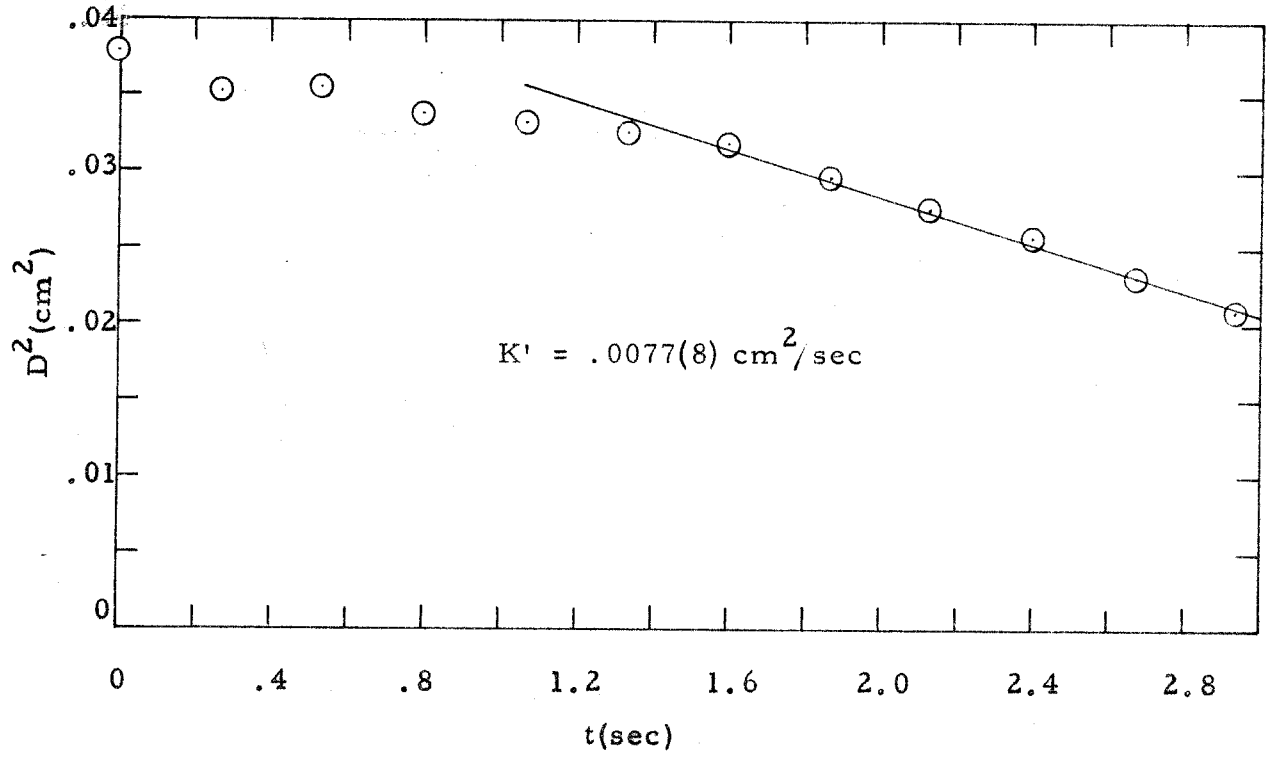

Figure 16 (continued). Experimental studies on the burning of RP-1 droplet in air.

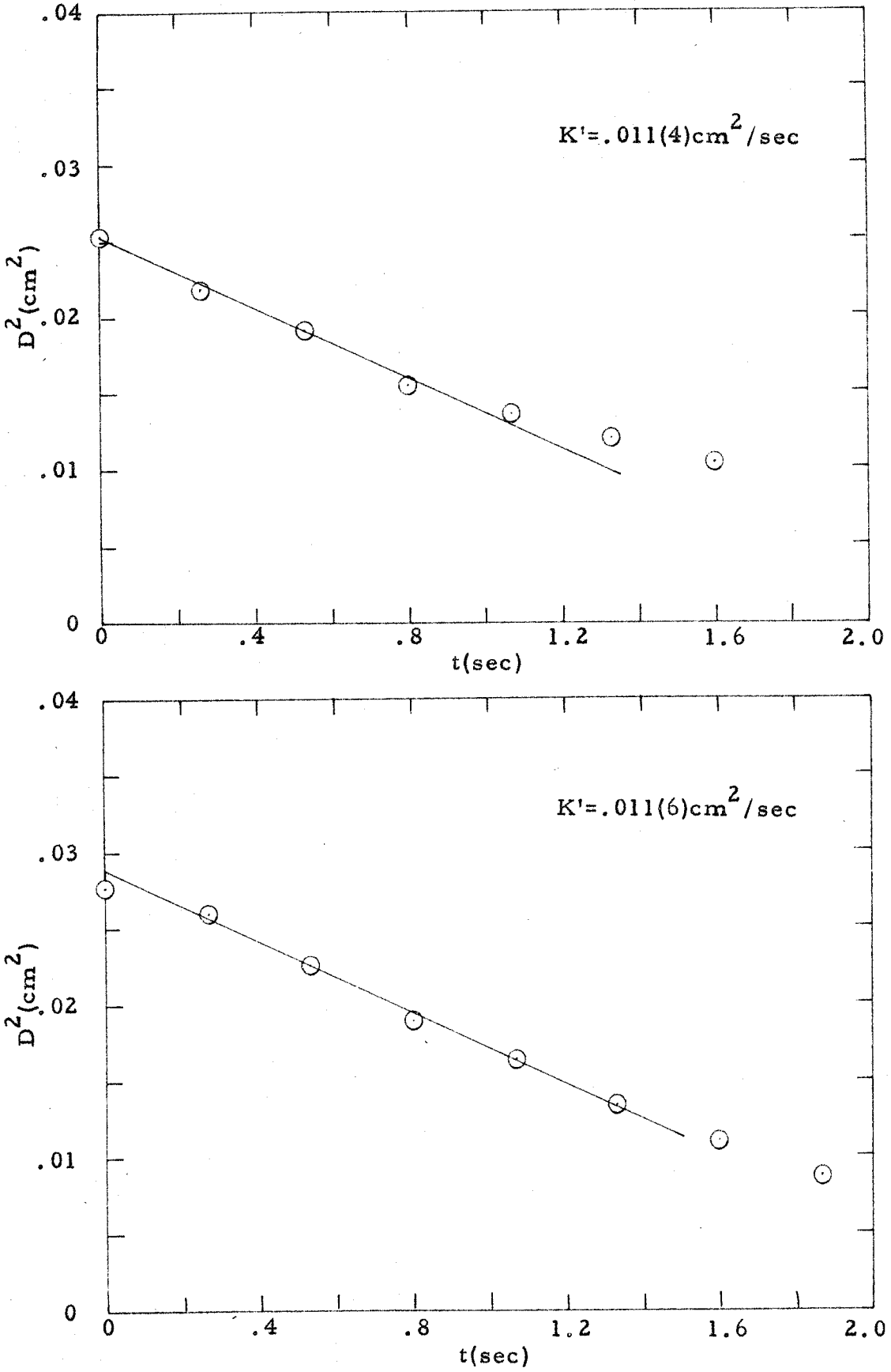

Figure 17. Experimental studies on the burning of UDMH in air.

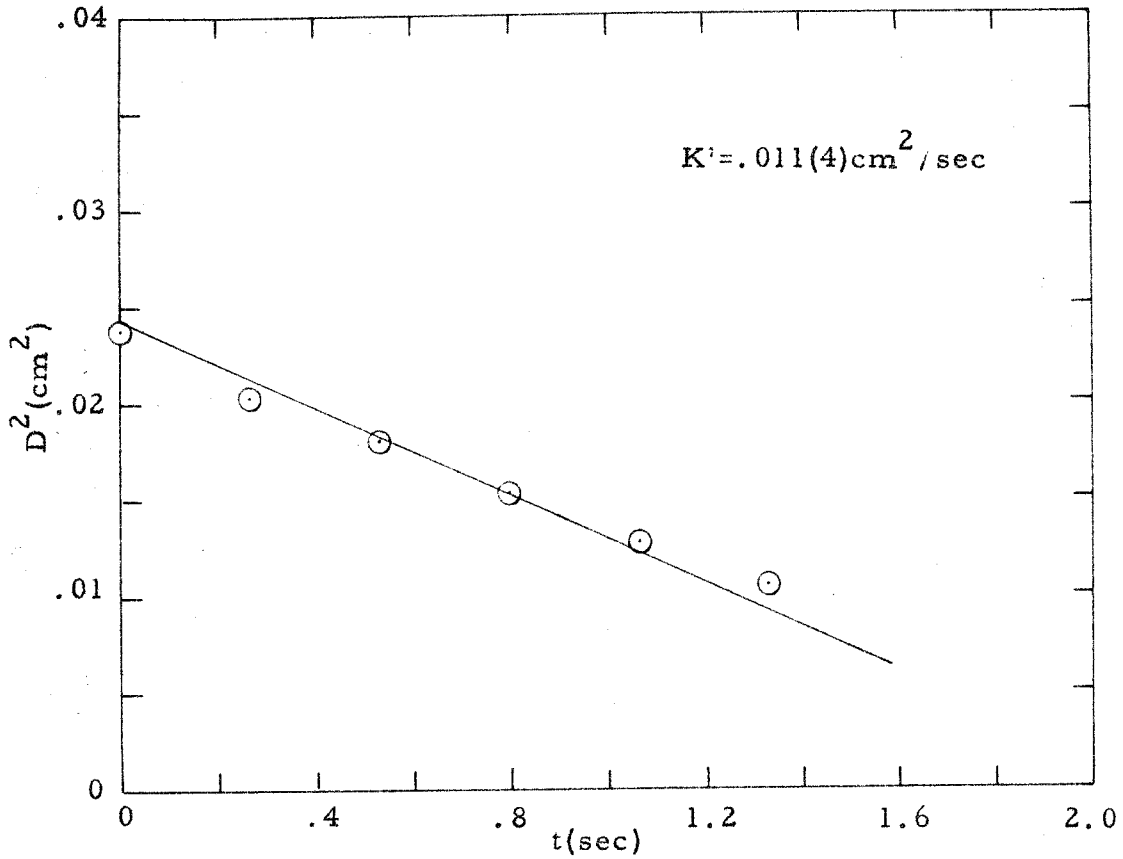

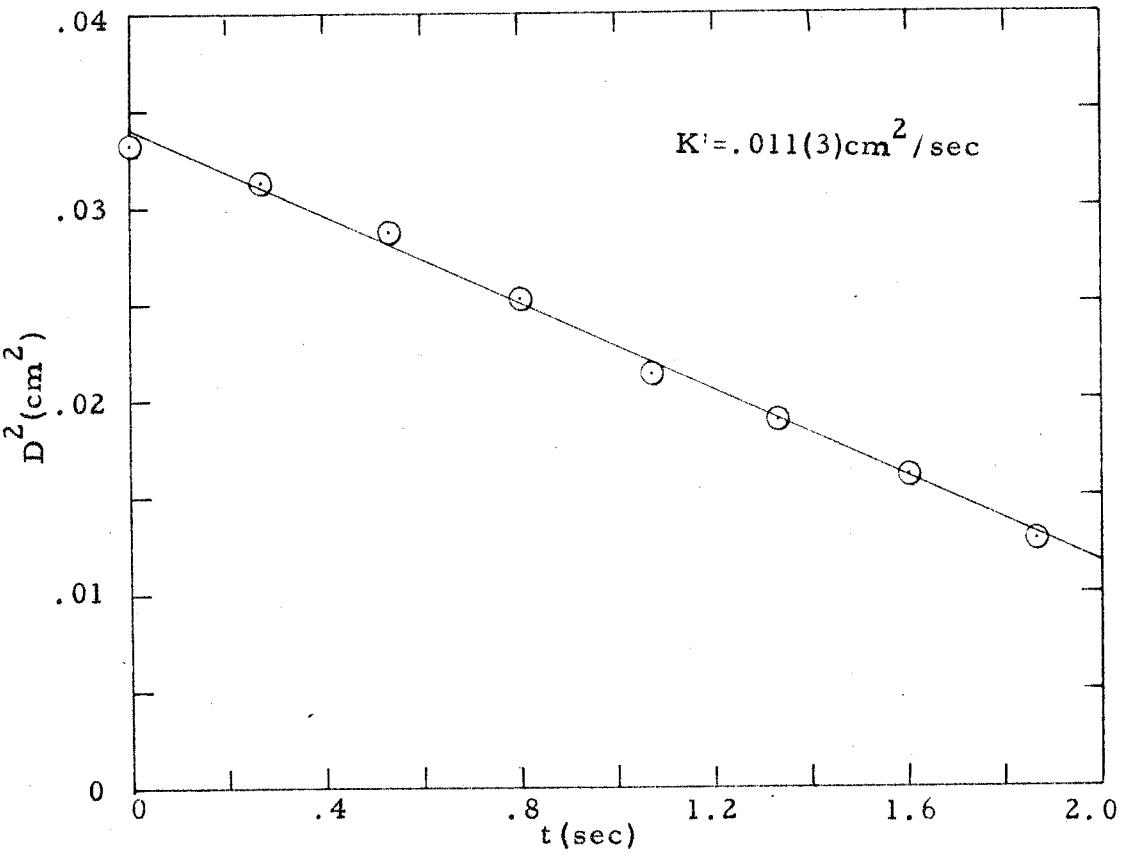

Figure 17 (continued). Experimental studies on the burning of UDMH in air.

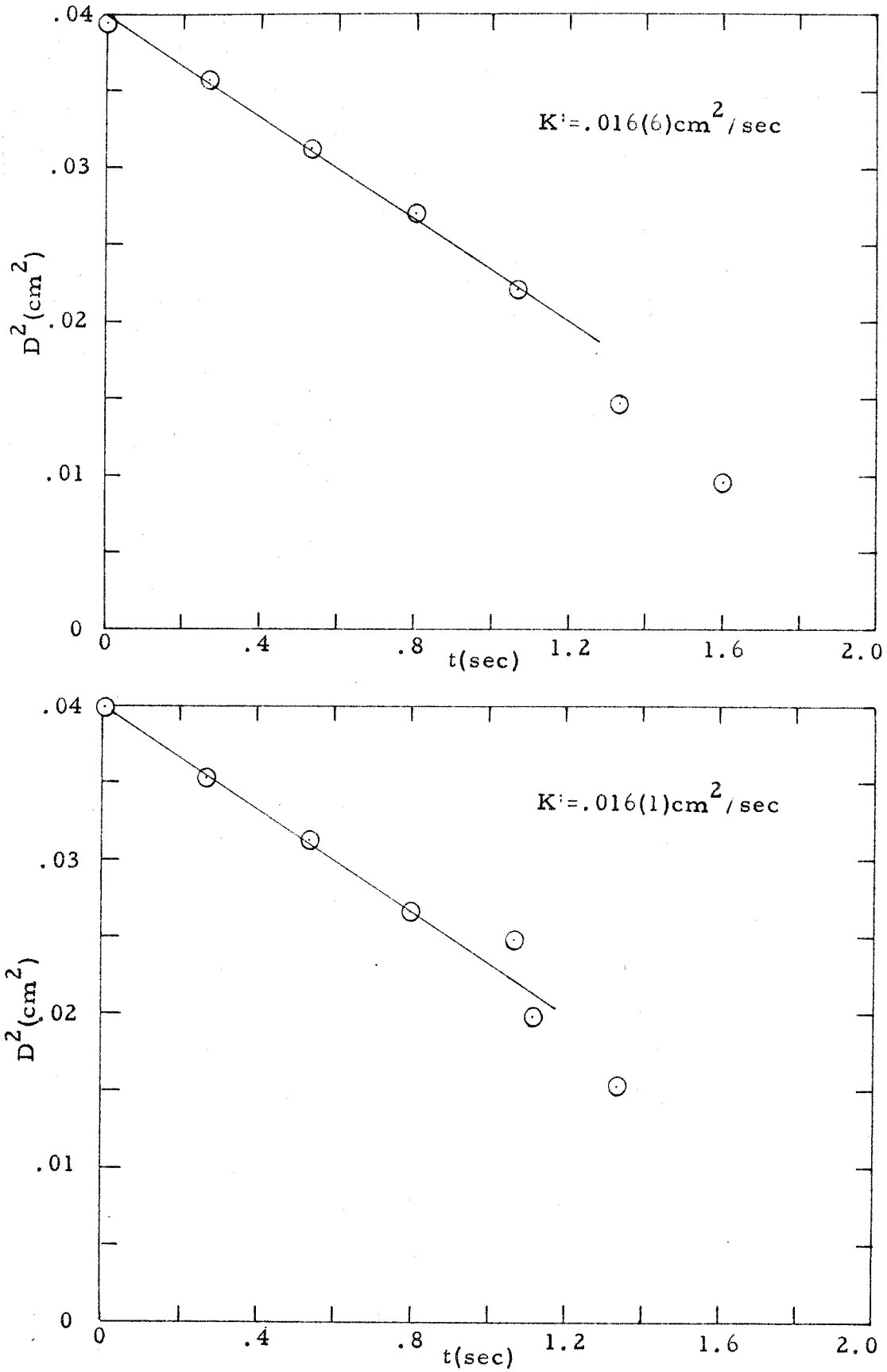

Figure 18. Experimental studies on the burning of N_2H_4 in air.

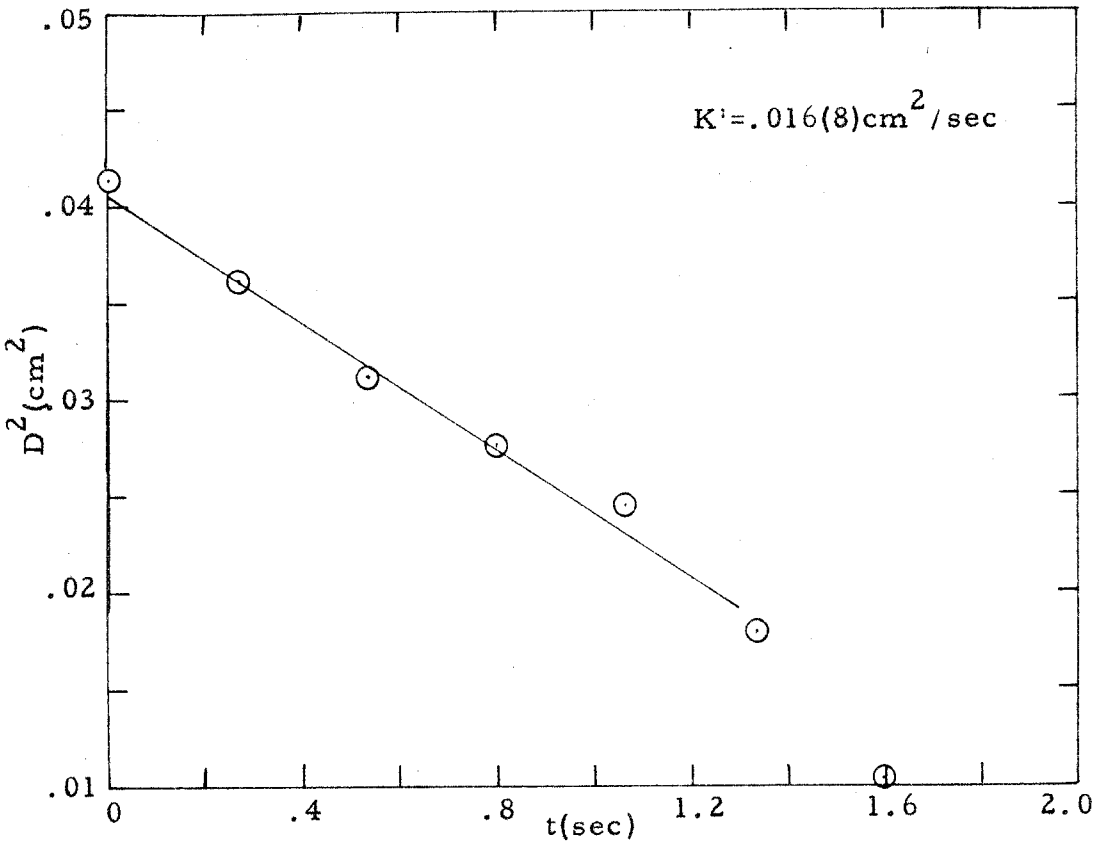

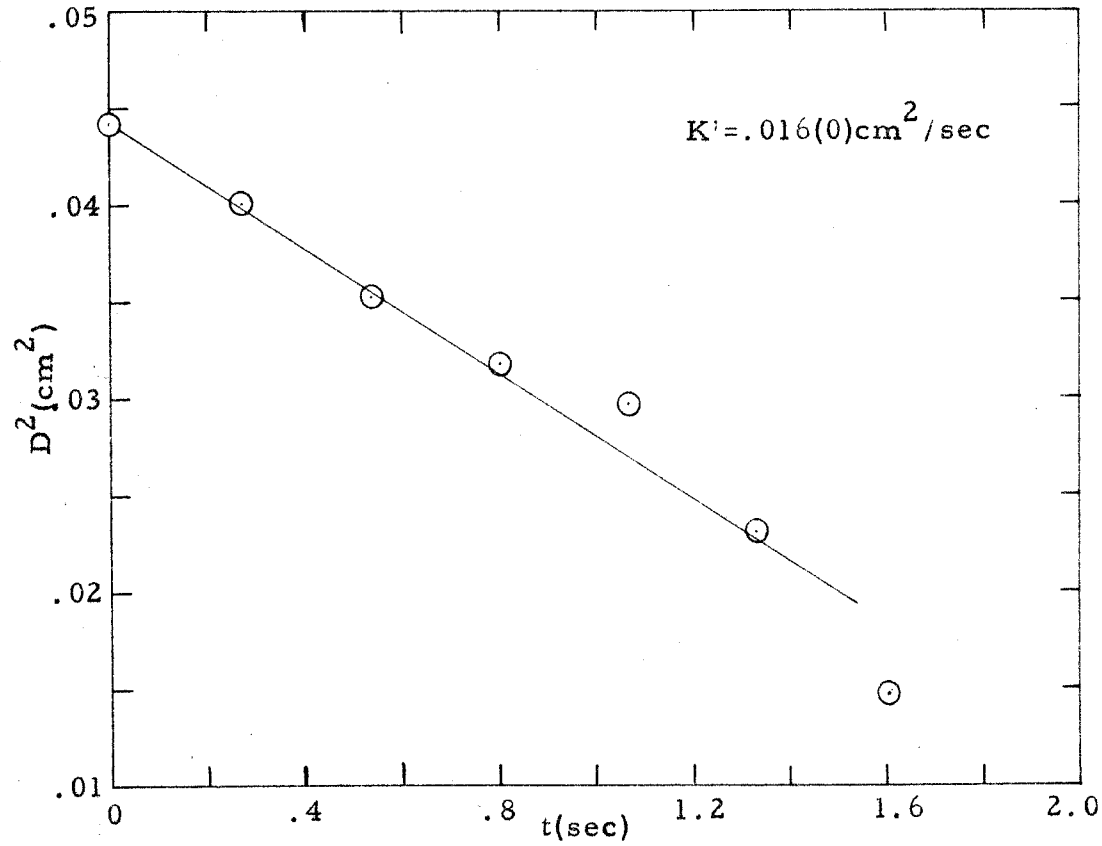

Figure 18 (continued). Experimental studies on the burning of N_2H_4 in air.

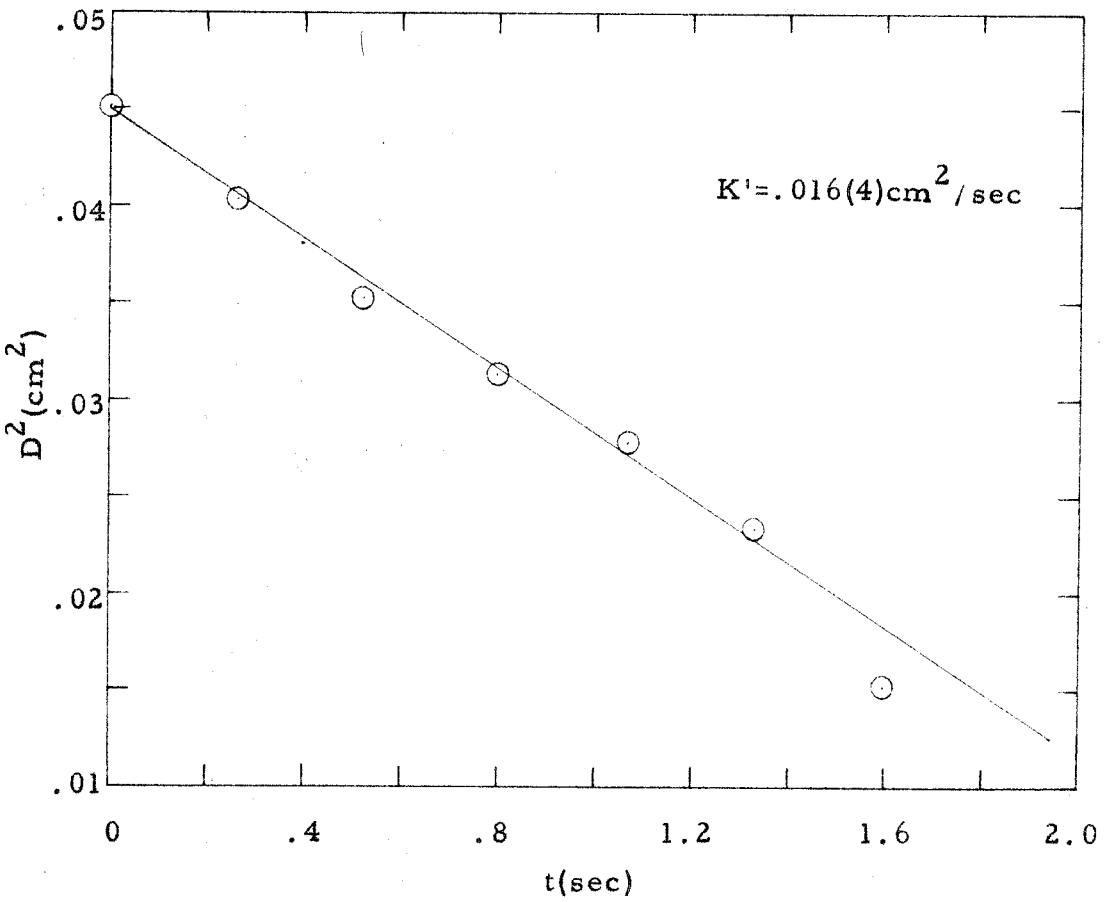

Figure 18 (continued). Experimental studies on the burning of N_2H_4 in air.

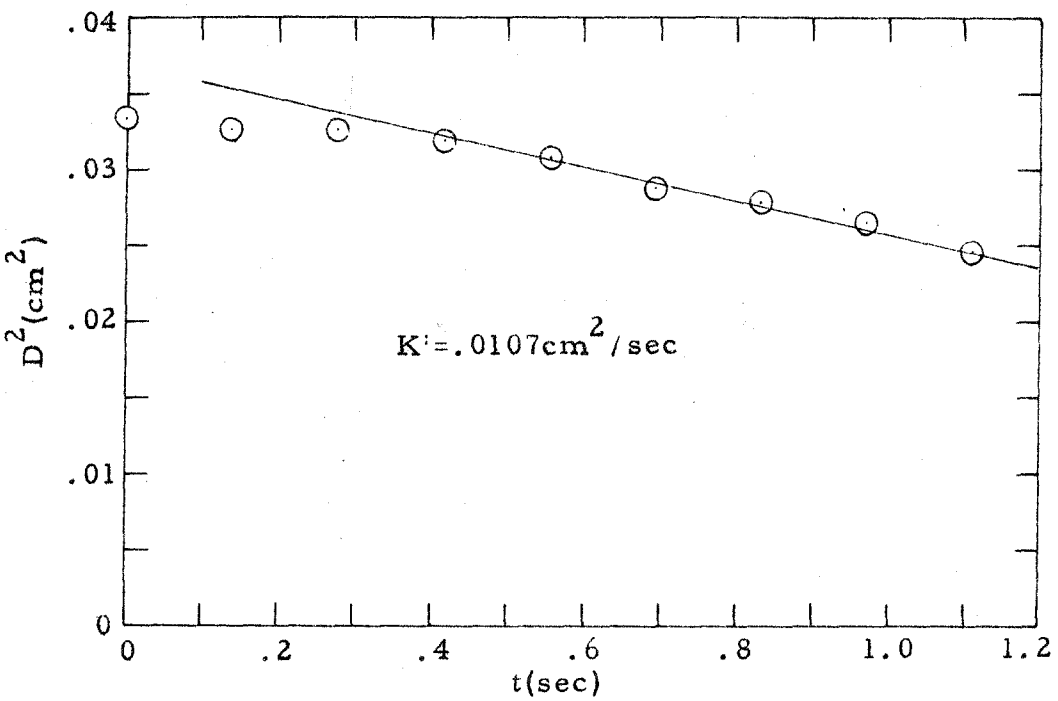

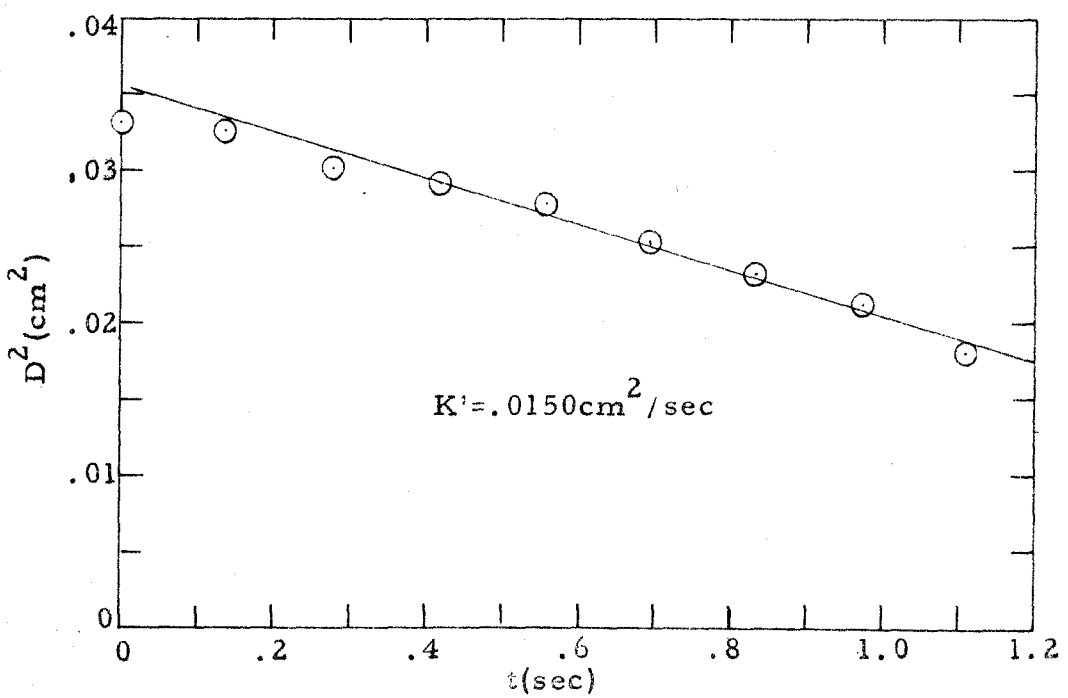

Figure 19. Experimental studies on the burning of RP-1 droplet in oxygen.

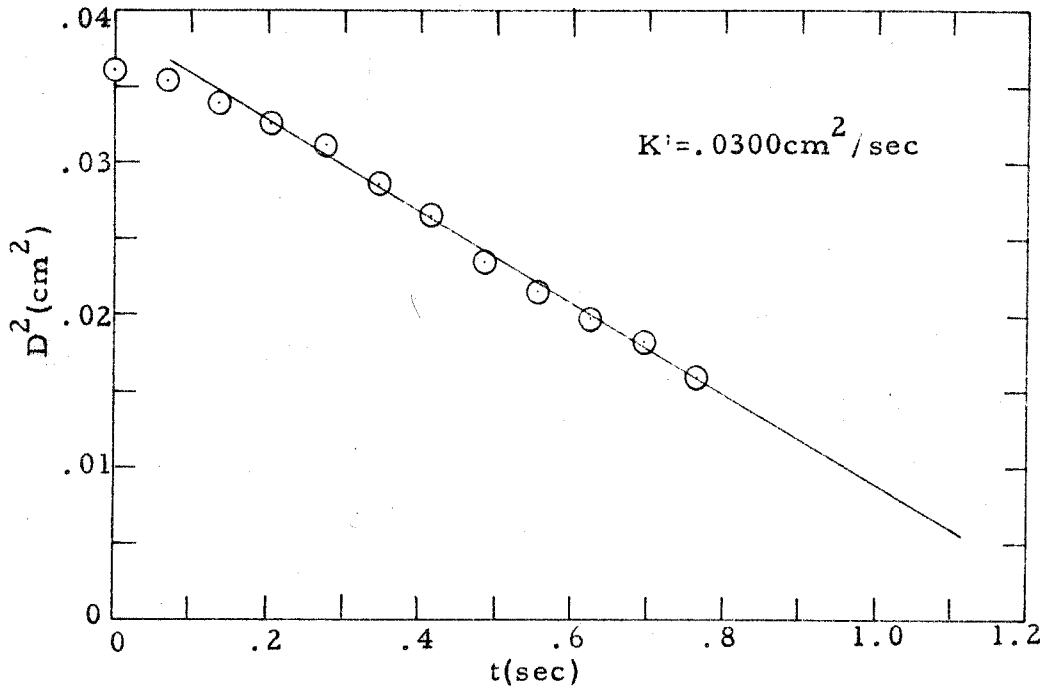

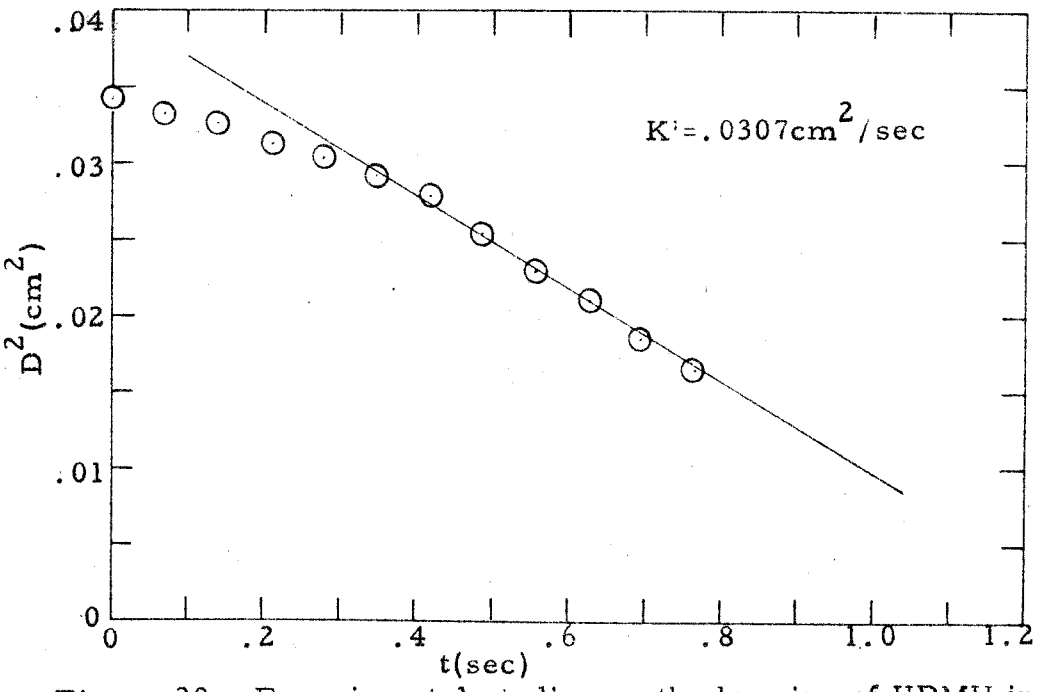

Figure 20. Experimental studies on the burning of UDMH in oxygen.

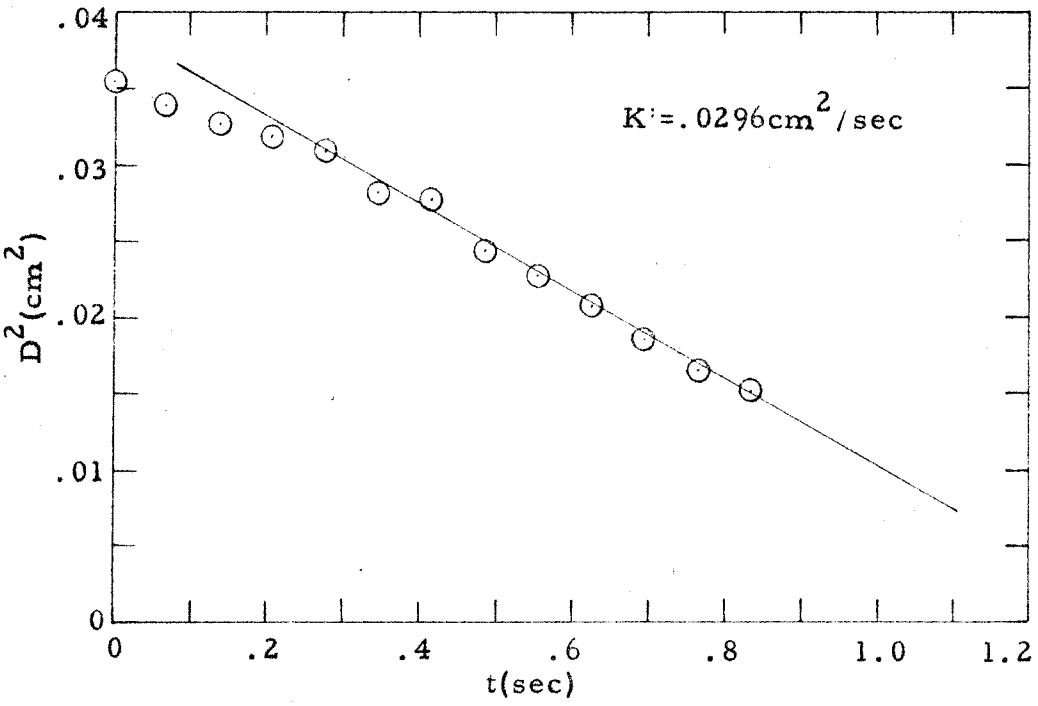

Figure 20 (continued). Experimental studies on the burning of UDMH in oxygen.

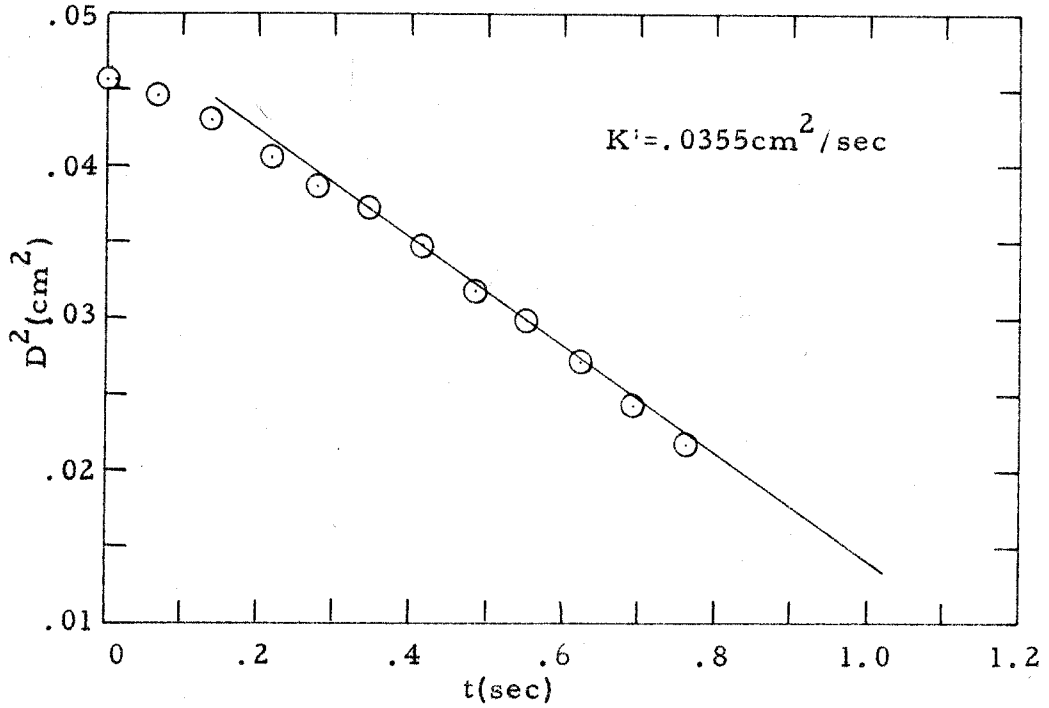

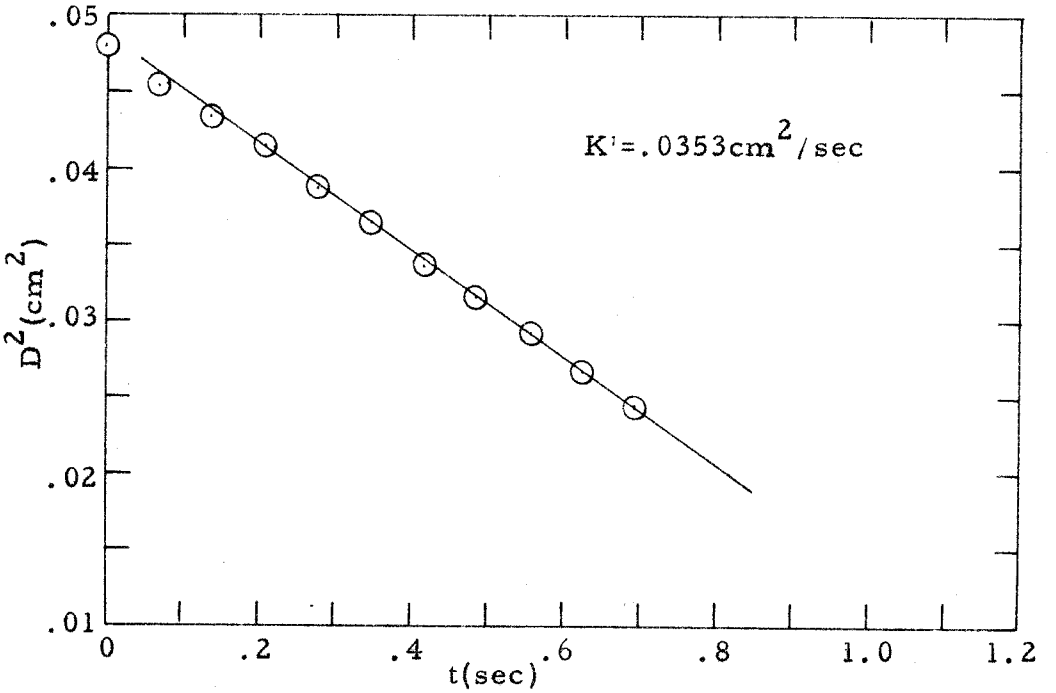

Figure 21. Experimental studies of the burning of N_2H_4 in oxygen.

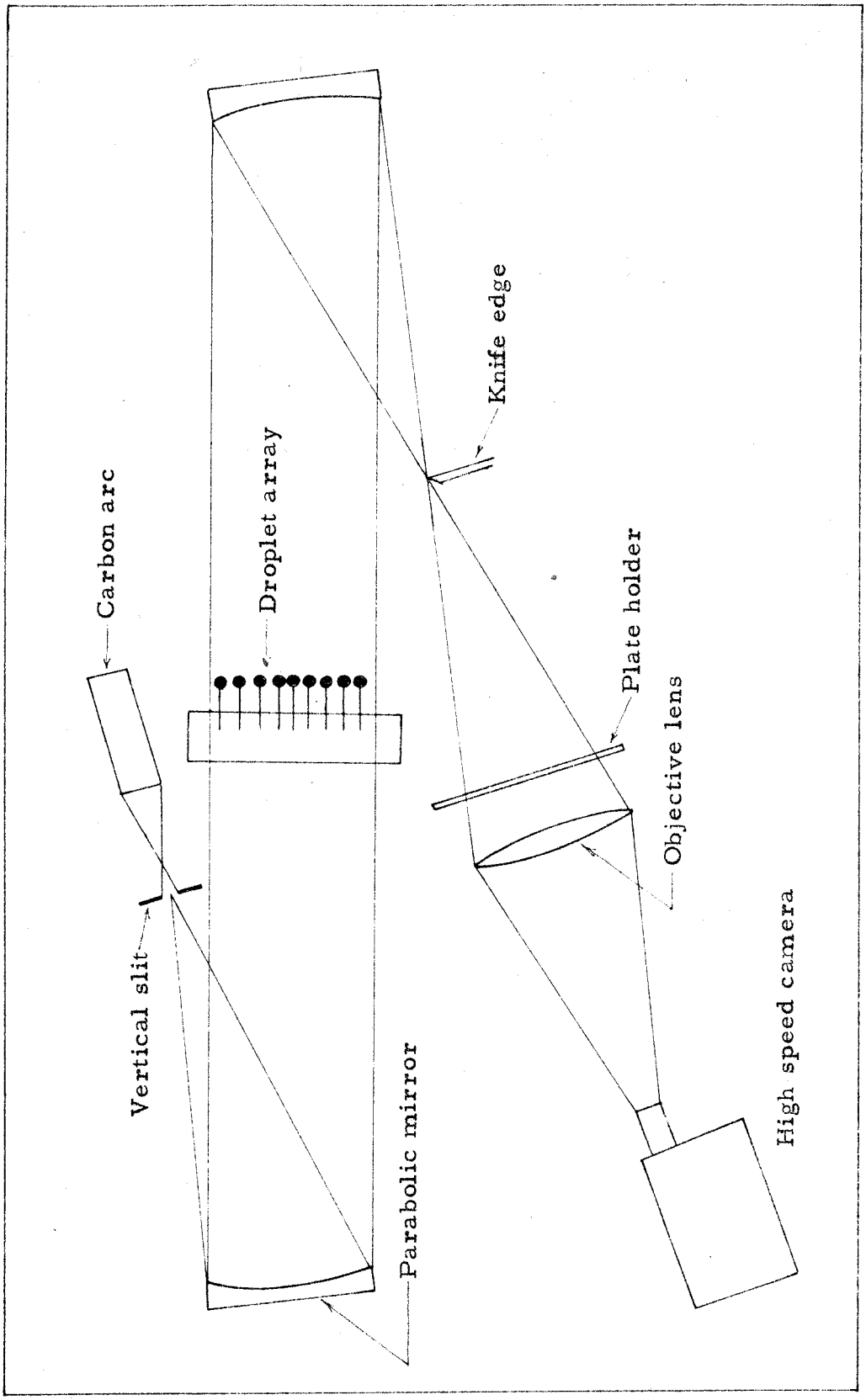

Figure 22. A schematic diagram of the apparatus used for determining the flame propagation rate in a one-dimensional droplet array.

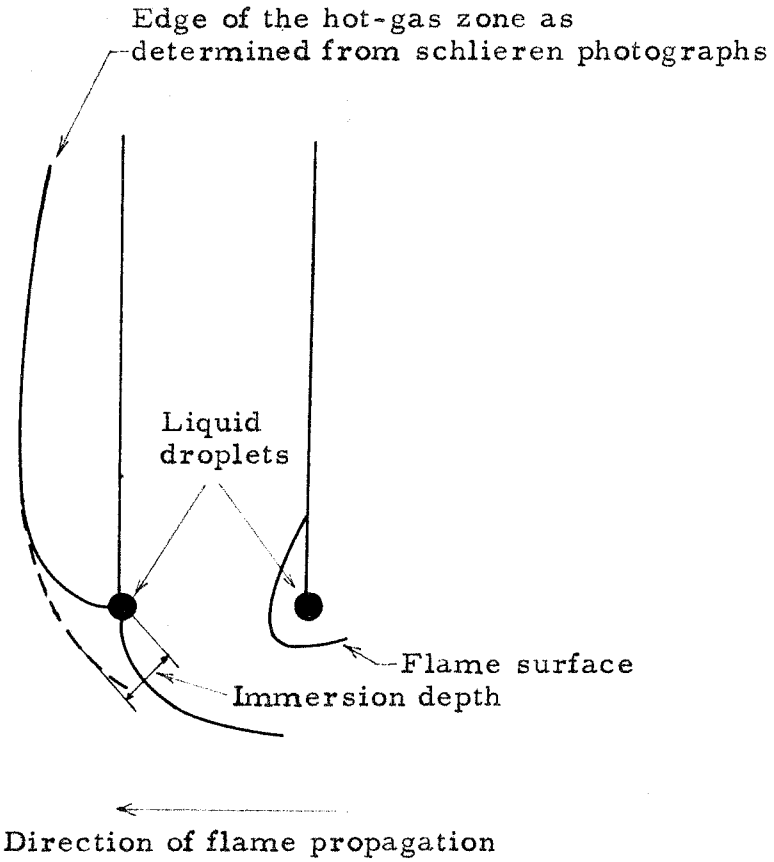

Figure 23. A schematic diagram showing the definition of immersion depth.

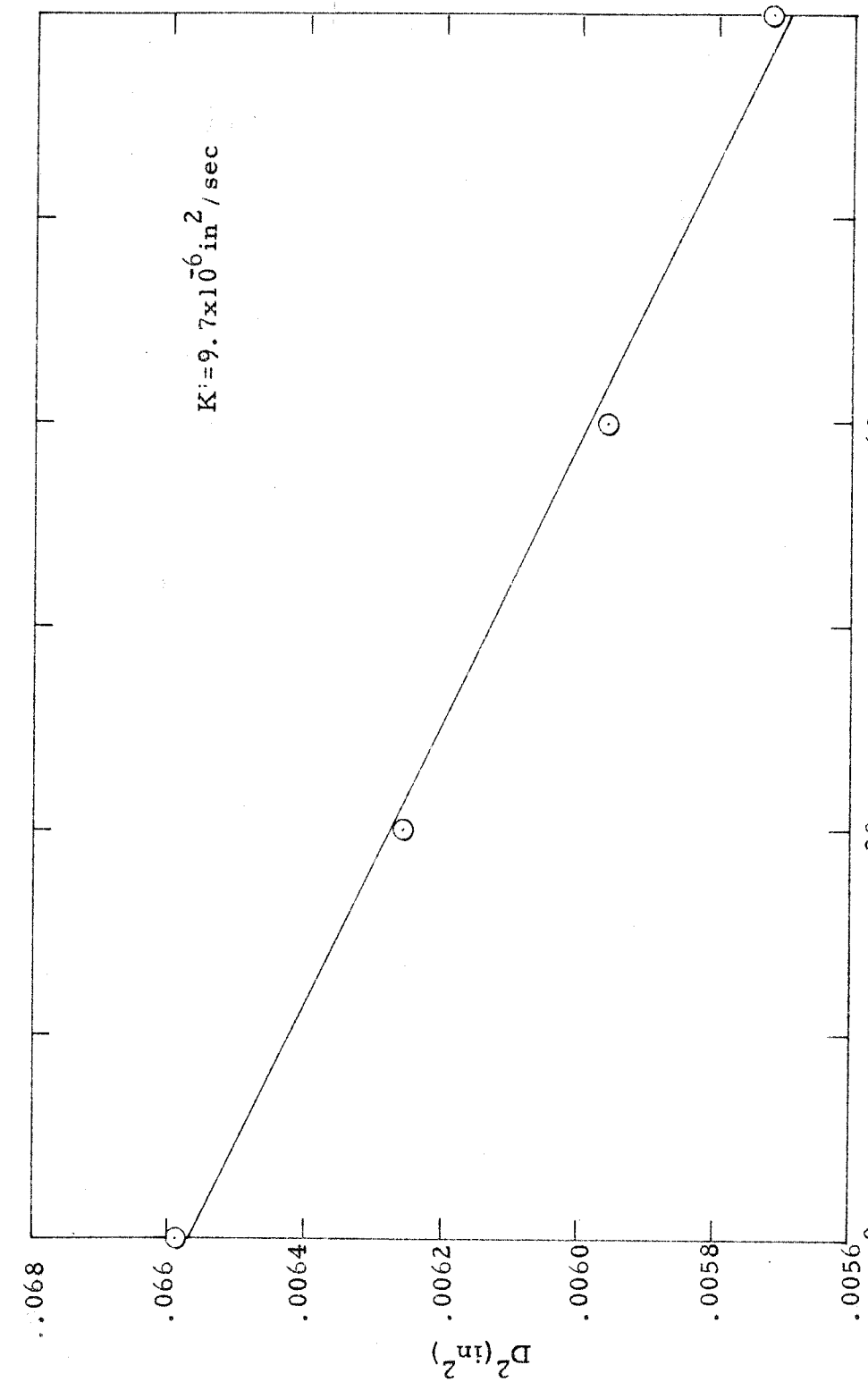

Figure 24. The evaporation constant for a non-burning n-octane droplet (i.e., not burning).

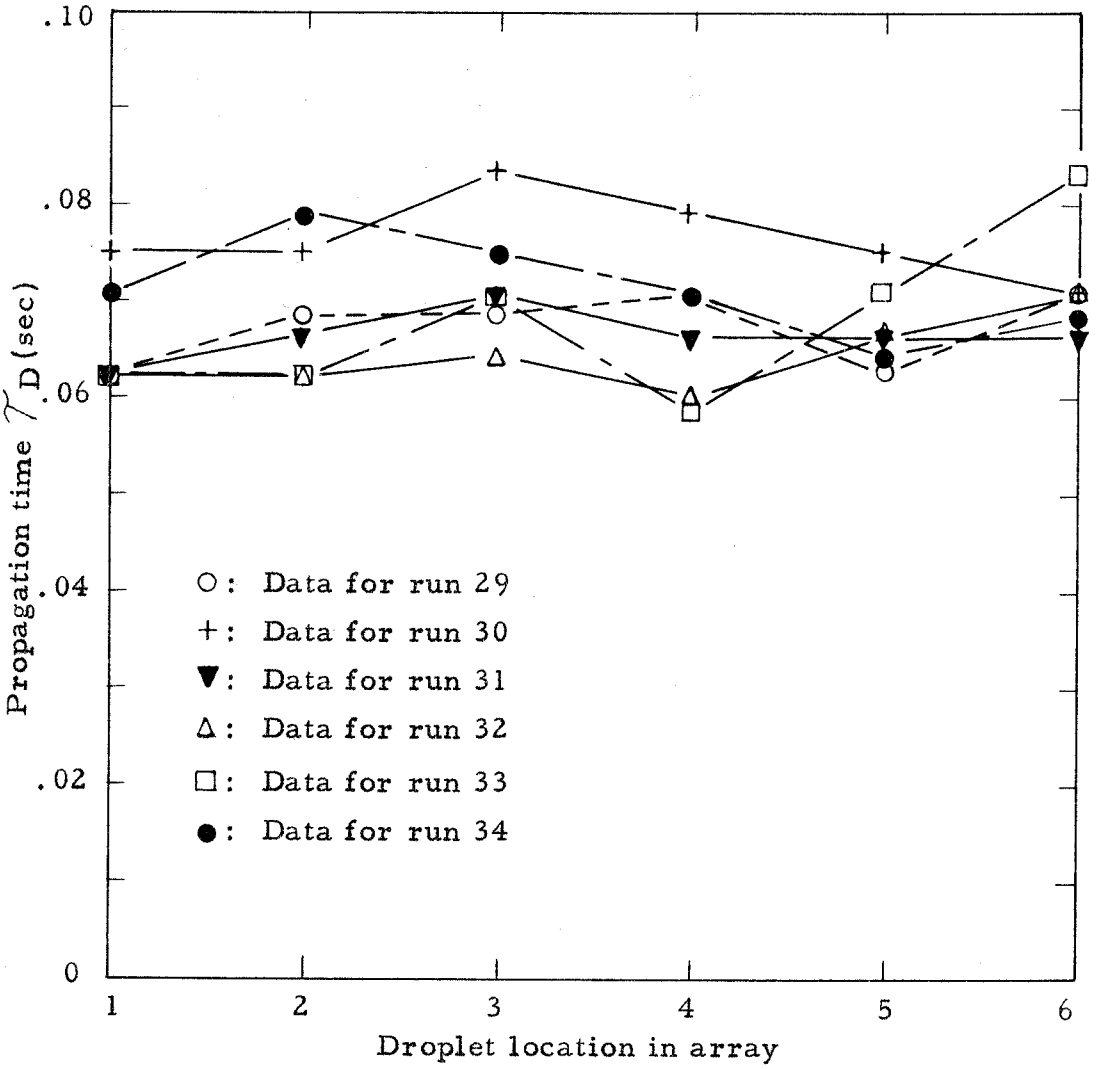

Figure 25. Representative propagation times τ_D for a spacing of 0.175 in and an initial droplet volume of 0.005 ml.

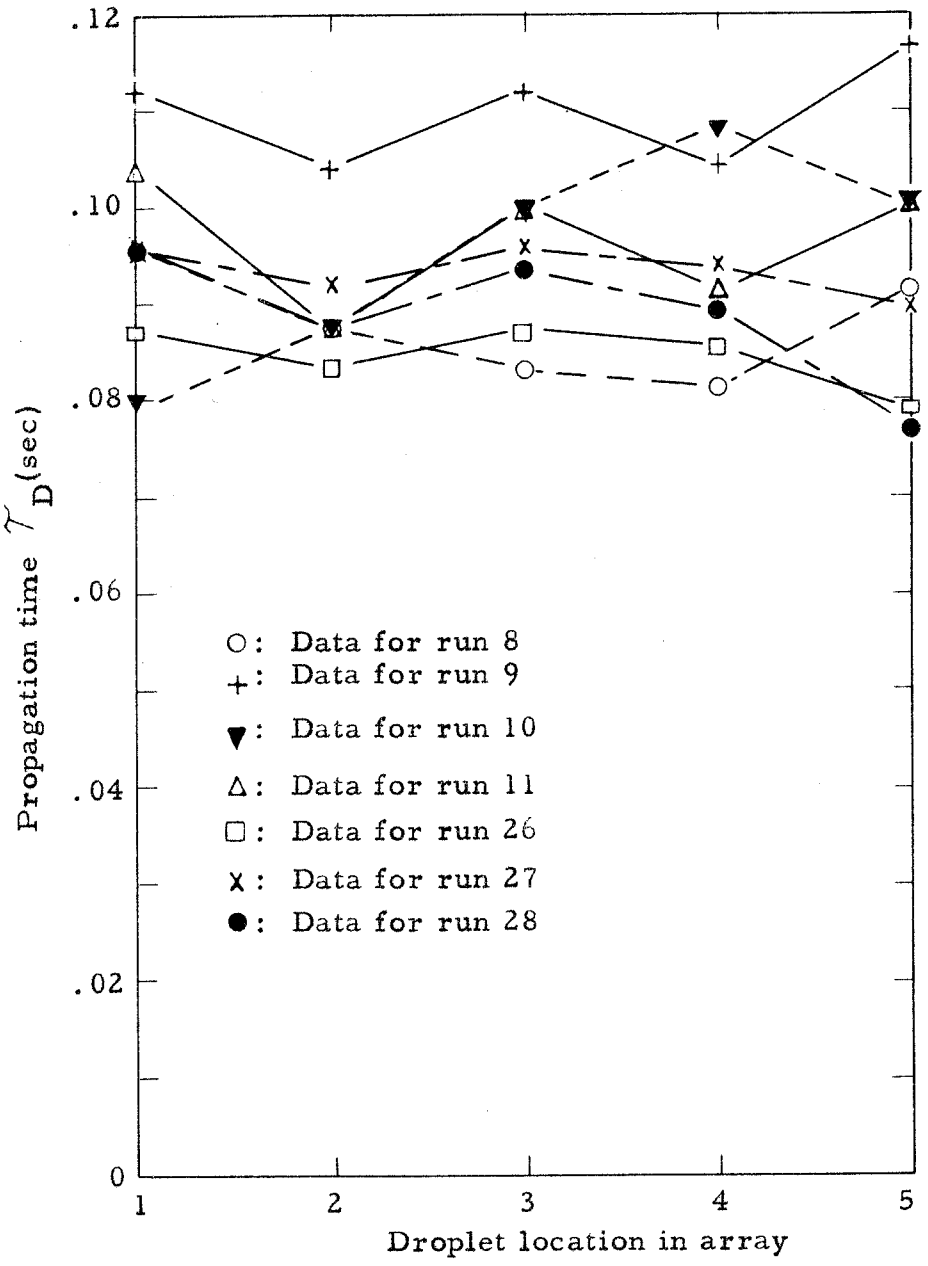

Figure 26. Representative propagation times for a spacing of 0.200 in and an initial droplet volume of 0.005 ml.

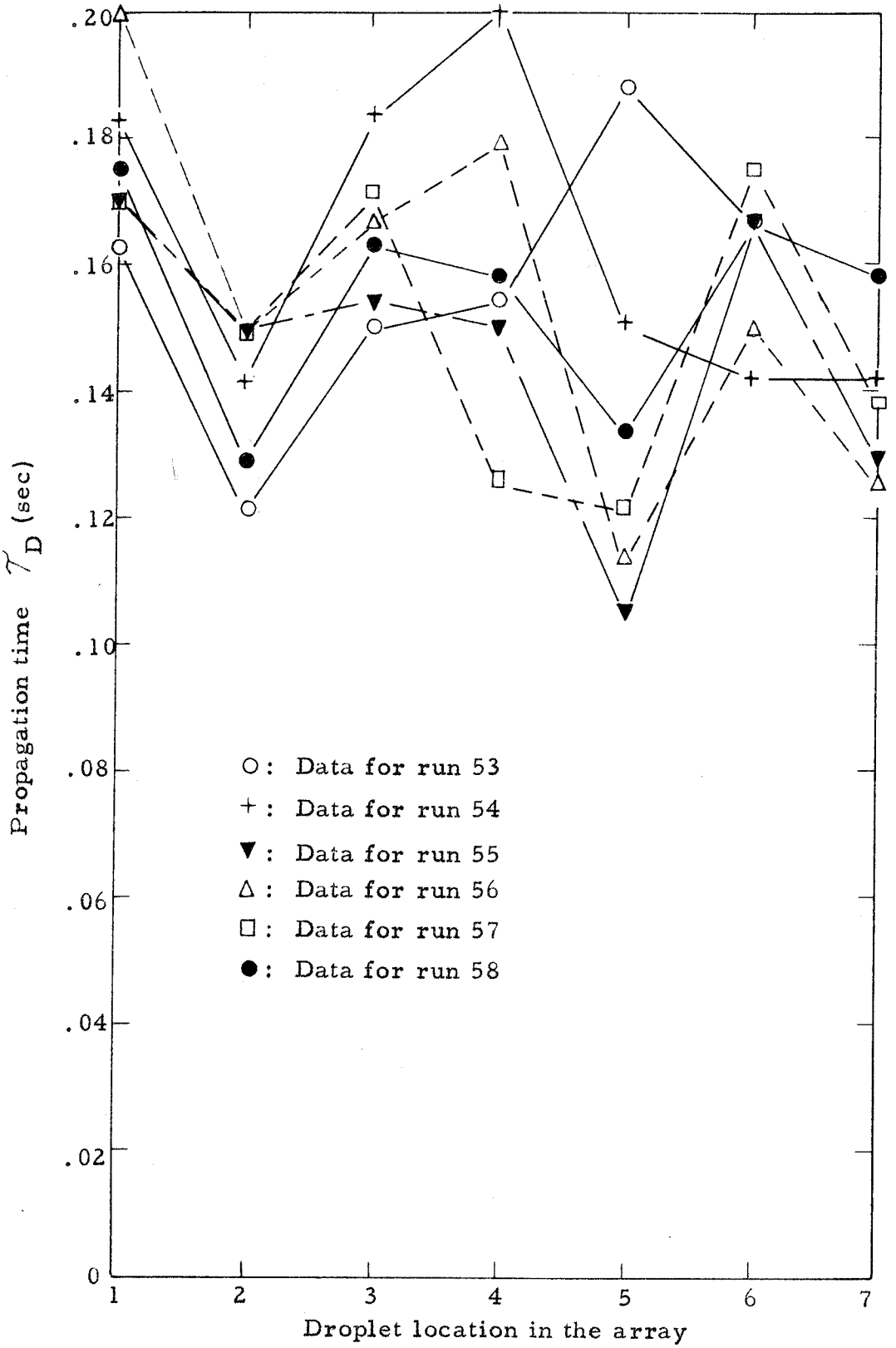

Figure 27. Representative propagation times τ_D for a spacing of 0.225 in and an initial droplet volume of 0.005 ml.

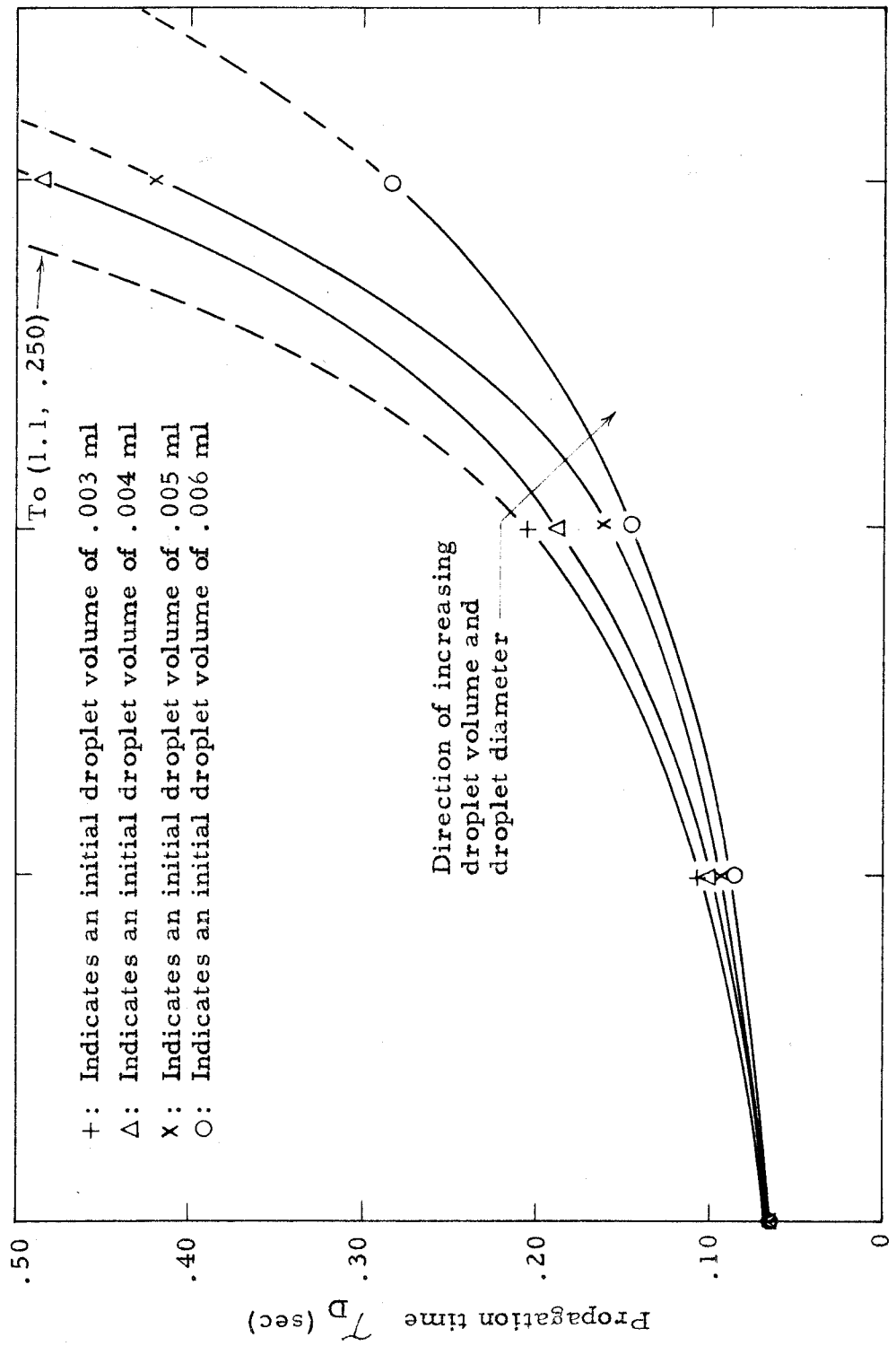

Figure 28. A plot of propagation time τ_D as a function of droplet spacing for variable droplet volumes.

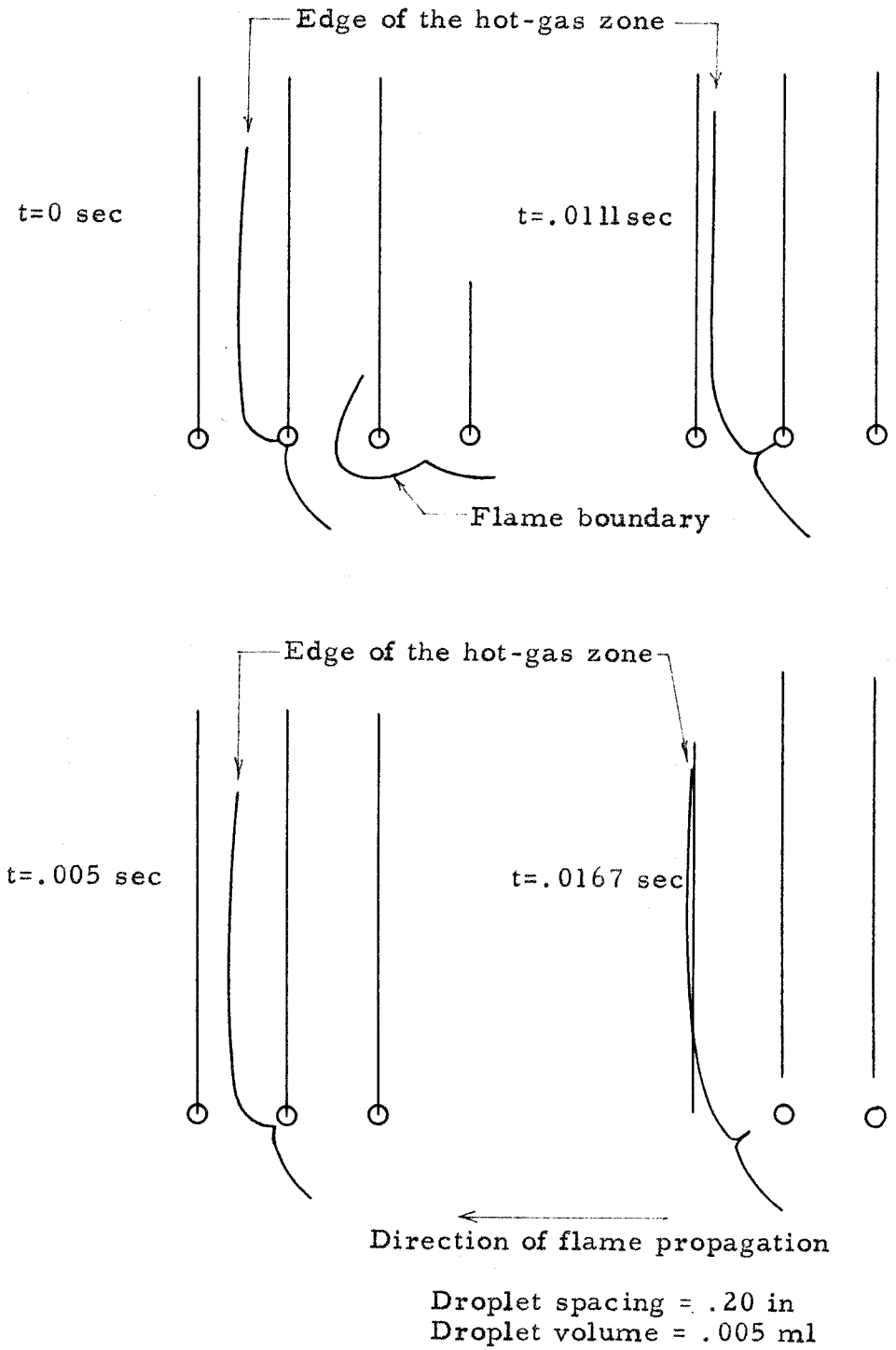

Figure 29. Schematic illustration of the ignition process for an n-octane droplet, as inferred from schlieren photographs.

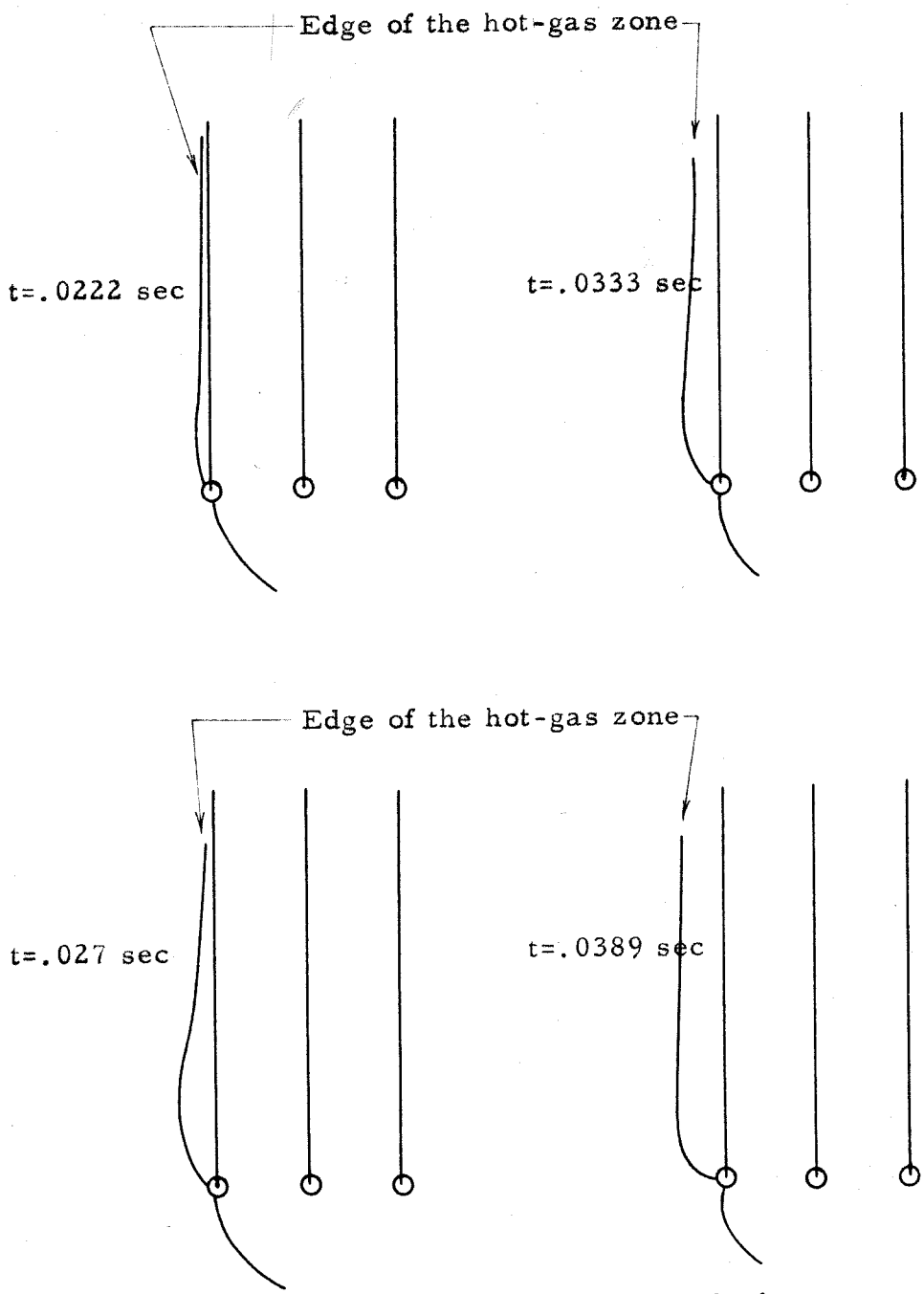

Figure 29 (continued). Schematic illustration of the ignition process for an n-octane droplet, as inferred from schlieren photographs.

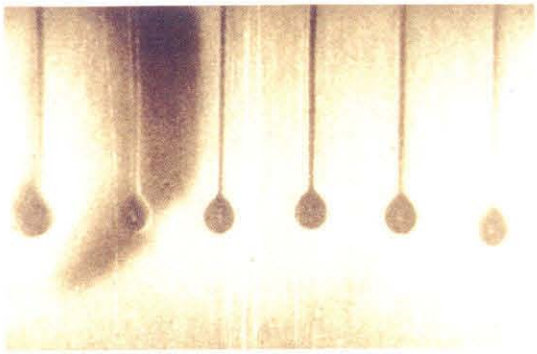

t=0

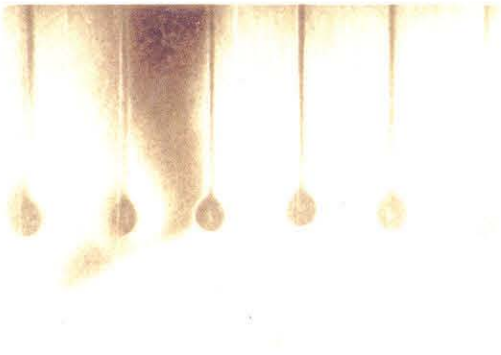

t=.0089

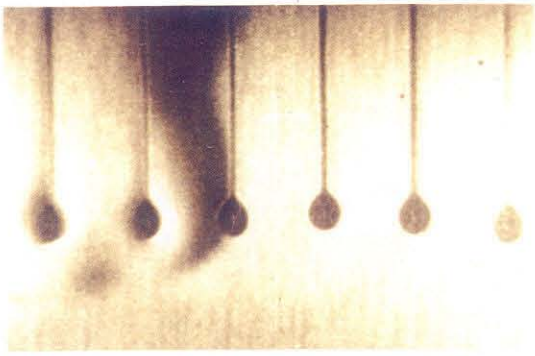

t=.0177

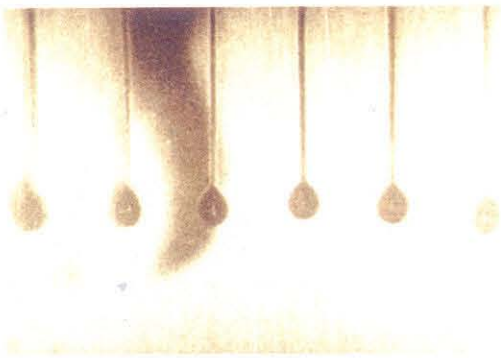

t=.0266

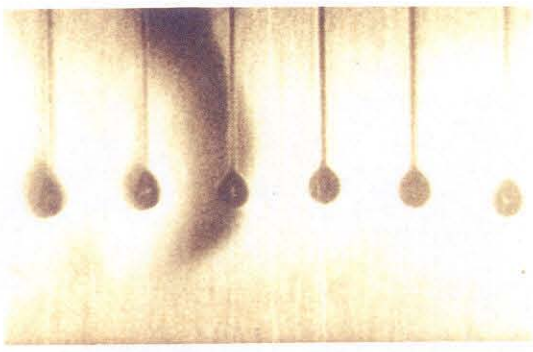

t=.0354

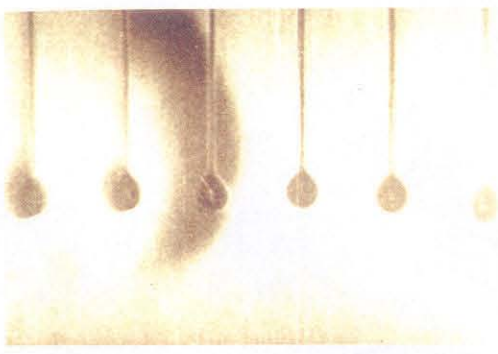

t=.0443

Figure 30. Schlieren photographs showing the hot-gas zone surrounding the unburnt droplet for a droplet spacing of 0.20 in and an initial droplet volume of 0.005 ml.

t=.0531 t=.0620

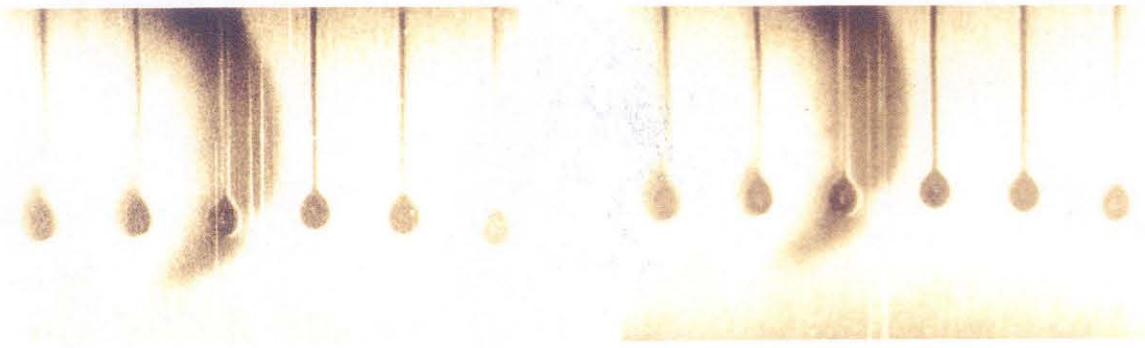

t=.0708 t=.0797

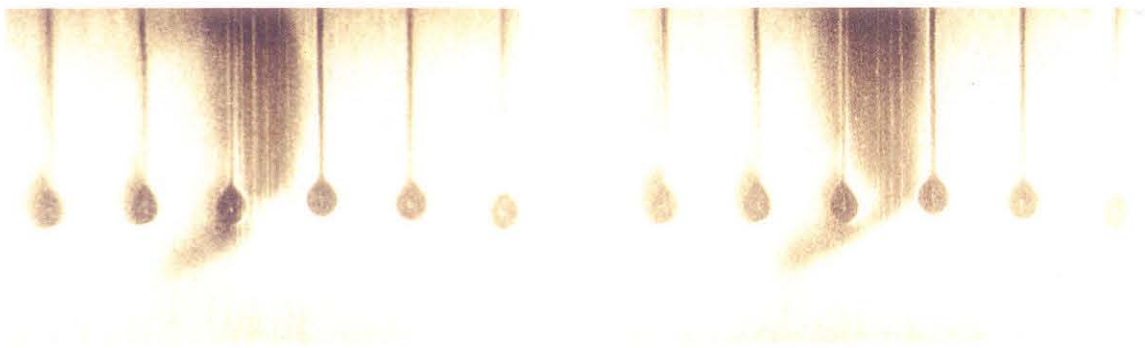

t=.0885 t=.0974

Figure 30 (continued). Schlieren photographs showing the hot-gas zone surrounding the unburnt droplet for a droplet spacing of 0.20 in and an initial droplet volume of 0.005 ml.

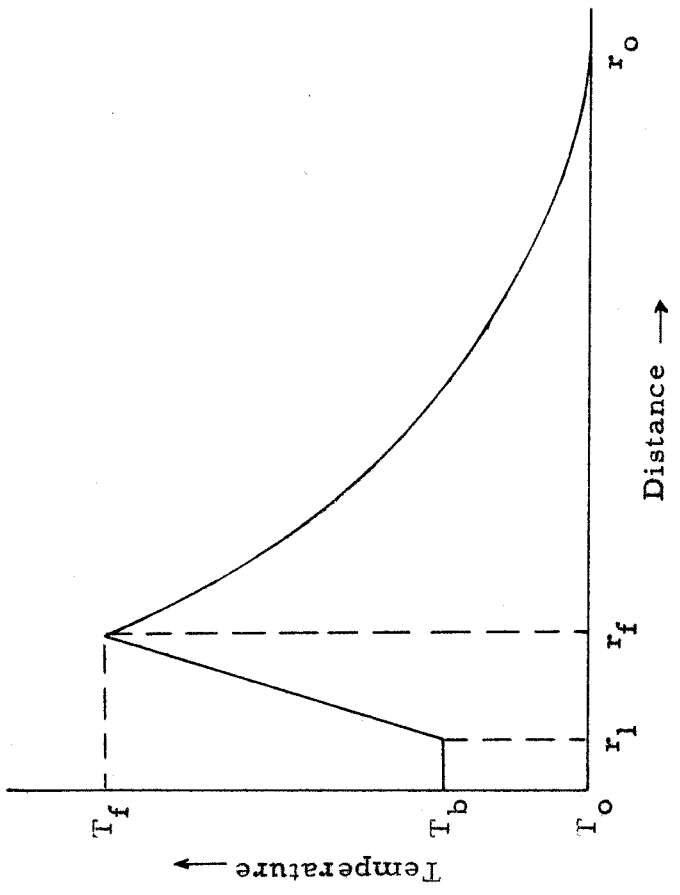

r_l = Droplet radius
r_f = Flame front radius
r_o = Radius of the hot-gas zone
T_f = Flame temperature
T_b = Boiling temperature of the fuel droplet
T_o = Ambient temperature of the surrounding atmosphere

Figure 31. A schematic sketch of the temperature as a function of distance as inferred from schlieren photographs.

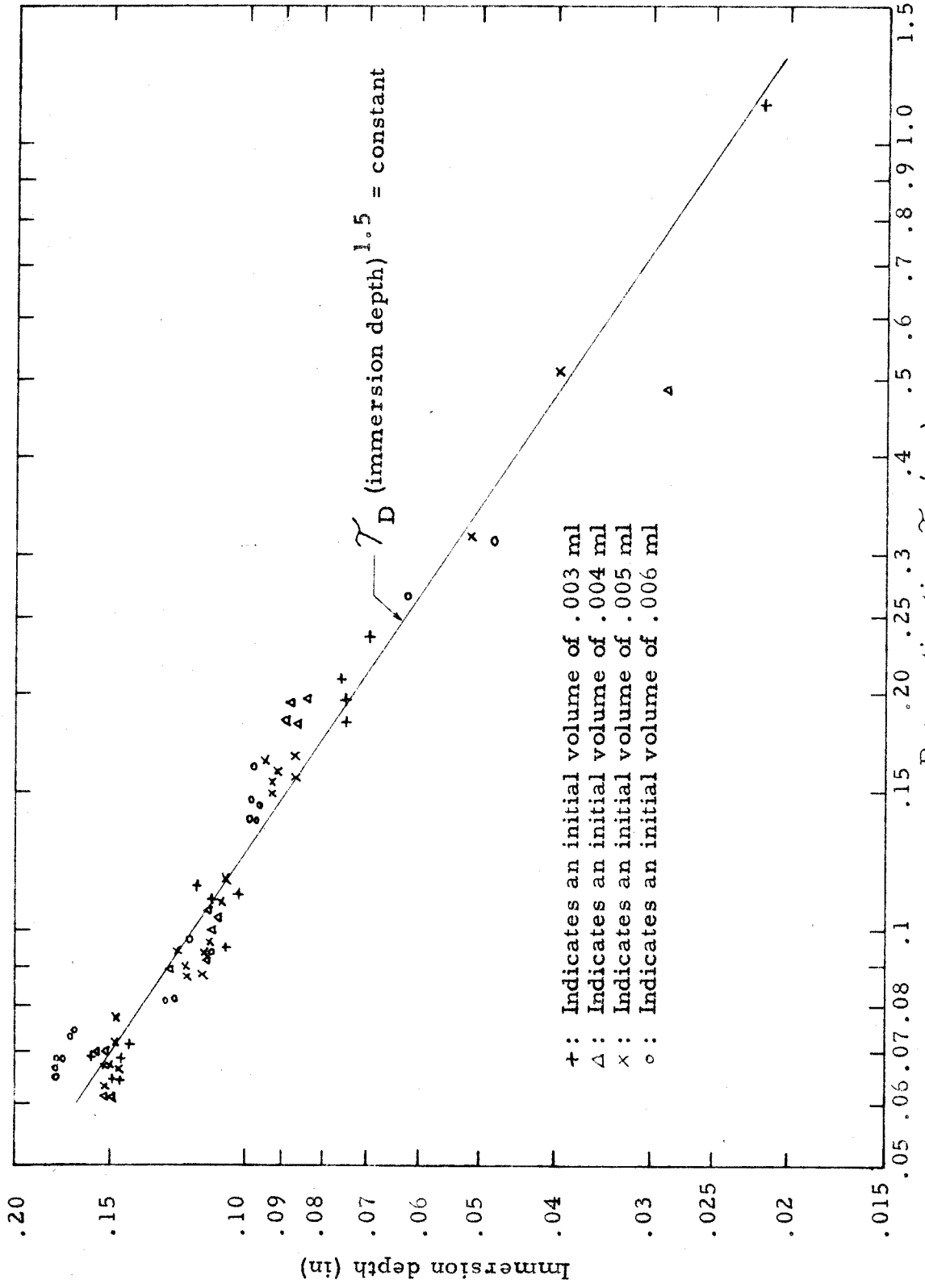

Figure 32. A plot of immersion depth vs. propagation time τ_D.

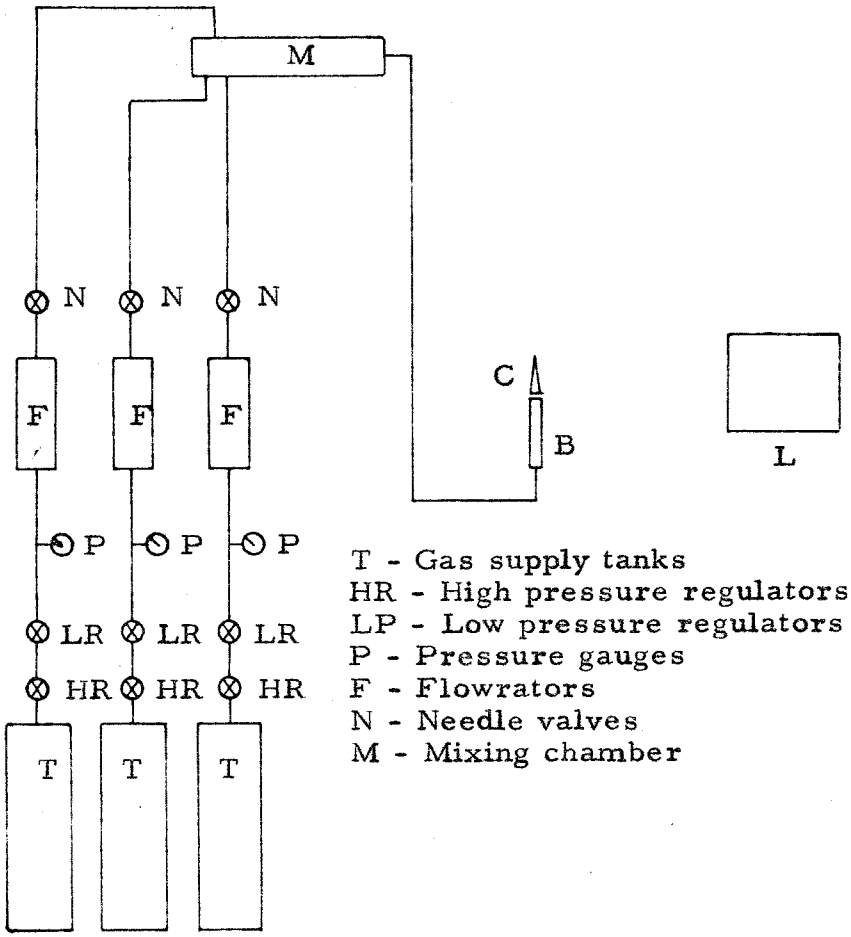

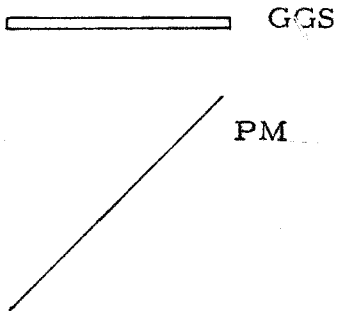

Figure 33. A schematic diagram of the apparatus used to obtain desired gas mixtures and laminar burning velocity data.

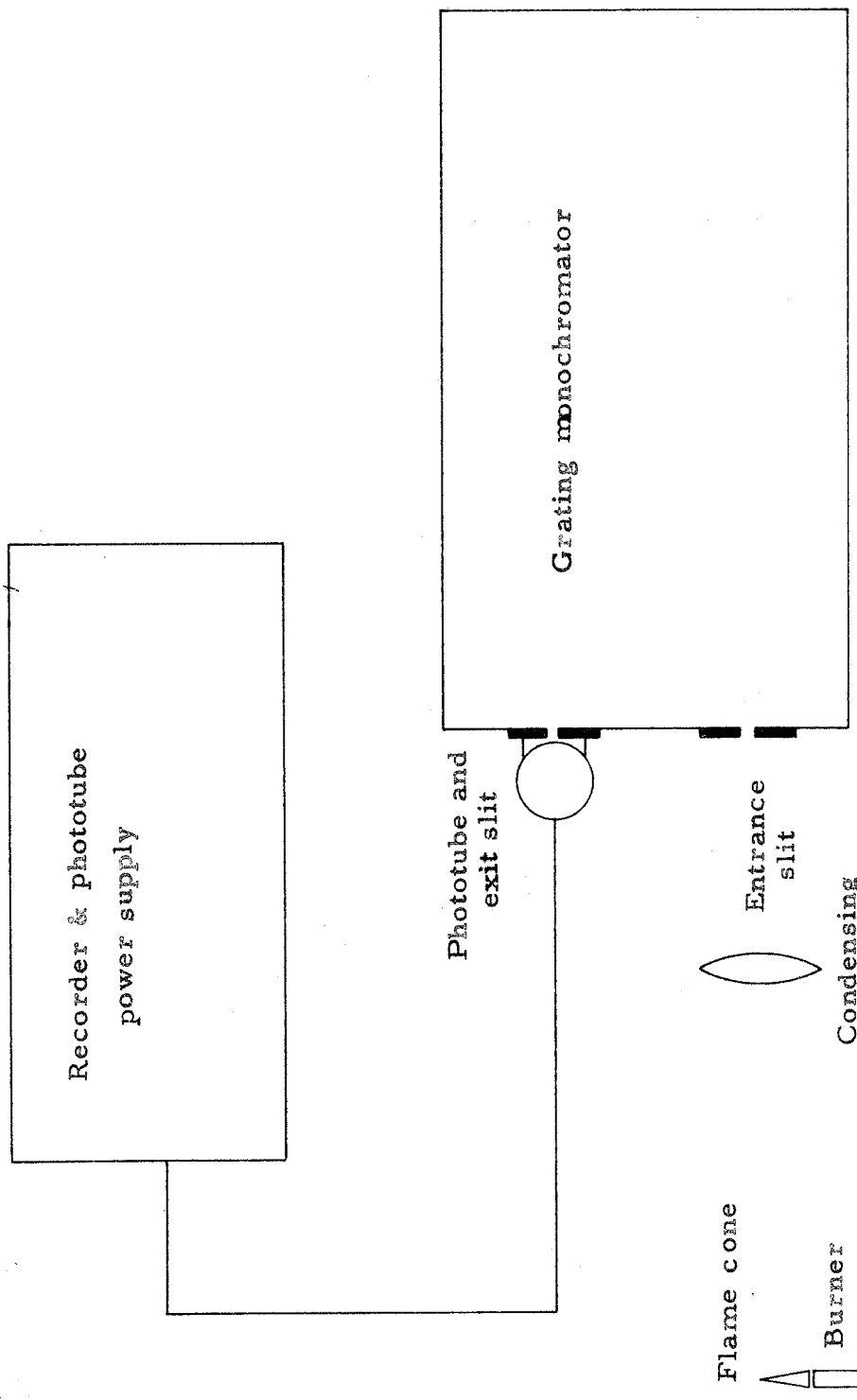

Figure 34. A schematic diagram of the apparatus used to obtain data for computation of the spectral intensity ratios.

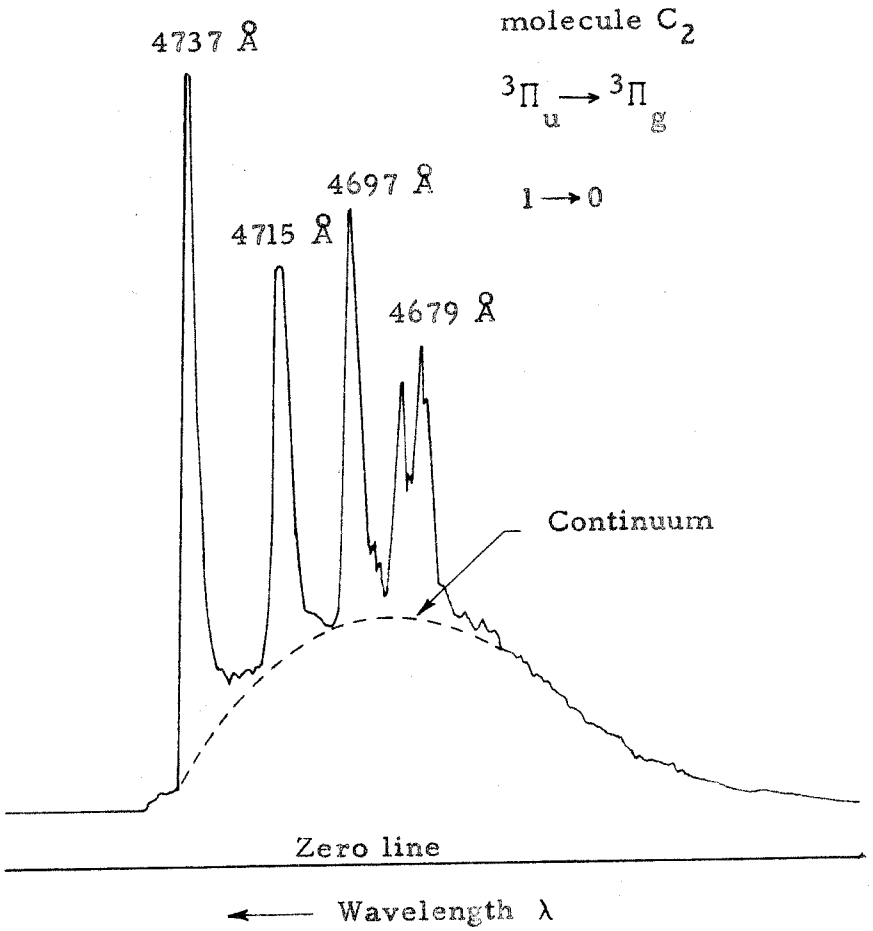

Figure 35. The apparent emission intensity as a function of wavelength.

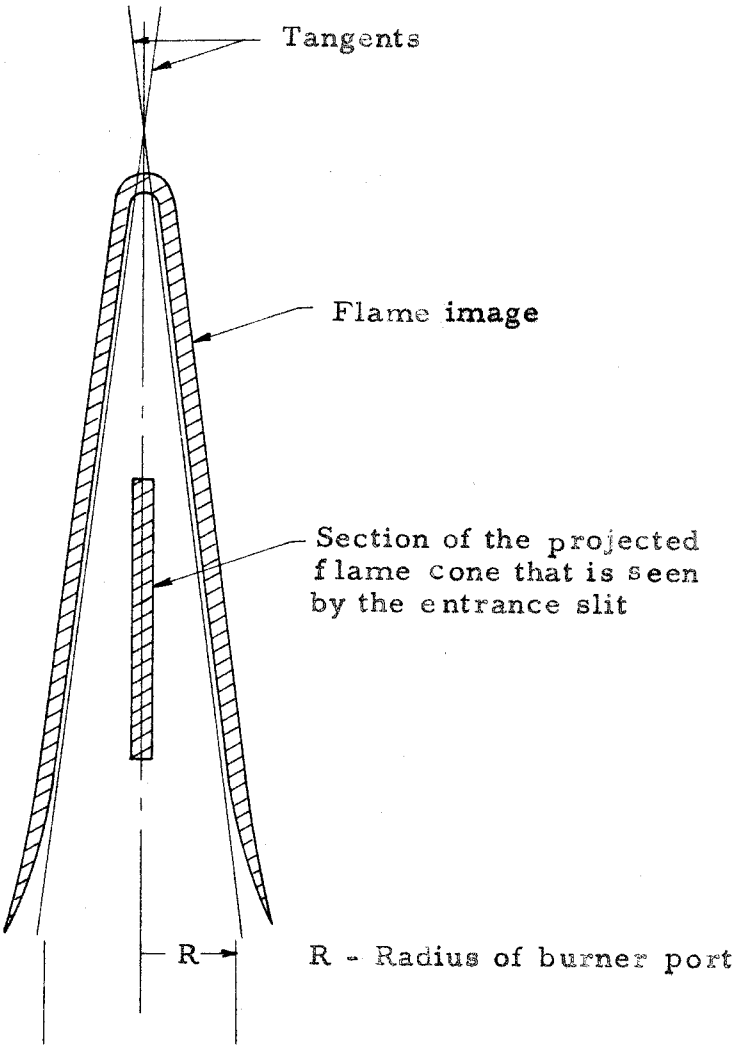

Figure 36. A diagram of a typical inner cone image.

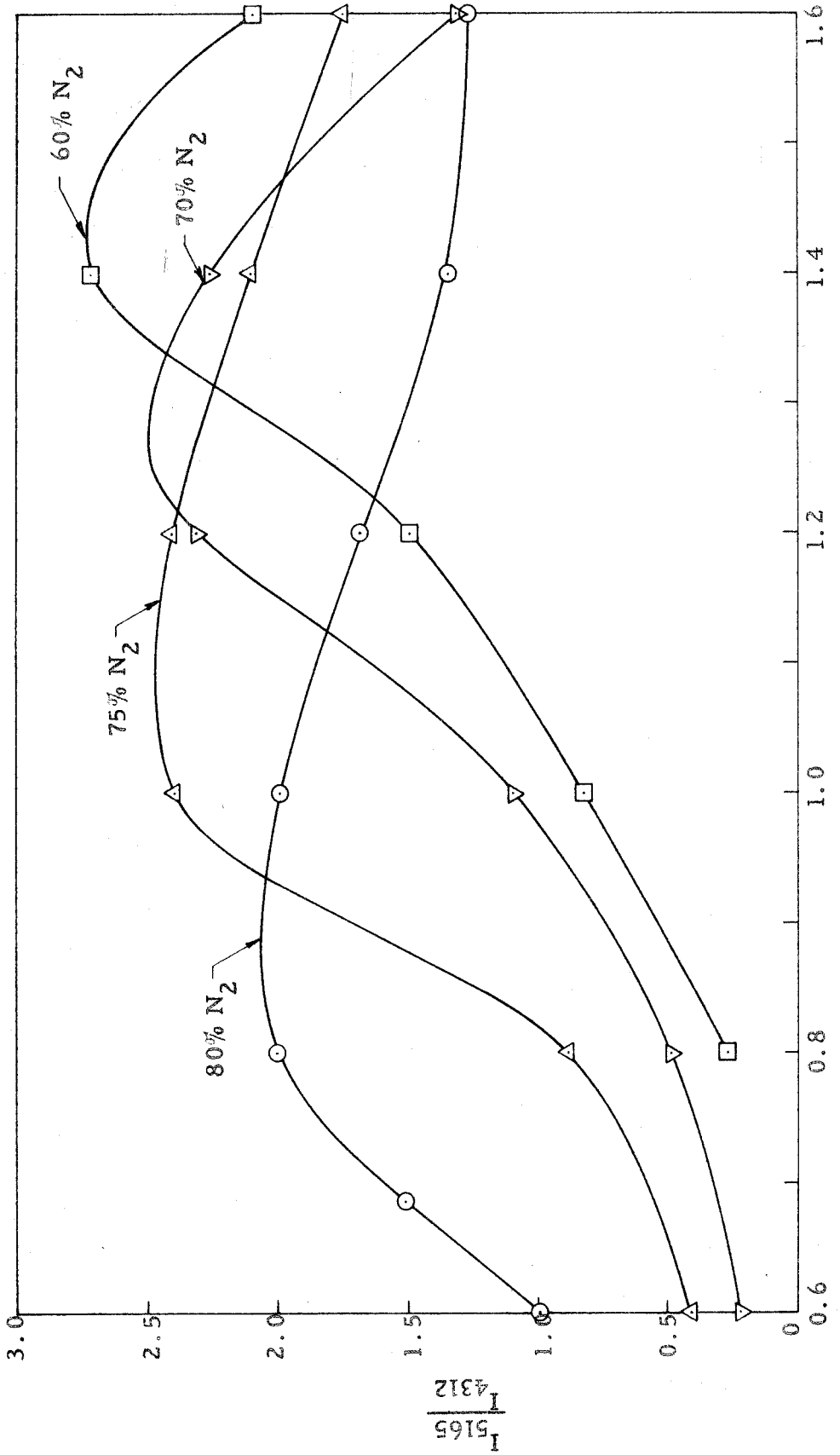

Figure 37. The spectral intensity ratio (I_{5165}/I_{4312}) as a function of equivalence ratio for various nitrogen contents (percentages by mass); 0.704 cm I.D. burner.

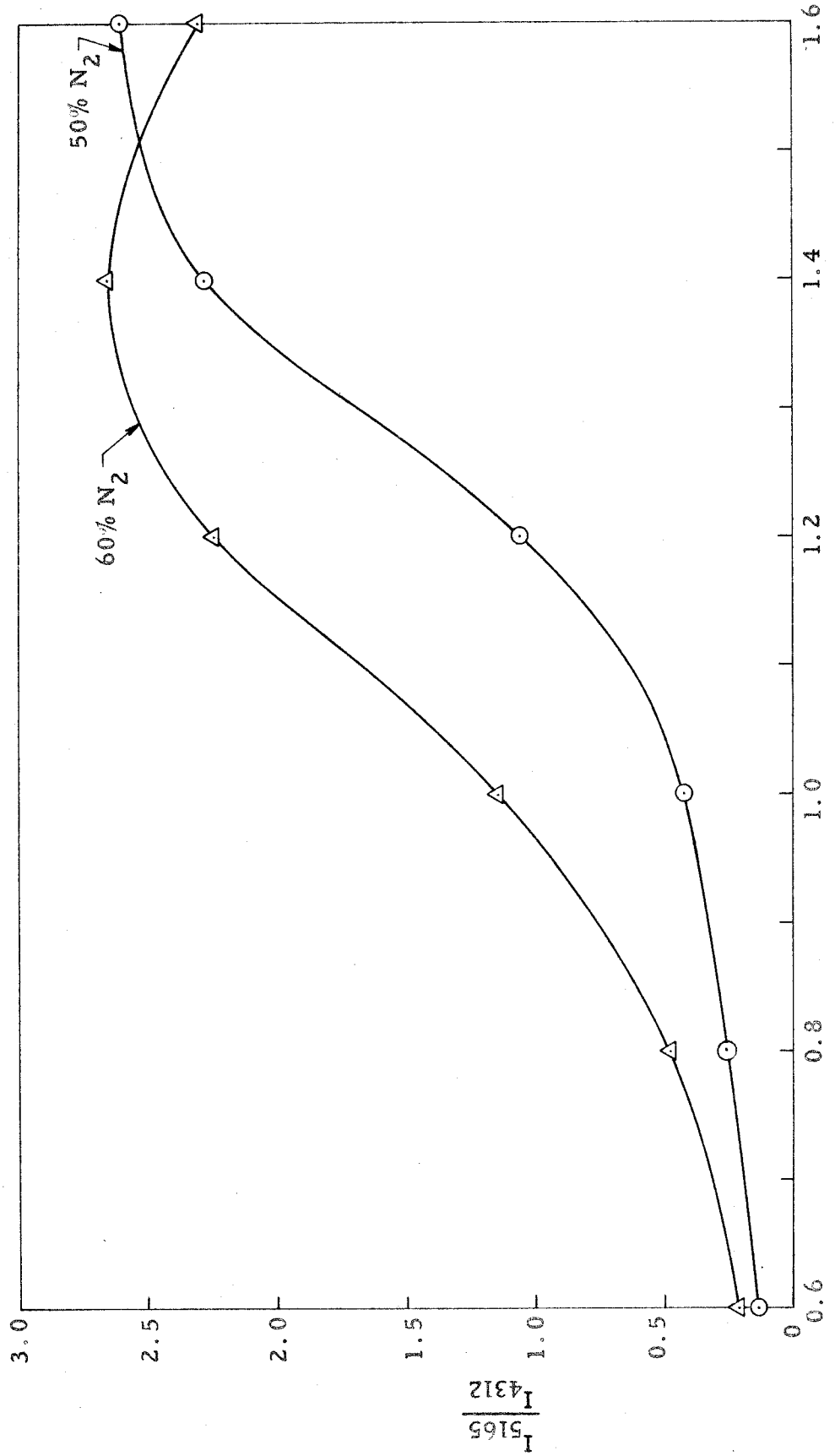

Figure 38. The spectral intensity ratio (I_{5165}/I_{4312}) as a function of equivalence ratio for various nitrogen contents (percentages by mass); 0.386 cm I.D. burner.

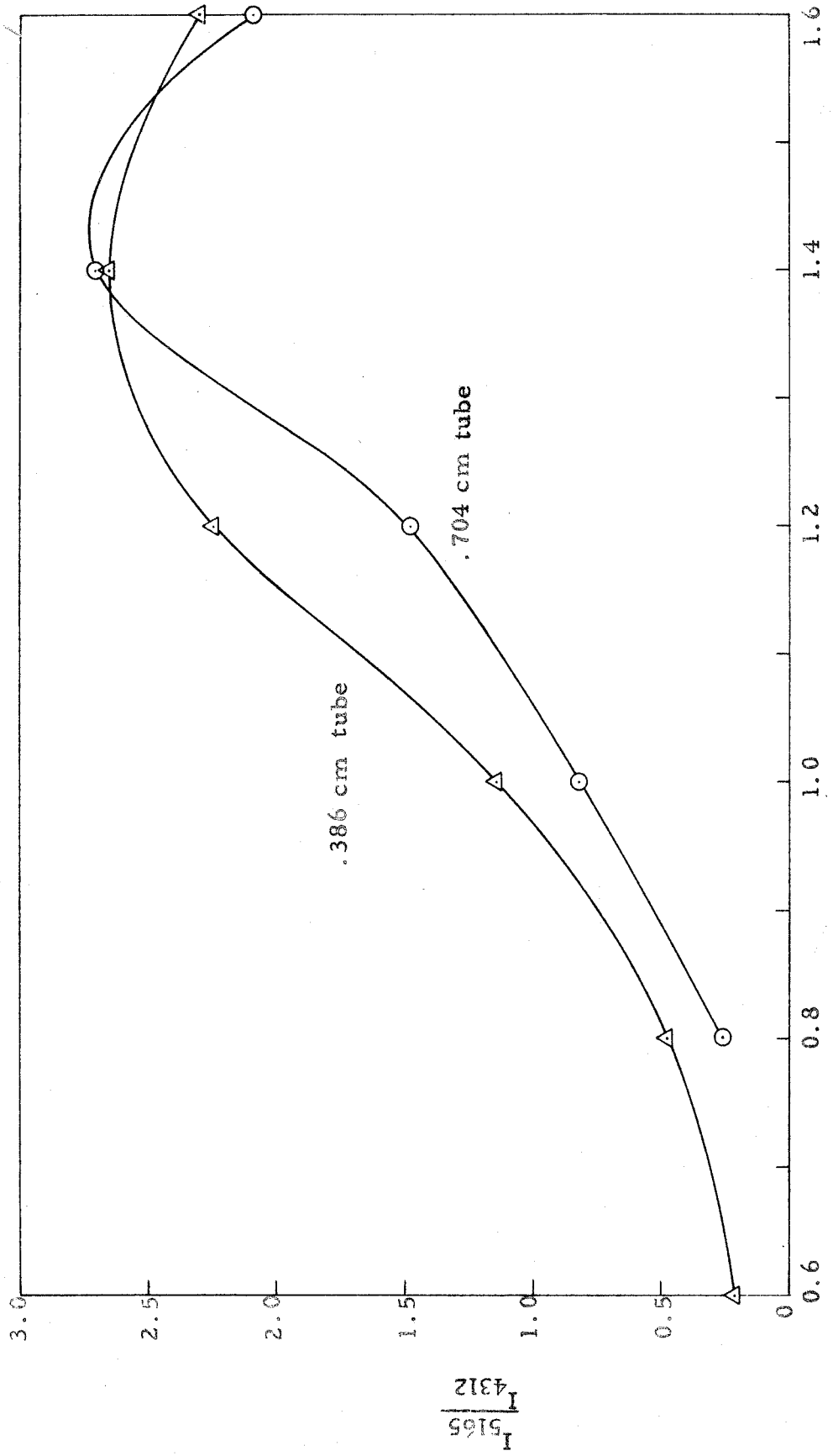

Figure 39. The spectral intensity ratio (I_{5165}/I_{4312}) as a function of equivalence ratio for 0.386 cm and 0.704 cm I.D. burners. Nitrogen content in mixtures: 60% by mass.

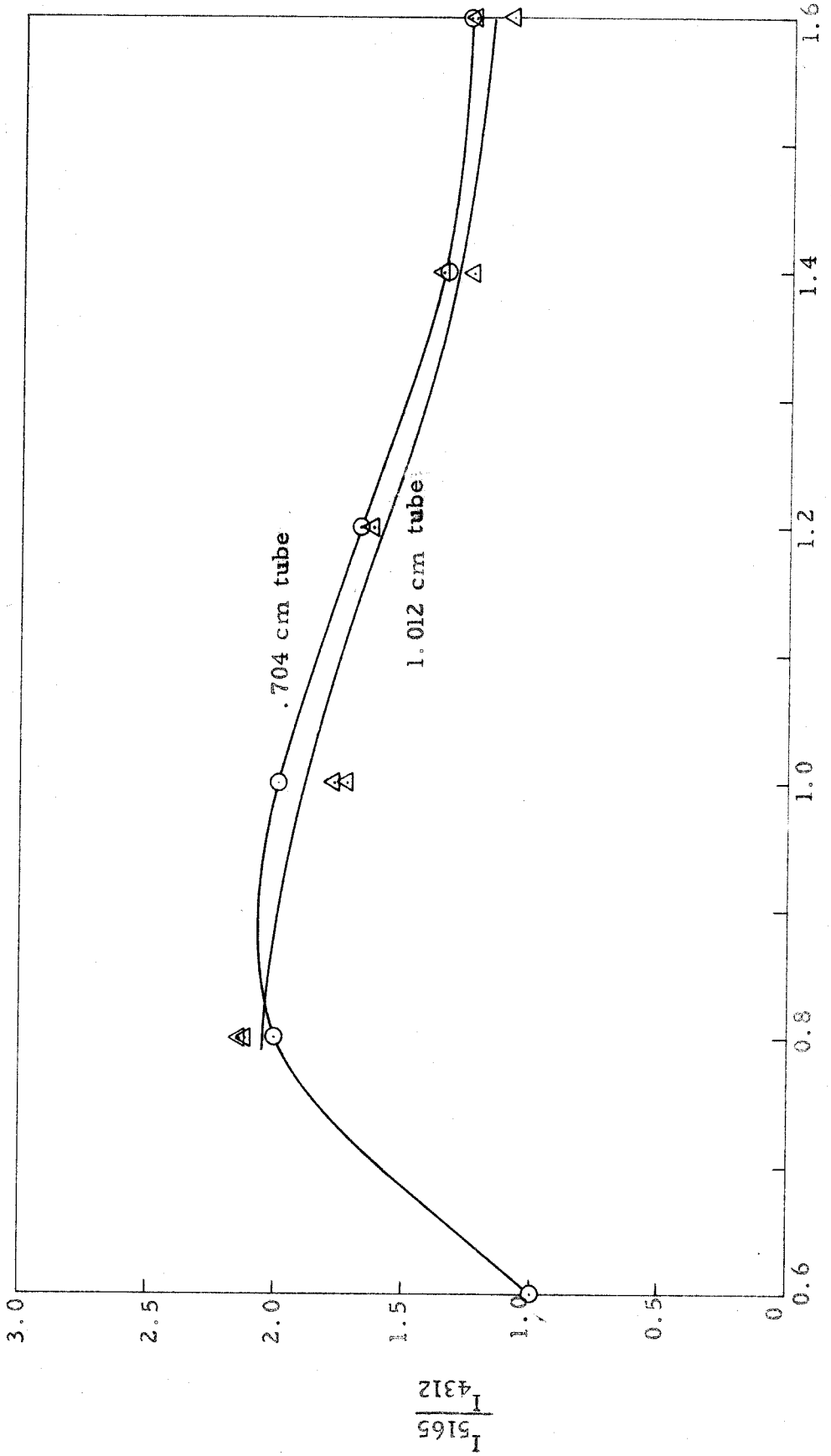

Figure 40. The spectral intensity ratio (I_{5165}/I_{4312}) as a function of equivalence ratio for 0.704 cm and 1.012 cm I.D. burners. Nitrogen content in mixtures: 80% by mass.

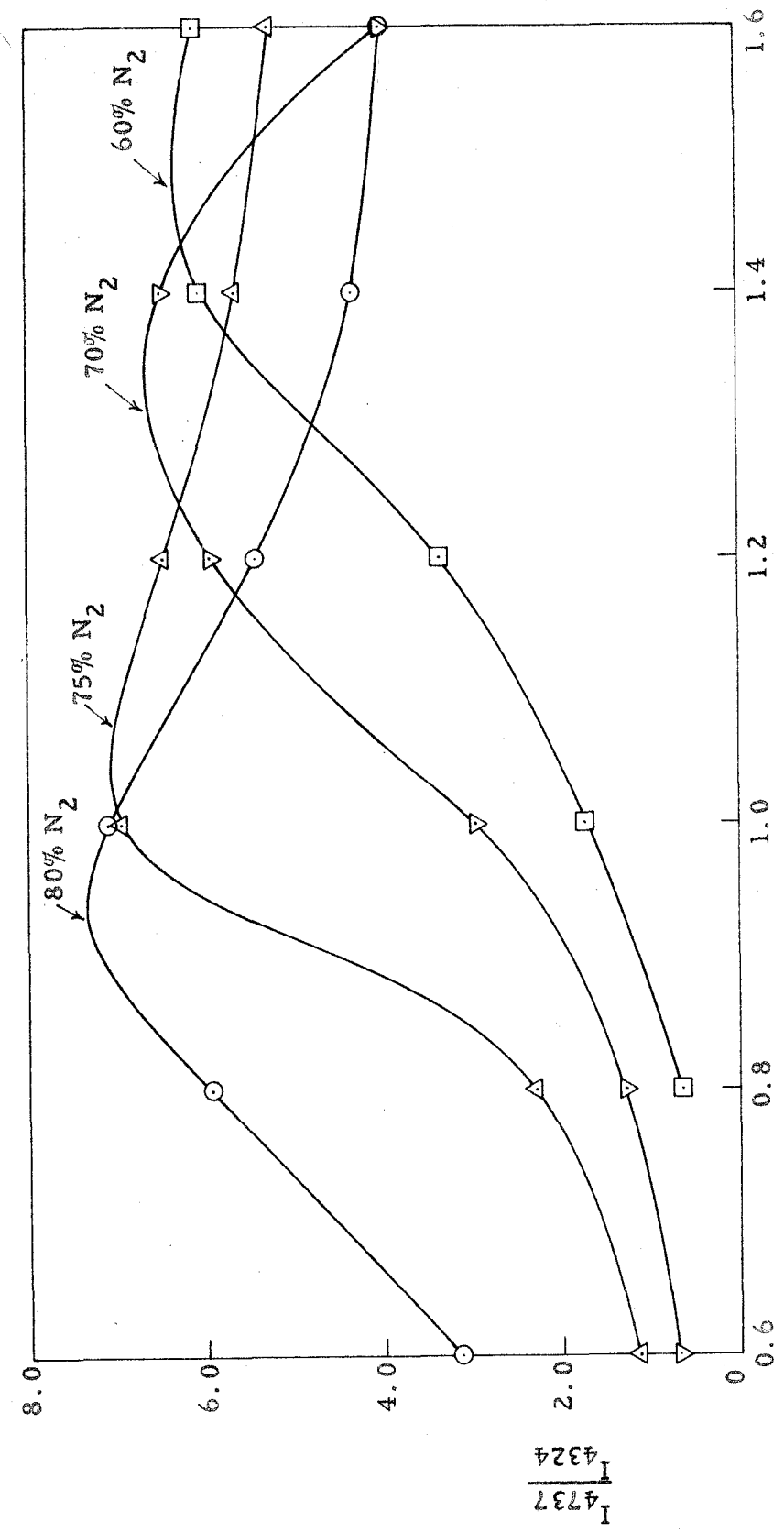

Figure 41. The spectral intensity ratio (I_{4737}/I_{4324}) as a function of equivalence ratio for various nitrogen contents (percentages by mass); 0.704 cm I.D. burner.

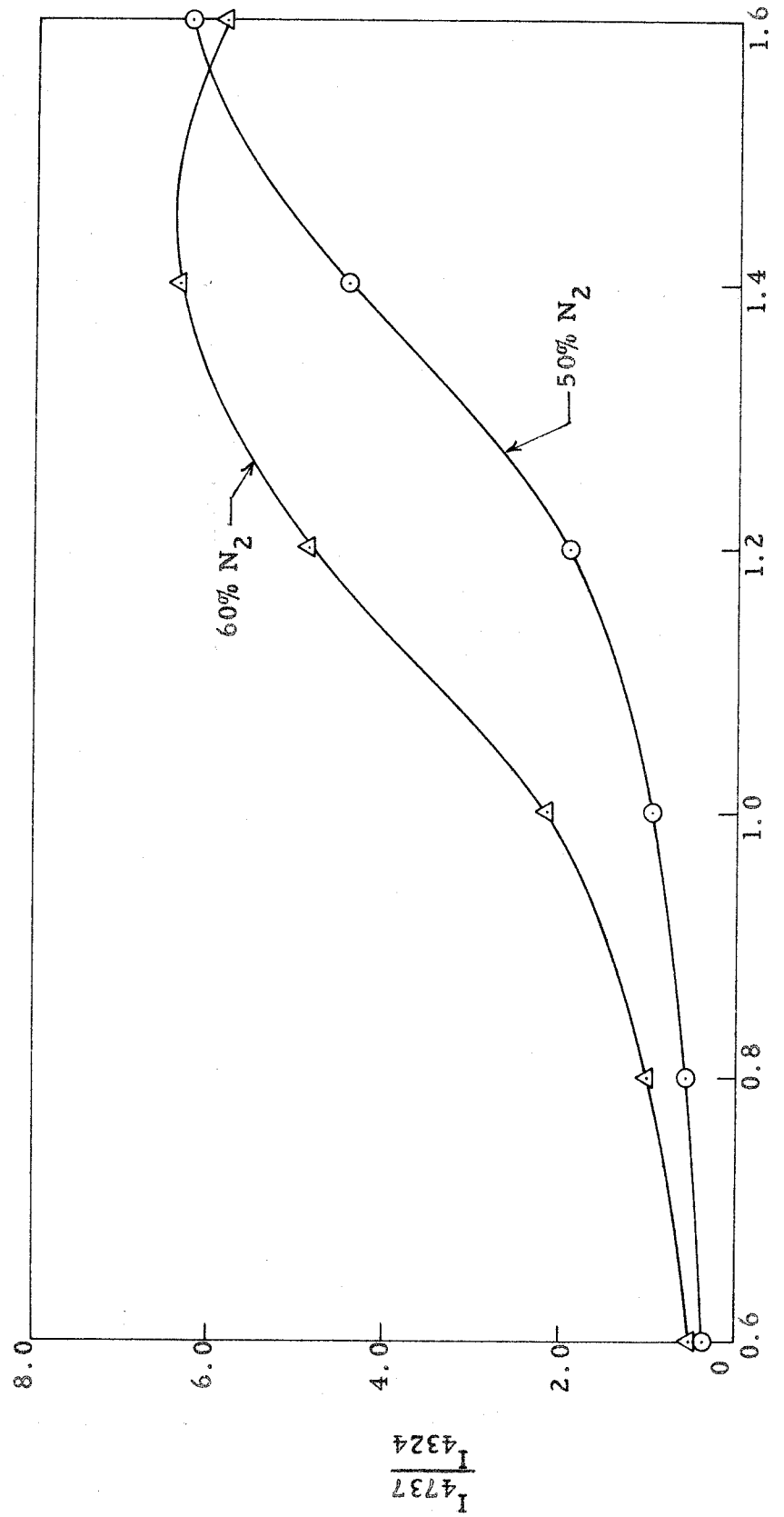

Figure 42. The spectral intensity ratio (I_{4737}/I_{4324}) as a function of equivalence ratio for various nitrogen contents (percentages by mass); 0.386 cm I.D. burner.

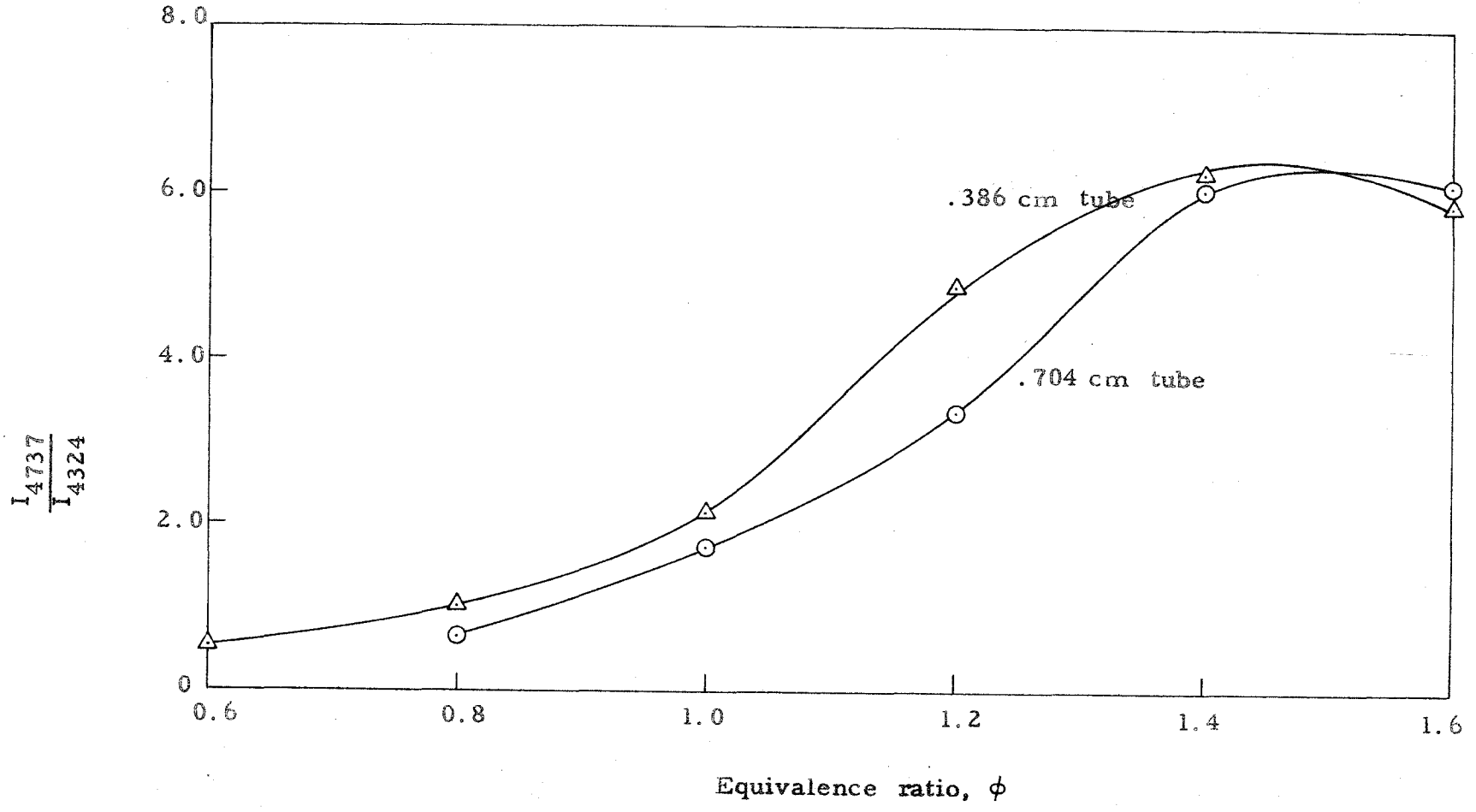

Figure 43. The spectral intensity ratio (I_{4737}/I_{4324}) as a function of equivalence ratio for 0.386 cm and 0.704 cm I.D. burners. Nitrogen content in mixtures: 60% by mass.

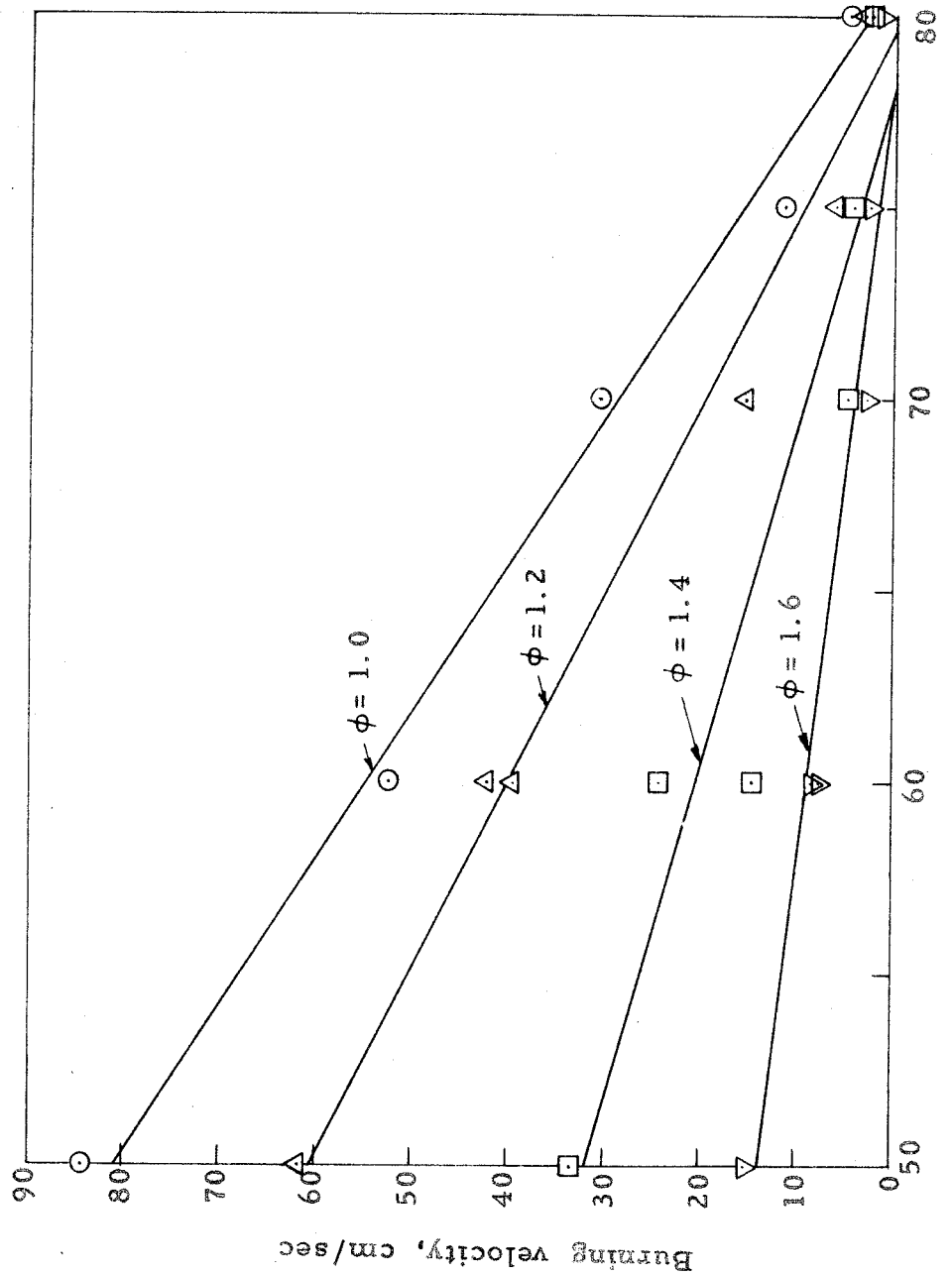

Figure 44. The laminar burning velocity as a function of nitrogen content (percentage by mass) for various equivalence ratios.